The Effect of Material Properties on Cartilage-like Tissue Formation

Towards the Development of Smart Biomaterials for Cartilage Regeneration

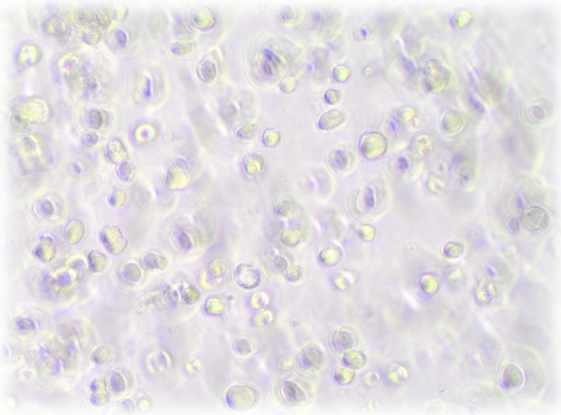

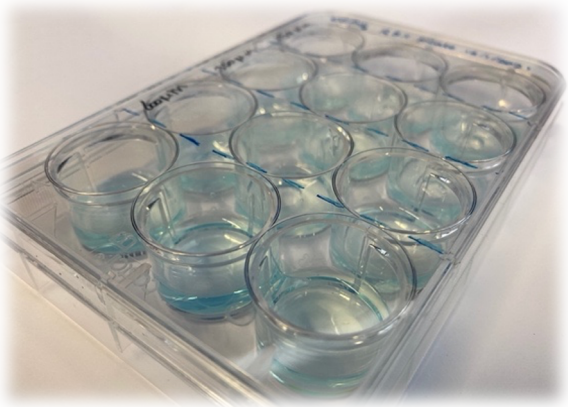

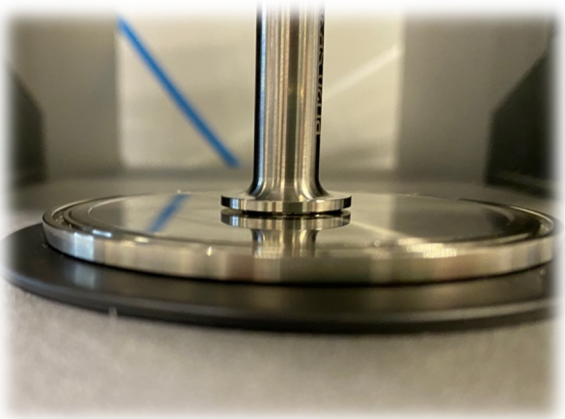

Erasmus MC
Universitair Medisch Centrum Rotterdam

TU Delft
Delft University of Technology

THE EFFECT OF MATERIAL PROPERTIES ON CARTILAGE-LIKE TISSUE FORMATION

TOWARDS THE DEVELOPMENT OF SMART BIOMATERIALS FOR CARTILAGE REGENERATION

Master Thesis

By

OSMAN ESEN

to obtain the degree of Master of Science
at the Delft University of Technology,
to be defended publicly on **28th of May, 2021** at 13:30 hours.

Student number	4400089
Supervisors:	prof. dr. G.J.V.M. van Osch (Erasmus MC & TU Delft) M. Fenu (Erasmus MC)
Thesis committee	prof. dr. G.J.V.M. van Osch (Erasmus MC & TU Delft) dr. I.A.A. Muntz (TU Delft) dr. M. Mirzaali Mazandarani (TU Delft)

Erasmus MC
Universitair Medisch Centrum Rotterdam

TU Delft Delft University of Technology

ACKNOWLEDGEMENTS

This project was completed thanks to the assistance and support from a few people. First of all, I would like to thank my daily supervisor, M. Fenu, for all his help, patience, and support during this project. Furthermore, I would like to thank prof. dr. G.J.V.M. van Osch and M. Fenu for taking me on this project and teaching me different techniques and theories related to cartilage tissue engineering topics. Both of them helped me solve many encountered challenges, and they helped me develop a more critical attitude towards experimental setup and writing. I would also like to thank the lab technicians, J.L.M. Koevoet, J. Witte-Bouma and N. Kops, for teaching and assisting me with many techniques I have learned in the lab. Next, I want to thank dr. I.A.A. Muntz for helping me with the rheological measurements. Finally, I would like to thank all my colleagues in the Connective Tissue Repair Lab at Erasmus MC and my friends and family for their guidance, encouragement, patience, and support. Without the help of all these people, I would not have completed my master thesis project.

ABSTRACT

Articular cartilage is an avascular tissue type with very limited self-repair capacity, making it prone to degenerative diseases such as osteoarthritis (OA). The current therapeutic strategy for OA patients is predominantly directed towards pain relief rather than preventing degeneration and promoting the regeneration of cartilage tissue. Mesenchymal stromal cells (MSCs) have been proposed as a potential cell source for articular cartilage tissue engineering purposes. MSCs are mechanosensitive cells capable of sensing, transmitting, and responding to mechanical cues from their microenvironment through a process known as mechanotransduction. Utilizing the mechanotransductive behaviour of MSCs, cell differentiation can be directed towards a specific phenotype, in our case a chondrogenic cell. Considerable effort has been put into the identification of mechanotransductional regulators for chondrogenic differentiation of MSCs. However, due to the interdependency of the material properties by the crosslinking density, the effect of isolated material properties on cells remains unknown, and limits researchers to develop smart biomaterials for tissue engineering purposes through the concept of mechanobiology.

This thesis will examine how material properties such as substrate stiffness and mesh size affect the chondrogenic differentiation potential of MSCs. A Unique approach based on the tunability of hydrogels to uncouple gel stiffness and mesh from each other will be used to assess the effect of isolated material properties. A hyaluronan based hydrogel with tyramine as a crosslinker (Ha-Tyr) enzymatically crosslinked with horseradish peroxidase (HRP) and hydrogen peroxide (H_2O_2) will be used within this study. As tunable parameters for the Ha-Tyr hydrogel, the polymer and H_2O_2 concentration were altered independently from each other. The evidence from this study confirmed that the gel stiffness of Ha-Tyr based hydrogels is polymer concentration and H_2O_2 concentration dependent. The tunability of these two parameters independently from each other enabled the production of different gel conditions having matching bulk stiffness. Unfortunately, the mesh size determination was not precise enough for complete uncoupling of the gel stiffness and mesh size from each other. Despite its limitations, the findings indicate that the mesh size shows a trend towards larger mesh size with increasing polymer concentration and lower H_2O_2 concentration. Thereby, indicating that difference in crosslinking density may have been the driving force for the observed trend.

Translation of the effect of material properties on the chondrogenic potential of MSCs indicated towards reduced cartilage-like matrix deposition with increasing crosslinking density. These findings suggest that in general the matrix deposition of cartilage-like tissue is driven by the crosslinking density rather than gel stiffness. Furthermore, gene expression levels for ECM remodelling genes like *MMP1* and *MMP3* showed increased expression patterns with higher crosslinking density, which hints towards the fact that these *MMPs* may have played a pivotal role in the observed matrix deposition.

The information obtained helps to identify mechanotransductional regulators that could be used for the development of smart biomaterials for tissue engineering purposes. Ultimately, it brings us a step closer to the development of functional cartilage tissue that could be used as a possible therapeutic strategy for OA patients.

TABLE OF CONTENTS

NOMENCLATURE 1

1 INTRODUCTION 5

1.1 Aims of the study 12

2 MATERIAL & METHOD 13

2.1 Cell isolation and expansion 13

2.2 3D culturing 14
2.2.1 Pellet formation 14
2.2.2 Hyaluronan-Tyramine hydrogel formation 14
2.2.3 Alginate beads formation 15

2.3 Experimental details 15
2.3.1 Evaluation of Cell density for chondrogenesis of encapsulated MSCs 15
2.3.2 Evaluation of TGF-β concentration for chondrogenesis of encapsulated MSCs 15
2.3.3 Evaluation of material properties for chondrogenesis of encapsulated MSCs 15

2.4 Cell retrieval for gene expression 16
2.4.1 Hyaluronan-Tyramine 16
2.4.2 Alginate beads 16
2.4.3 Pellets 16

2.5 Gene expression quantification 16
2.5.1 RNA isolation 16
2.5.2 cDNA preparation 17
2.5.3 qPCR 17

2.6 Biochemical assays 19
2.6.1 Sample digestion for biochemical assay 19
2.6.2 DNA assay 19
2.6.3 DMB assay 20

2.7 Histology staining 21
2.7.1 Cryostat sectioning 21
2.7.2 Hematoxylin Eosin Staining 21
2.7.3 Thionin staining 21
2.7.4 Safranin O staining 22

2.8 Rheological measurements 22
2.8.1 Mesh size calculation based on the compression test 22

2.9 Flory-Rehner model 23

2.10 Statistics 24

3 RESULTS 25

3.1 How do different crosslinking densities influence the gene expression of ECM remodeling genes and result in different matrix deposition? 25
3.1.1 Expression of ECM deposition related genes in cartilage like tissue 25
3.1.2 Expression of ECM remodeling related genes in cartilage like tissue 27

3.2 Which gel conditions are required to investigate the effect of the isolated material properties on Ha-Tyr based hydrogels? 30
3.2.1 Gel stiffness 30

3.2.2 Mesh size 32
3.2.3 Uncoupling mesh size & stiffness 33
3.3 What is the effect of material properties on the matrix deposition of chondrogenic differentiation of MSCs? 35
3.3.1 Expression levels chondrogenic markers 35
3.3.2 Biochemical assays 36
3.3.3 Expression levels of ECM remodeling related genes 36
4 DISCUSSION 38
5 FUTURE RECOMMENDATION 44
6 CONCLUSION 46
7 REFERENCE 47
A APPENDIX 53
B APPENDIX 54
C APPENDIX 59
D APPENDIX 60
E APPENDIX 62
F APPENDIX 63
G APPENDIX 64
H APPENDIX 65
I APPENDIX 70
J APPENDIX 73
K APPENDIX 75
..... 76

NOMENCLATURE

Greek/Mathematical symbols

$Ø$	Diameter
ξ	Mesh size
λ	Wavelength
F	Force
a	Diameter
η	Viscosity
$\dot{\varepsilon}$	Compressive strain rate
G'	Storage modulus
$\overline{M_c}$	Average molecular weight between crosslinks of the gel
V_1	Molar volume solvent
χ	Flory polymer solvent interaction parameter
k	Permeability
ρ_p	Polymer density
W_s	Swollen weight of the gel
W_d	Dry weight of the gel

Abbreviations

α-MEM	Alpha-minimum essential medium
$CaCl_2$	Calcium chloride
cDNA	Copy DNA
CO_2	Carbon dioxide
CS	Chondroitin sulphate C
DMB	1,9-Dimethylmethylene-Blue
DMEM	Dulbecco's modified eagle's medium with glutamax
DS_{mol}	Degree of substitution
ECM	Extracellular matrix
EDTA	Ethylenediaminetetraacetic acid salt
EtOH	Ethanol
FBS	Fetal bovine serum
FGF_2	Fibroblast growth factor 2
GAG	Glycosaminoglycan
H_2O_2	Hydrogen peroxide
Ha-Tyr	Hyaluronan-Tyramine
HCl	Hydrochloric acid
HEPES	4-(2-hydroxyethyl)-1-piperazineethanesulfonic acid
HRP	Horseradish peroxidase
ITS	Insulin, transferrin and selenium
KCl	Potassium chloride
MSCs	Mesenchymal stromal cells
NaCl	Sodium chloride
Na_2EDTA	Ethylenediaminetetraacetic acid disodium salt
$Na_2HPO_4.2H_2O$	Sodium phosphate dibasic dihydrate
NaH_2PO_4	Sodium phosphate monobasic
NaOH	Sodium hydroxide
OA	Osteoarthritis
OCT	Optimal cutting temperature compound
PBS	Phosphate buffer saline
PBS-EDTA	Phosphate buffer saline-ethylenediaminetetraacetic acid salt
P-MSCs	Pediatric mesenchymal stromal cells

qPCR	Quantitative polymerase chain reaction
RCF	Relative centrifugal force
RNASTAT-60	RNA signal transducer and activation on transcription-60 REAGENT
Saline	0.9% sodium chloride
SD	Standard deviation
T175	Culture flask with a surface area of 175 cm^2
TGF-β1	Transforming growth factor beta 1
Tris	Tromethamine
Vit-C	Ascorbic acid-2-phosphate
w/v	Weight to volume ratio

Gene names (human)

ACAN	Aggrecan
ADAMTS-4	A disintegrin and metalloproteinase with thrombospondin motifs 4
ADAMTS-5	A disintegrin and metalloproteinase with thrombospondin motifs 5
B2M	Beta-2-microglobulin
COL2A1	Collagen type II alpha-1-chain
GAPDH	Glyceraldehyde-3-phosphate dehydrogenase
MMP-1	Matrix metalloproteinase-1
MMP-2	Matrix metalloproteinase-2
MMP-3	Matrix metalloproteinase-3
MMP-13	Matrix metalloproteinase-13
MMP-14	Matrix metalloproteinase-14
RPS27A	Ribosomal protein S27A
TIMP-1	Tissue inhibitor of metalloproteinases-1
TIMP-2	Tissue inhibitor of metalloproteinases-2
UBC	Ubiquitin C

1

INTRODUCTION

Articular cartilage is a 2 to 4 mm thick layer of tissue covering the edges of long bones between diarthrodial joints that functions as a smooth friction-reducing and shock-absorbing layer [1, 2, 3]. The extracellular matrix (ECM) of this tissue type predominantly consists of collagen type II and aggrecan molecules, which yields 20 to 35 % of the tissue wet weight and 90 to 95 % of the tissue dry weight [1, 2, 4]. Within cartilage tissue, collagen type II functions as the tissues main framework and provides tensile strength to maintain swelling pressure in cartilage [1, 2, 4]. Simultaneously, the negatively charged aggrecan molecules are responsible for the compressive strength by attracting water into the tissue [1, 2, 4]. The compressive and tensile strength within cartilage tissue together allows the inflow and outflow of water during dynamic loading of cartilage and gives it the unique property to function as a shock-absorbing tissue [1, 2, 4].
Only 2 % of the total cartilage tissue volume (wet weight) yields for a specialised cell population called chondrocytes [1, 5]. These specialised cells are responsible for the remodelling and homeostasis of the ECM of cartilage tissue and functions as mechanical sensors within the tissue [1, 5, 6]. In addition, these cells are known for having a low metabolism with limited proliferative capabilities [7, 8, 9, 10, 11]. As a consequence of the avascular nature of cartilage tissue, chondrocytes function in low oxygen conditions and obtain their nutrient supply through diffusion at the articular surface of cartilage [7, 8, 9, 10, 11]. A schematic representation of the articular cartilage environment is presented in fig. 1.

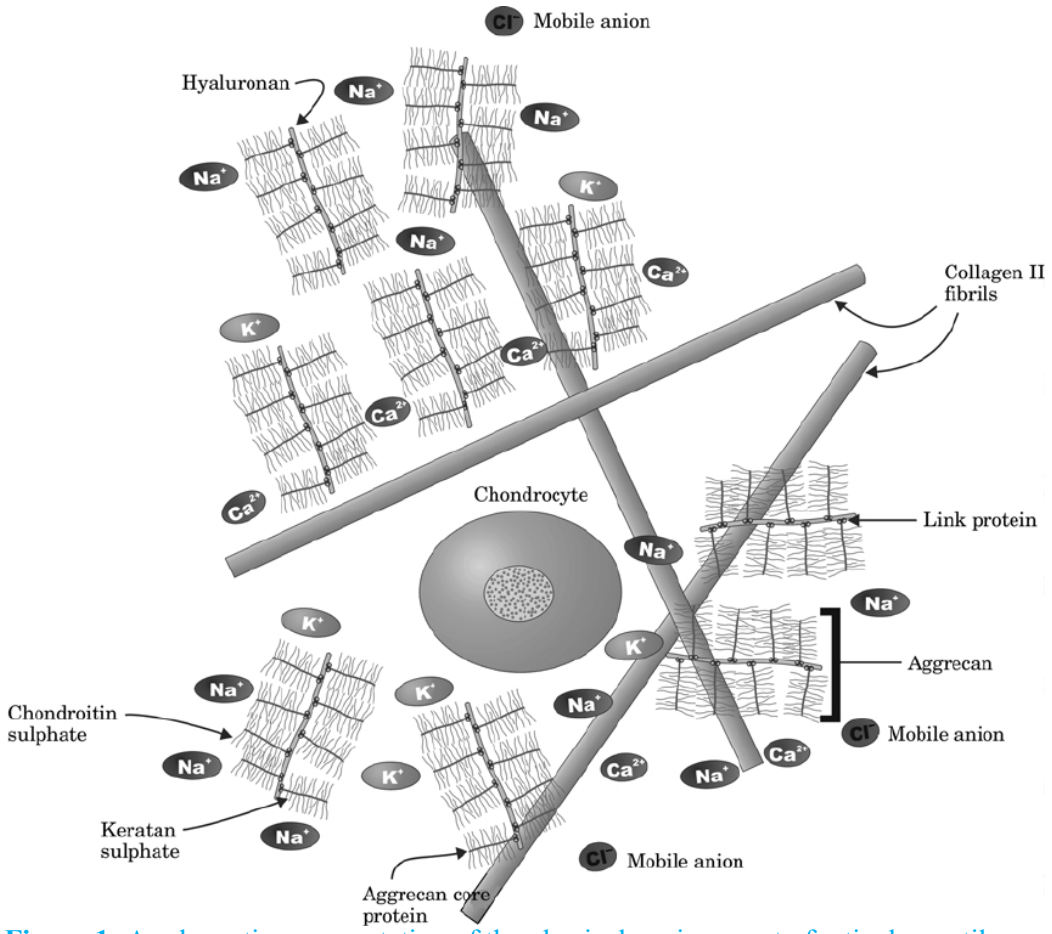

Figure 1: A schematic representation of the physical environment of articular cartilage with the main components of the extracellular matrix and a chondrocyte cell [4].

Cartilage tissue has a minimal self-repair capacity due to the tissues avascular nature and the low proliferative capabilities of chondrocytes, making the tissue prone to degenerative diseases like osteoarthritis (OA) [8, 9, 10, 11]. OA is a chronic joint disease characterised by the deterioration of cartilage and subchondral bone that leads to the development of chronic pain, joint stiffness, and movement disability [10, 12, 13]. Typically, the degeneration of cartilage in OA consists of two phases: a biosynthetic phase, where chondrocytes try to repair damaged parts within the ECM; and a degradative phase, where the matrix production is inhibited and digestion of the ECM of cartilage is activated [14]. At the end of the two phases, a deteriorated joint is obtained, which is schematically illustrated for an OA knee joint in fig. 2 [14]. More than 25 % of the world population (age 18 >) suffers from some type of OA, making it one of the most disabling diseases worldwide [11, 13, 15, 16]. Several risk factors may lead to the development of OA, such as genetics, ageing, inflammation, rheumatism, bone deformation, and obesity as well as environmental factors like mechanical stress and trauma [11, 16, 17, 18]. Furthermore, the unhealthier lifestyle (causing more obesity) and increasing life expectancy will lead to an annual increase in the OA patient population [13, 15, 18, 19]. In the US alone, approximately 27 million OA patients already result in annual health cost expenses of roughly $90 billion, which will only increase further with the increasing population of OA patients [19]. Adding up the fact that it is estimated that 30 % of the world population will have some type of OA by 2030 clearly emphasises the huge burden of this disease on the society [18, 19].

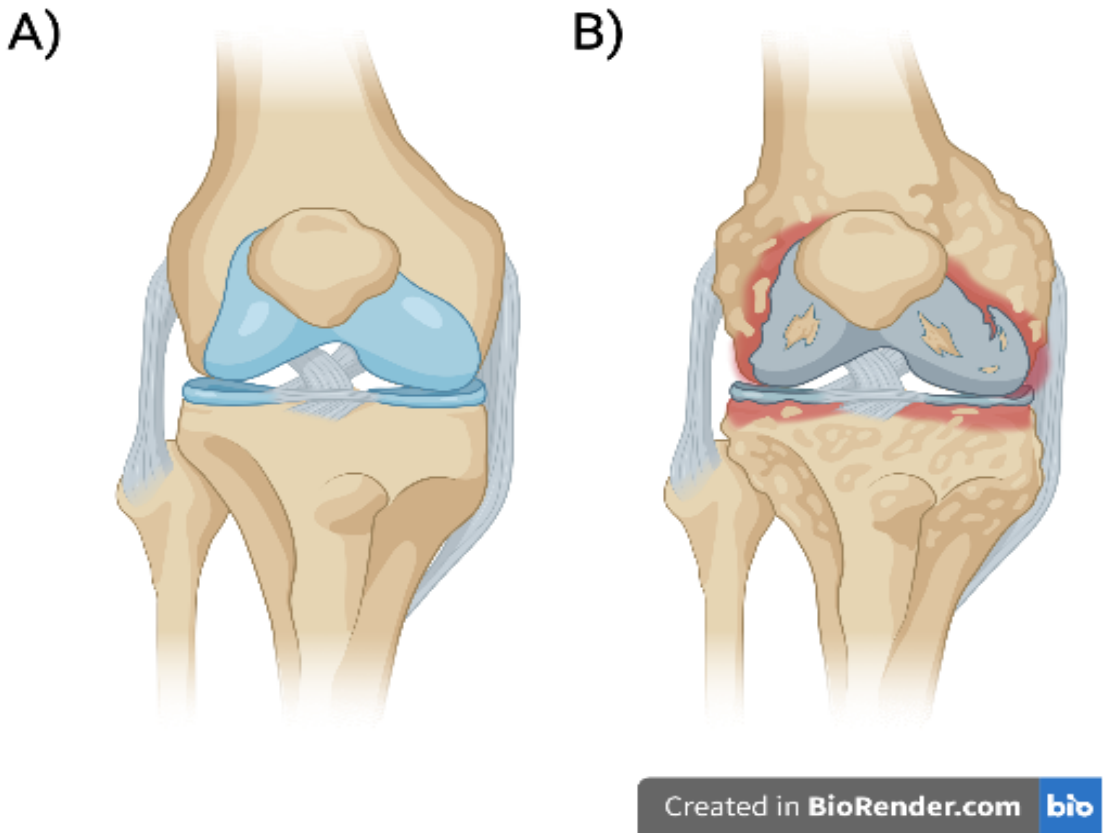

Figure 2: A schematic representation of a human knee joint. A) representation of a healthy human knee joint with intact cartilage tissue. B) representation of an osteoarthritic knee joint with deteriorated cartilage and subchondral bone tissue.

The current therapeutic strategy for OA patients predominantly focused on pain relief via pharmaceuticals, physiotherapy, and surgical replacement of the affected joint at the end-stage [10, 11, 16]. However, the therapeutic strategy should be more directed towards preventing the degeneration of cartilage and promoting the regeneration of new cartilage. But as a consequence of the very limited self-repair capacity of cartilage tissue, the regeneration of cartilage remains an unsolved challenge in new/alternative OA treatments [8, 9, 10, 11]. The concept of tissue engineering that combines engineering and biological sciences principles have been proposed to facilitate the regeneration of (new) articular cartilage [9, 20, 21]. According to the definition provided by Langer and Vacanti (1993) [22], tissue engineering is "an interdisciplinary field which applies the principles of engineering and life sciences toward the development of biological substitutes that restore, maintain, or improve tissue function''. The initial aim of tissue engineering was for repairing, replacing and maintaining functional tissue substitutes *in vitro* for implantation as biological substitutes [20, 22, 23]. Recently, it gained a second purpose for the development of *in vitro* models of healthy and diseased organs for the sake of drug screening and therapy evaluation [23]. The concept of tissue engineering consists of four main parts, which are: cell source, scaffold/hydrogel, biochemical cues (growth factors), and biophysical cues (mechanical environment) [9, 21]. A schematic representation of the concept of tissue engineering is shown in fig 3.

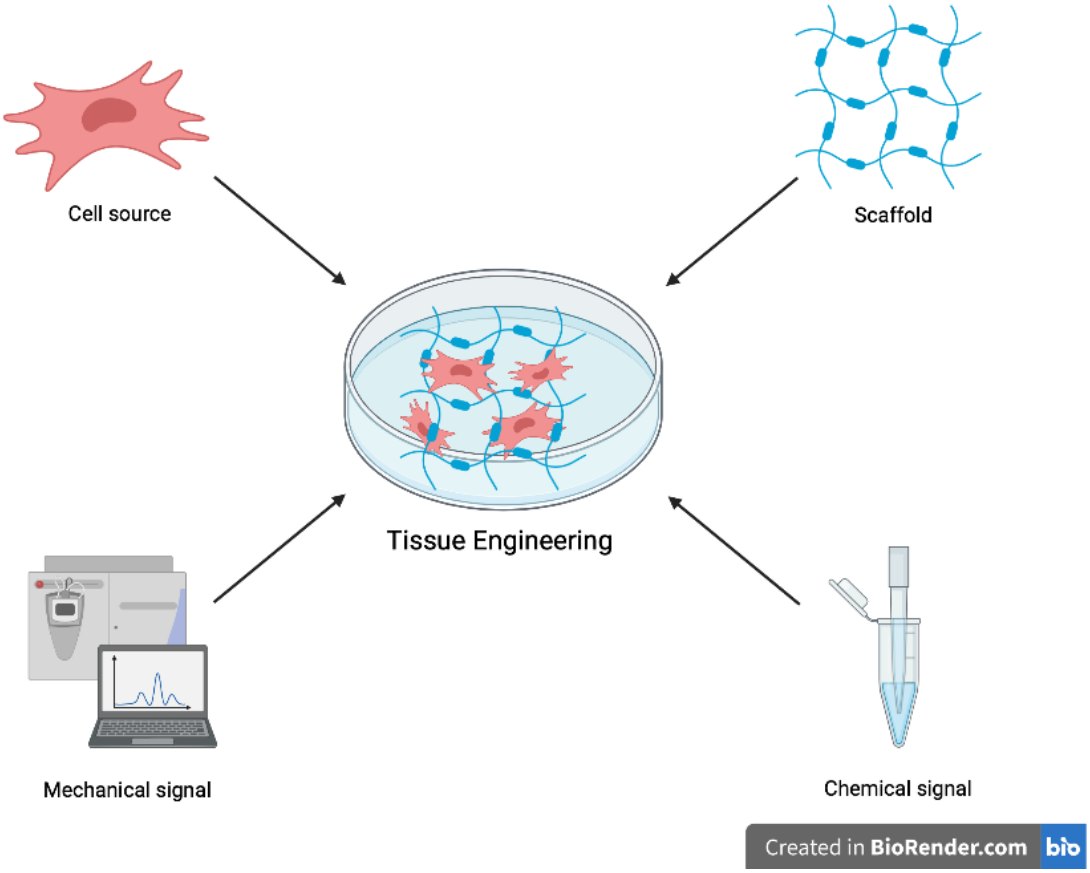

Figure 3: A schematic representation of the concept of tissue engineering, which consists of four main parts. These parts are the cell source, scaffold, chemical factors, and mechanical factors.

Autologous chondrocytes harvested from low load-bearing areas of the patients own cartilage has been suggested as a relevant cell source for cartilage tissue engineering purposes [3, 24]. However, their low proliferative capacity, nonabundancy, and phenotype loss during *in vitro* expansion make chondrocytes unfavourable as cell source [8, 24, 25]. Therefore, alternative cell sources capable of chondrogenic differentiation, such as mesenchymal stromal cells (MSCs), gained more interest over the years [4, 26, 27]. MSCs are attractive cell sources since they can be harvested from various locations (i.e. bone marrow, adipose tissue); have a high proliferative capacity; and are multipotent stem cells capable of differentiating into osteogenic, chondrogenic, or adipogenic cells during *in vitro* expansion when exposed to the right combination of stimuli [8, 26, 27]. These stimuli could be either of mechanical or chemical origin [28, 29].

Cells within the body are continuously exposed to various forces such as fluid flow stress due to blood pumping or compressive force resulting from joint loading and muscle activity during locomotion [30, 31]. These type of forces can be defined as external forces or extrinsic forces acting on cells [30, 31]. Additionally, mechanical properties of the ECM surrounding the cells as a consequence of the cell-matrix interaction do play a role in force sensing within cells [30, 31]. During cell-matrix interaction, cell generated contractile force results in deformation of the cell [30, 31]. These cellular deformations due to cell-matrix interaction or application of external forces are translated to cellular responses through a process known as mechanotransduction, which has been schematically represented in fig. 4 [30, 31, 32]. Mechanotransduction has been defined as a continuous process of sensing, transmitting and

responding to the forces acting on cells, which are essential for the maintenance and cellular functioning of cells [30, 32]. Like MSCs, mechanosensitive cells sense forces via specific receptors that function as attachment points for cell-matrix interaction; via mechanosensitive ion channels or by generating contractile forces to sample its microenvironment to determine its surrounding mechanical properties [30, 31, 32]. This information is then translated into intracellular responses via cytoskeletal rearrangement within the cell, resulting in cellular and nuclear deformation [30, 31, 32]. These deformations can trigger intracellular signaling pathways and downstream cascades that ultimately regulate many cellular processes, including cell proliferation, differentiation, migration, apoptosis, and the remodelling of the ECM [30, 31, 32]. Utilizing the mechanotransductive behaviour of MSCs, cell differentiation can be directed towards a specific phenotype, in our case chondrogenic cells [31, 33, 34]. Novel approaches are required to understand which mechanotransductional regulators do play a pivotal role in cartilage tissue engineering to stimulate the development of smart biomaterials [31, 33, 34]. Ultimately, this will bring us a step closer to the development of smart biomaterials capable of directing cell differentiation for tissue engineering purposes and eliminating the need for additional chemical stimulators.

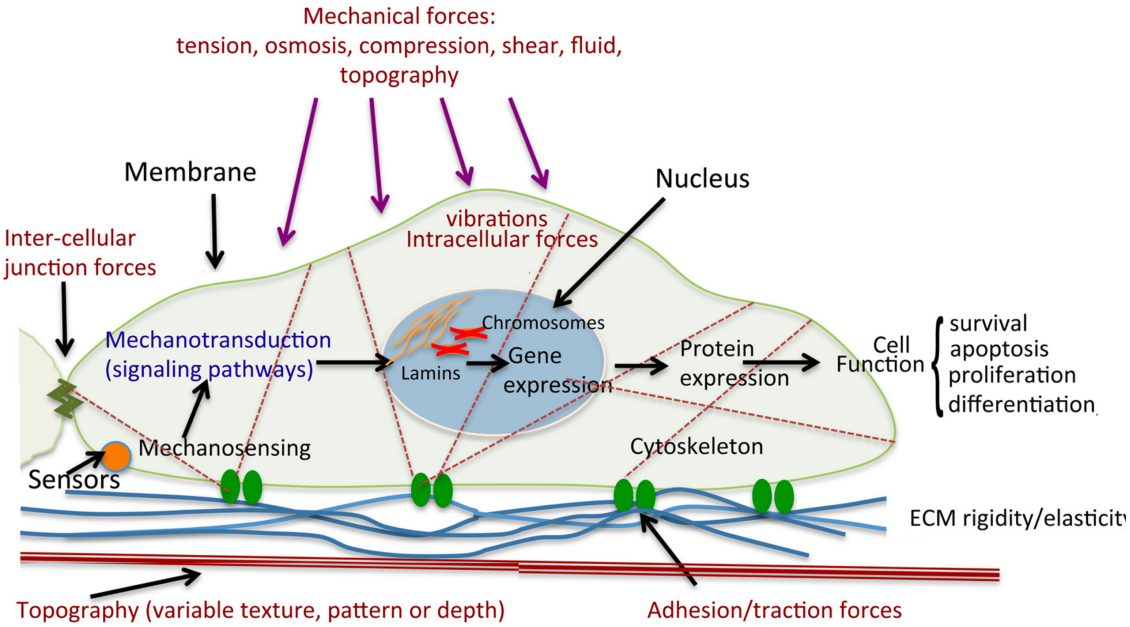

Figure 4: A schematic representation of the concept of mechanotransduction that represents the continuous process of sensing, transmitting and responding to forces acting on cells. The forces acting on cells are denoted in red. Force acting on the cell are sensed via cell-matrix interaction using receptors as attachment points with their microenvironment. Mechanical signals initiate cytoskeletal rearrangements within cells, resulting in cellular and nuclear deformation that triggers intracellular signaling cascaded. These signaling cascades results in specific cellular responses like cell proliferation, differentiation and apoptosis [32].

Hydrogels gained a lot of attention throughout the years for cartilage tissue engineering purposes, since the material properties of hydrogels can be tuned to mimic the hydrophilic composition of cartilage; their capability to carry cells and drugs; and they support the matrix deposition of cartilage-like tissue [28, 31, 33, 35]. Typically, a hydrogel is a viscoelastic material capable of maintaining its volume and shape, and they have both properties of a solid and liquid material [36]. The solid part consists of polymer chains cross-linked to each other, creating a structure that looks similar to a net (fig. 5). These net like structures are

called mesh. According to Rehmann et al. (2017) [37], the mesh size is defined as the correlation length as the linear distance between two adjacent cross-links. It is a key structural parameter of a hydrogel [36, 37]. Via alterations in the density of polymer chains connected to each to create a polymer network (crosslinking density), different crosslinking densities are generated that yields different mechanical properties within the hydrogels [36, 38]. However, alteration of the crosslinking density in hydrogels results in changes of multiple material properties of the material as a consequence of the interdependency of material properties to the crosslinking density [36]. This interdependency of the material properties is schematically represented in fig. 5. It illustrates that an increase in crosslinking density results in an increase in gel stiffness, while the mesh size, diffusivity and degradation rate of the gel decreases [36].

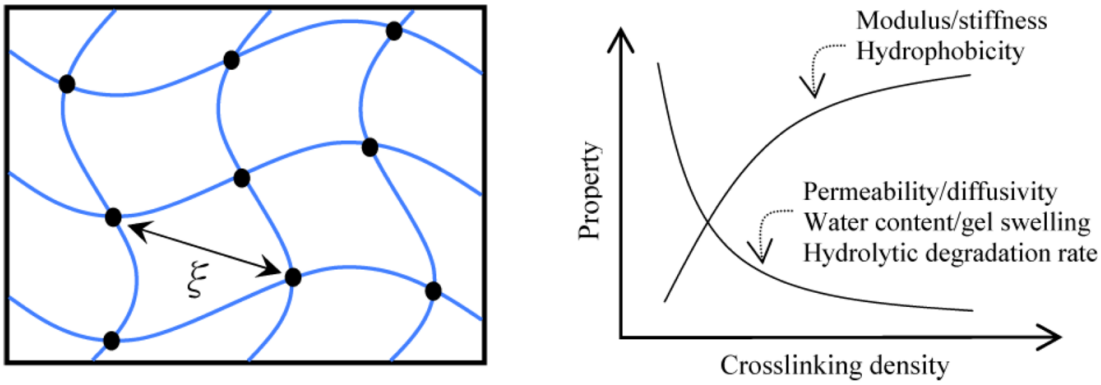

Figure 5: A schematic representation of a crosslinked hydrogel network resulting in a net-like structure. The black dots represent crosslinking points in the network, and ξ denotes the mesh size of the hydrogel. A schematic illustration of material properties as a function of crosslinking density [36].

In the last decade, many researchers tried to identify mechanotransductional regulators for chondrogenic differentiation of MSCs [29, 39, 40]. In particular, gel stiffness received much attention [39, 41, 42, 19]. However, the large variability between material use and stiffness of the gels resulting in chondrogenic differentiation of MSCs, makes it challenging to define an optimal stiffness for chondrogenic differentiation independently of the biomaterial [39, 41]. When comparing these studies, it was observed that the majority of studies did not take into account the interdependency of mechanical properties of gels as a consequence of the crosslinking density [39, 41, 42, 19]. Therefore, it remains unknown whether the cell responds to the change in gel stiffness or changes in other material properties, such as mesh size, degradation rate, fiber rigidity or a combination of them. Eventually, it limits researchers to develop smart biomaterials for tissue engineering purposes through the concept of mechanobiology.

One of the material parameters that have been overlooked when investigating the effect of material properties on cells is the mesh size. The mesh size depends on the hydrogels crosslinking density, the polymer volume fraction and molecular weight of the polymer [43, 44]. A strategy was reported that enables researchers to investigate the effect of mesh size and gel stiffness on cells independently from each other by creating different gel conditions and grouping them afterwards [44, 45]. This strategy relies on the fact that the crosslinking density depends on several independent parameters such as polymer type, molecular weight of the polymer, polymer concentration, crosslinking method, and environmental parameters like pH and temperature [44, 45]. By changing one of the crosslinking density parameters and maintaining the rest of the parameters constant, different crosslinking densities could be

obtained, resulting in gels with different material properties. Application of this uncoupling strategy to the dataset obtained from Bian et al. (2013) [43] indicated that uncoupling of gel stiffness and mesh size was possible (fig. 6).

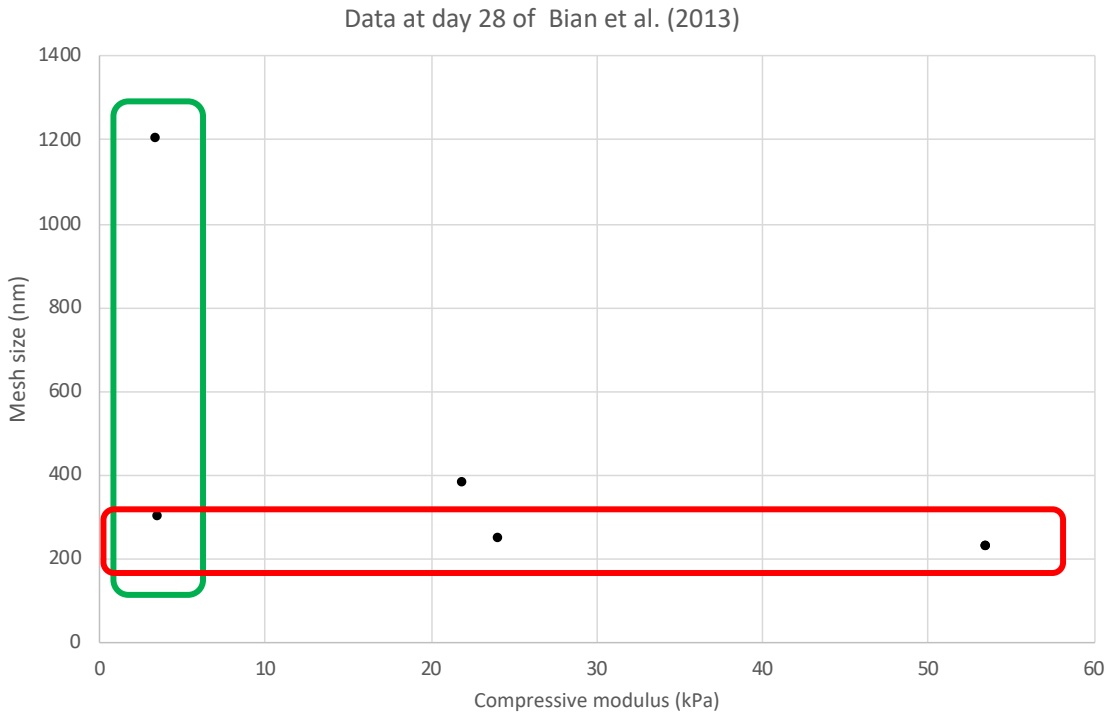

Figure 6: Rearrangement of the measured dataset from the study of Bian et al. (2013) [43] to uncouple the substrate stiffness and mesh size from each other.

Harnessing the mechanosensitivity of MSCs and their potential to differentiate towards a chondrogenic phenotype, this thesis aimed to investigate the effect of isolated material properties on the chondrogenic differentiation potential of MSCs. Chondrogenesis and the quality of the produced cartilage will be assessed based on gene expression levels, biochemical assays, and histological staining for chondrogenic markers [26, 19, 39, 40]. Thereby, the expression of *SOX9, COL2A1* and *ACAN* is associated with chondrogenic differentiation since *SOX9* plays a key transcription factor for chondrogenesis while *COL2A1* and *ACAN* denote for the two main components in articular cartilage [26, 19, 39, 40]. A hyaluronan based hydrogel with Tyramine as a crosslinker (Ha-Tyr) will be used within this study. Ha-Tyr hydrogels can be enzymatically crosslinked by the enzyme horseradish peroxidase (HRP), which uses hydrogen peroxide (H_2O_2) as an oxidant [46]. Ha-Tyr hydrogels have already been used in the study of Vaineri et al. (2020) [46], which illustrated that by varying the H_2O_2 concentration while maintaining the same polymer concentration, different gel stiffness could be obtained. Based on these findings, we hypothesized that via alteration in H_2O_2 and polymer concentration, different crosslinking densities with varying sizes of mesh and gel stiffnesses could be obtained [45]. We hypothesized that by increasing the H_2O_2 concentration during crosslinking of Ha-Tyr hydrogels, a stiffer gel with a constant mesh size would be obtained. We also hypothesize that by lowering the polymer concentration of Ha-Tyr softer hydrogels increasing the mesh size will be generated. Plotting the measured gel stiffness and mesh size against each other should reveal which gel conditions enable the investigation of isolated material properties.

1.1 Aims of the study

The overarching aim of this study was to investigate the effect of mesh size and gel stiffness independently on MSCs. Therefore, the following research question has been defined: ‘’What are the effects of substrate stiffness and mesh size on the chondrogenic differentiation potential of MSCs?’’
To answer the research question, we divided the research question into the following three sub-questions:

- How do different cross-linking densities influence the gene expression of ECM remodelling genes and result in a difference in matrix deposition?
- Which gel conditions are required to investigate the effect of the isolated material properties on Ha-Tyr based hydrogels?
- What is the effect of material properties on the matrix deposition of chondrogenic differentiation of MSCs?

2

MATERIAL & METHOD

2.1 Cell isolation and expansion

Paediatric mesenchymal stromal cells (P-MSCs) from a single donor (10 years old boy) were used for cell culture related experiments. P-MSCs were harvested from leftover iliac crest bone chip material obtained from a patient undergoing alveolar bone graft surgery. P-MSCs were isolated after the medical ethics committee's approval at Erasmus Medical Centre (MEC-2014-16). Isolation of MSCSs was performed following the standard protocol as explained in Knuth et al. (2018) [47]. Isolated P-MSCs were expanded in culture flasks (T175; Corning, New York, United States) containing 20 mL of expansion medium made of alpha-Minimum Essential Medium (α-MEM; Gibco, Carlsbad, California, United States) supplemented with 10% fetal bovine serum (FBS; Gibco, Carlsbad, California, United States), 50 µg/mL gentamycin (Gibco, Carlsbad, California, United States), 1.5 µg/mL fungizone (Gibco, Carlsbad, California, United States), 1 ng/mL fibroblast growth factor 2 (FGF2; AbD Serotec, Puchheim, Germany), and 25 µg/mL ascorbic acid-2-phosphate (vit-C; Sigma-Aldrich, Saint Louis, MO) and cultured in a humidified atmosphere at 37 °C and 5% carbon dioxide (CO_2). The medium was changed after 3 days of cultivation. The cell seeding density was 2300 cells/cm^2, and cells were passed at approximately 70-80 % confluency using 0.05 % trypsin (Gibco, Carlsbad, California, United States). An overview of the used passages for each experiment is shown in table 1.

Table 1: Summary table of the cell type, source, and passage number that has been used for each experimental setup.

Experiment name	Cell source	Passage number
Cell density	P-MSCs	7
TGF-β concentration	P-MSCs	9
Mesh effect experiment	P-MSCs	6

2.2 3D culturing

2.2.1 Pellet formation

Cell pellet cultures were achieved by spinning down $0.2 \cdot 10^6$ cells/0.5mL of full chondrogenic medium in 15-mL conical polypropylene tubes (Techno Plastic Products AG, Trasadingen, Switzerland) at 230 relative centrifugal force (RCF) for 8 minutes. Pellets formed a spherical construct after 24 hours in an incubator cultured in a humidified atmosphere at 37 °C and 5% CO_2. The spherical pellets were loosened after 24 hours of incubation by gently tapping the tubes.
The full chondrogenic medium consists of Dulbecco's modified Eagle's medium with Glutamax (DMEM; Gibco, Carlsbad, California, United States) with the addition of 1 % Insulin transferrin selenium (ITS, Sigma Aldrich, Missouri, United States), 50 µg/mL fungizone, 1.5 µg/mL gentamicyn, 1 mM sodium pyruvate (Gibco, Carlsbad, California, United States), 40 µg/mL proline (Sigma Aldrich, Missouri, USA), 100 nM Dexamethasone (Sigma Aldrich, Missouri, USA), and with10 ng/mL Transforming Growth Factor beta 1 (TGF-β1; R&D System, Minnesota, USA) unless stated otherwise. The medium was changed every second day.

2.2.2 Hyaluronan-Tyramine hydrogel formation

The Ha-Tyr hydrogel functionalized with a degree of substitution (DS_{mol}) of 6% Tyramine was received as a gift from the AO Research Institute Davos, located in Switzerland. The Ha-Tyr hydrogels were polymerized after overnight reconstitution of the gel suspension. The desired weight-to-volume ratio (w/v) of Ha-Tyr (1.5, 2.5 or 3.5 % w/v of final hydrogel volume) (AO Research Institute Davos, Switzerland**)** was weighted down and UV-sterilized for 1 hour. Sterilised Ha-Tyr was mixed in 0.5 volumes M-buffer with the addition of 0.2 U/mL of horse radish peroxidase (HRP; Sigma Aldrich, Missouri, USA) enzyme and homogenised overnight using a bench rotator at 4 °C. The M-buffer consist of 20 mM 4-(2-hydroxyethyl)-1-piperazineethanesulfonic acid (HEPES; Sigma Aldrich, Missouri, United States), 109 mM sodium chloride (NaCl; Sigma Aldrich, Missouri, United States), and 5.36 mM potassium chloride (KCl; Sigma Aldrich, Missouri, United States) and pH was adjusted to 7.3 via dropwise addition of 6 M sodium hydroxide (NaOH; Sigma Aldrich, Missouri, United States) and 6 M hydrochloric acid (HCl; Sigma Aldrich, Missouri, United States) before filter sterilisations using a 0.2 µm syringe filter (Whatman, Ohio, United States). Stock solutions of 2 mM and 1 mM hydrogen peroxide were prepared by diluting 9.8 M hydrogen peroxide (H_2O_2; Merck, Darmstadt, Germany) in M-buffer before filter sterilisation using a 0.2 µm syringe filter freshly for every experiment.

The Ha-Tyr/HRP/M-buffer suspension, M-buffer and H_2O_2 stock solutions were chilled on ice for 20 minutes before casting the gels. For encapsulated cell experiments, the cells were resuspended at a cell density of $15 \cdot 10^6$ cells/mL in DMEM. 50 µL of cell suspension per 250 µL final Ha-Tyr gel volume was added to obtain a final cell density concentration within the Ha-Tyr gel of $3 \cdot 10^6$ cells/mL. The cell suspension was added to the Ha-Tyr/HRP/M-buffer suspension and homogenised in a bench rotator for 10 minutes at 4 °C.
The gels were casted by mixing the Ha-Tyr/HRP/M-buffer (with cells) suspensions with varying concentrations of H_2O_2 to obtain different gel conditions. All gel conditions were gelled for 30 min at 37 °C and filled with 800 µL of complete chondrogenic medium. The medium was changed every second day.

2.2.3 Alginate beads formation

The alginate beads were casted after overnight reconstitution of the alginate suspension. 1.2 % of alginate powder (Novomatrix, Lillerød, Denemarken) was reconstituted in 0.9 % sodium chloride (saline; Sigma Aldrich, Missouri, United States) and stirred overnight. The alginate solution was sterilised using a 0.2 µm syringe filter. The desired amount of cells was spinned down at 290 RCF for 8 minutes after tripsinisation and resuspended in the leftover medium after discarding the supernatant. Sterile alginate suspension was added to the cell suspension and homogenised by gently up and down pipetting to achieve the desired final cell density concentration.
The cell/alginate suspension was transferred in a sterile syringe while avoiding air bubbles. Using a 23 gauge needle (B. Braun, Mulsungen, Germany), the alginate suspension was purged dropwise roughly 1 cm above 25 mL of sterile 102 mM calcium chloride ($CaCl_2$; Sigma Aldrich, Missouri, United States) for crosslinking of the alginate beads. Thereby, 3 mL of alginate bead suspension should be prepared in 2 minutes. The beads were incubated in 102 mM $CaCl_2$ for 10 minutes before washing twice with saline for 5 minutes. The beads were transferred into DMEM medium before using the beads for the desired experiments. All used media were full chondrogenic medium. The medium volume was calculated based on the ratio of 0.5 mL medium per $0.2 \cdot 10^6$ cells.

2.3 Experimental details

2.3.1 Evaluation of Cell density for chondrogenesis of encapsulated MSCs

To evaluate the effect of cell density on the chondrogenic potential of MSCs, cells were encapsulated at a cell density of $2 \cdot 10^6$ or $10 \cdot 10^6$ cells/mL in alginate. The alginate beads were cultured in chondrogenic medium containing either 0 or 10 ng/mL TGF-β1. Samples were cultured for 14 days and harvested for gene expression analyses.

2.3.2 Evaluation of TGF-β concentration for chondrogenesis of encapsulated MSCs

To evaluate TGF-β1 concentration on chondrogenesis of MSCs, $2 \cdot 10^6$ cells/mL were encapsulated in alginate and cultured in chondrogenic medium with either 0, 1, 2.5 or 10 ng/mL TGF-β1. Samples were cultured for 14 days and harvested for gene expression analyses.

2.3.3 Evaluation of material properties for chondrogenesis of encapsulated MSCs

To evaluate chondrogenesis of MSCs encapsulated in Ha-Tyr hydrogels, cells were encapsulated at a cell density of $3 \cdot 10^6$ cells/mL Ha-Tyr having a gel volume of 250 µL. The Ha-Tyr hydrogels were crosslinked with varying concentrations of H_2O_2 (150, 300 and 600 µM) and polymer concentration (1.5 and 3.5 % w/v Ha-Tyr) to obtain different gel conditions. A hydrogel disk was prepared using a 24 well plate. The samples were cultured in full chondrogenic medium for 14 days and harvested for gene expression analyses and biochemical assays.

2.4 Cell retrieval for gene expression

2.4.1 Hyaluronan-Tyramine

P-MSCs/Ha-Tyr constructs were harvested into sterile 1,5 mL Eppendorf tubes. 4 mg/mL hyaluronidase (Sigma Aldrich, Missouri, United States) in phosphate buffer saline solution (PBS, ThermoFisher, Carlsbad, California, United States) was freshly prepared and filter sterilized using a 0.2 µm syringe filter. 1 mL of hyaluronidase solution per sample was added and incubated in a bench rotator at 37°C for up to 2 hours. After visual inspection of Ha-Tyr complete dissolution, the cell suspensions were spined down at 400 RCF, 4 °C for 8 minutes. The pellets were resuspended in 1 mL of RNA signal transducer and activation on transcription-60 REAGENT (RNASTAT-60, Gentaur, Kampenhout, Belgium) per 10^6 cells to stop the RNA expression in cells and stored at -80 °C before RNA isolation.

2.4.2 Alginate beads

P-MSCs/alginate constructs were harvested into sterile 1.5 mL Eppendorf tubes. 100 µL of sodium citrate buffer per alginate bead was added to dissolve the alginate beads by rotating the alginate beads in buffer with a bench rotator at 4 °C for 8 minutes. Sodium citrate buffer contains 150 mM NaCl, 55 mM Na-citrate (Sigma Aldrich, Missouri, United States), and 20 mM EDTA.$2H_2O$ (Sigma Aldrich, Missouri, United States). After visual inspection of the alginate beads complete dissolution, the cell suspensions were spined down at 400 RCF, 4 °C for 8 minutes. Cells were resuspended in 1 mL of RNASTAT-60 per 10^6 cells to stop the RNA expression in cells and stored at -80 °C before RNA isolation.

2.4.3 Pellets

P-MSC pellets were harvested into a sterile 1,5 mL Eppendorf tube. 1 mL of RNASTAT-60 per 10^6 cells was used to stop the RNA expression in cells. Pellets were manually homogenised using sterile pellet pestles before storing the sample at -80 °C before RNA isolation.

2.5 Gene expression quantification

2.5.1 RNA isolation

RNA was isolated using the miRNeasy micro Kit (Qiagen, Hilden, Germany). Briefly described, 0.2 volumes of chloroform (Sigma Aldrich, Missouri, United States) was added and mixed vigorously with the samples before incubating for 10 minutes on ice. The supernatant of incubated samples was collected and dissolved in 70% ethanol (EtOH; BOOM, Meppel) after centrifuging samples at 12000 RCF for 15 min. Resuspended supernatants were loaded in QiaSpin columns (Qiagen, Hilden, Germany) and spinned down at 8000 RCF for 30 sec. The columns were washed with 350 µL of RW1 buffer (Qiagen, Hilden, Germany) per column and spinned down at 8000 RCF for 30 sec. 10 µL of DNase I stock solution (Qiagen, Hilden, Germany) and 70 µL Buffer RDD (Qiagen, Hilden, Germany) were mixed before transferring 75 µL of DNaseI/RDD buffer to each column and

incubated for 30 minutes at room temperature. The columns were washed with 350 µL RW1 buffer and 500 µL RPE buffer (Qiagen, Hilden, Germany) respectively and after each addition of the solution spinned down at 8000 RCF for 30 sec. 500 µL 80% EtOH was added to each column and spinned down at 8000 RCF for 2 minutes before drying it by centrifuging the columns at 8000 RCF for 5 minutes. 16 µL of RNase free water (Qiagen, Hilden, Germany) was added onto the filters and incubated for 60 seconds at room temperature before centrifuging the columns in RNase free 1.5 mL Eppendorf tubes at 8000 RCF at 4 °C. RNA quantity and quality were assessed utilising the NanoDrop ND100 UV–VIS spectrophotometer (Isogen Life Science B.V, de Meern, the Netherlands).

2.5.2 cDNA preparation

Isolated RNA was converted into copy DNA (cDNA) using the RevertAid First Strand cDNA Synthesis Kit (ThermoFisher, Carlsbad, California, United States) and following the manufacturer's instructions. Briefly described, 0.5 µL of Oligo-d(T)18 primer (ThermoFisher, Carlsbad, California, United States), 0.5 µL of Random Hexamer primer (ThermoFisher, Carlsbad, California, United States), 240 ng of RNA isolation, and filled up till 12 µL of a mixture with RNAse free water. Gently mix the suspension and spin down before incubating the cDNA mix for 5 min at 70 °C. Spin the cDNA mixture again down and set them on ice for 5 min. 4 µL of 5X Reaction buffer (ThermoFisher, Carlsbad, California, United States), 2 µL of 10 mM dNTPs (ThermoFisher, Carlsbad, California, United States), 1 µL of 20 U/µL Ribolock inhibitor (ThermoFisher, Carlsbad, California, United States), and 1 µL of 200 U/µL RevertAid M-MuLV Reverse Transcriptase (ThermoFisher, Carlsbad, California, United States) were added to each sample and spinned down before putting the cDNA samples in the following thermocycling program of 5 min at 25 °C, 60 min at 42 °C, 10 min at 72 °C, and 12 °C ∞. After thermocycling, all cDNA samples were diluted with 100 µL of RNA free water to obtain a cDNA solution of 120 µL with a cDNA concentration of 2 ng/mL.
A control sample for DNA contamination was prepared by sampling the RNA isolation from 4 samples and substituting the Revertaid M-MuLV Reverse Transcriptase with RNAse free water. A water control sample was also included to validate if the used RNAse free water was contaminated with DNA. Therefore, the RNA extraction content was substituted with RNAse free water. All incubation steps (except ice) were performed using a PTC-100® Thermal Cycler (Bio-Rad Laboratories, California, United States).

2.5.3 qPCR

For quantitative analyses of gene expression, quantitative polymerase chain reaction (qPCR) with either Taqman Universal PCR mastermix (Applied Biosystem, Foster City, CA, USA) or SyberGreen (Eurogenetc, Seraing, Belgium) has been used in 10 µL reactions on ABI Prism 7000 system (Applied Biosystem, Foster City, CA, USA). A list of all used genes with their respective sequences are presented in table 2. *GAPDH, B2M, RPS27A*, and *UBC* were used to calculate the best housekeeper index (B to determine the relative gene expression in cells at different conditions and time points. These housekeeper genes were also used to calculate the best housekeeper index. The relative gene expression in each sample was calculated using equations 1 to 3.

$$Best\ housekeeper\ index = \sqrt[3]{housekeeper\ gene\ 1 \cdot housekeeper\ gene\ 2 \cdot housekeeper\ gene\ 3} \quad (1)$$

$$\Delta Cq = Cq_{gene\ of\ interest} - Cq_{Best\ houskeeper\ index\ or\ housekeeper\ gene} \quad (2)$$

$$quantity = 2^{-\Delta cq} \quad (3)$$

Table 2: A list of primer sets and their respective sequences used within this study.

Name	Primer sequence
Aggrecan (*ACAN*)	Forward: 5'- TCGAGGACAGCGAGGCC -3' Reverse: 5'- TCGAGGGTGTAGCGTGTAGAGA -3' Probe[1]: 5'- ATGGAACACGATGCCTTTCACCACGA -3'
A disintegrin and metalloproteinase with thrombospondin motifs 4 (*ADAMTS-4*)	Forward: 5'- CAAGGTCCCATGTGCAACGT -3' Reverse: 5'- CATCTGCCACCACCAGTGTCT -3' Probe[1]: 5'- CCGAAGAGCCAAGCGCTTTGCTTC -3'
A disintegrin and metalloproteinase with thrombospondin motifs 4 (*ADAMTS-5*)	Forward: 5'- TGTCCTGCCAGCGGATGT -3' Reverse: 5'- ACGGAATTACTGTACGGCCTACA -3' Probe[1]: 5'- TTCTCCAAAGGTGACCGATGGCACTG -3'
Beta-2-Microglobulin (*B2M*)	Forward: 5'- TGCTCGCGCTACTCTCTCTTT -3' Reverse: 5'- TCTGCTGGATGACGTGAGTAAAC -3'
Collagen type II α1-chain (*COL2a1*)	Forward: 5'- GGCAATAGCAGGTTCACGTACA -3' Reverse: 5'- CGATAACAGTCTTGCCCCACTT -3' Probe[1]: 5'- CCGGTATGTTTCGTGCAGCCATCCT -3'
Glyceraldehyde-3-phosphate dehydrogenase (*GAPDH*)	Forward: 5'- ATGGGGAAGGTGAAGGTCG -3' Reverse: 5'- TAAAAGCAGCCCTGGTGACC -3' Probe[1]: 5'- CGCCCAATACGACCAAATCCGTTGAC -3'
Matrix metalloproteinase-1 (*MMP-1*)	Forward: 5'- CTCAATTTCACTTCTGTTTTCTG -3' Reverse: 5'- CATCTCTGTCGGCAAATTCGT -3' Probe[1]: 5'- CACAACTGCCAAATGGGCTTGAAGC -3'
Matrix metalloproteinase-2 (*MMP-2*)	Forward: 5'- TCAAGTTCCCCGGCGAT -3' Reverse: 5'- TGTTCAGGTATTGCACTGCCA -3' Probe[1]: 5'- TCGCCCCCAAAACGGACAAAGA -3'
Matrix metalloproteinase-3 (*MMP-3*)	Forward: 5'- TTTTGGCCATCTCTTCCTTCA -3' Reverse: 5'- TGTGGATGCCTCTTGGGTATC -3' Probe[1]: 5'- AACTTCATATGCGGCATCCACGCC -3'
Matrix metalloproteinase-13 (*MMP-13*)	Forward: 5'- AAGGAGCATGGCGACTTCT -3' Reverse: 5'- TGGCCCAGGAGGAAAAGC -3' Probe[1]: 5'- CCCTCTGGCCTGCGGCTCA -3'
Matrix metalloproteinase-14 (*MMP-14*)	Forward: 5'- TGCCTGCGTCCATCAACACT -3' Reverse: 5'- CATCAAACACCCAATGCTTGTC -3' Probe[1]: 5'- AAGACGAATTTGCCATCCTTCCTCTCGT -3'
Ribosomal Protein S27A (*RPS27A*)	Forward 5'- TGGCTGTCCTGAAATATTATAAGGT -3' Reverse 5'- CCCCAGCACCACATTCATCA -3'
Tissue inhibitor of metalloproteinases (*TIMP-1*)	Forward: 5'- TGCCGCATCGCCGAGAT -3' Reverse: 5'- ATGGTGGGTTCTCTGGTG -3' Probe[1]: 5'- CCAGCGCCCAGAGAGAC -3'
Tissue inhibitor of metalloproteinases 2 (*TIMP-2*)	Forward: 5'- CACCAGGCCAAGTTCTTC -3' Reverse: 5'- CGGTACCACGCACAGGA -3' Probe[1]: 5'- CCTGCATCAAGAGAAGTGAC -3'
Ubiquitin C (*UBC*)	Forward: 5'- ATTTGGGTCGCGGTTCTTG -3' Reverse: 5'- TGCCTTGACATTCTCGGATGGT -3'

[1] Probe FAM-TAMRA for Taqman PCR reaction

2.6 Biochemical assays

2.6.1 Sample digestion for biochemical assay

2.6.1.1 Proteinase K digestion

Each pellet was digested in 250 µL of proteinase K solution at 56 °C for at least 16 hours. After visual inspection of complete dissolution, the proteinase K digestion solution was heat-inactivated by boiling the samples for 10 minutes. The proteinase K solution contains 1 mg/mL of proteinase K (Sigma Aldrich, Missouri, United States), 50 mM tromethamine (tris; Sigma Aldrich, Missouri, United States), 1mM ethylenediaminetetraacetic acid (EDTA; Sigma Aldrich, Missouri, United States) buffer at a pH of 7.6, 1 mM iodoacetamide (Sigma Aldrich, Missouri, United States), and 10 µg/mL pepstatin A (Sigma Aldrich, Missouri, United States).

2.6.1.2 Papain digestion

Alginate beads were dissolved in 50 µL of sodium citrate buffer per alginate bead using a bench rotator at 4 °C for 10 to 60 minutes. 50 µL of papain digestion solution was added to each sample before incubating the samples overnight at 60 °C. The next day, the samples were spinned down at 400 RCF for 3 minutes and incubated for an additional hour at 60 °C. The papain buffer contains 0.2 M sodium phosphate monobasic (NaH_2PO_4; Sigma Aldrich, Missouri, United States) and 0.01 M EDTA dissolved in distilled water, and the pH was adjusted to 6.0.

2.6.1.3 Hyaluronidase digestion

Each Ha-Tyr sample was dissolved in 250 µL of 4.0 mg/mL hyaluronidase dissolved in PBS at 37 °C for up to 2 hours. After visual inspection for complete dissolution, the samples were further digested according to the proteinase K digestion protocol.

2.6.2 DNA assay

Quantitative DNA measurements were performed on digested samples using a CyQUANT Cell Proliferation Assay kit (ThermoFisher, Carlsbad, California, United States), flat 96-well plates (ThermoFisher, Carlsbad, California, United States), and the Spectramax iD3 (Molecular Devices, California, United States) measuring at an excitation/emission wavelength (λ) respectively at $\lambda_{excitation}$ 480 nm and $\lambda_{emission}$ 520 nm. For the DNA quantification, 50 µL of each sample was mixed with 100 µL of heparin solution (Leo Pharma BV, Amsterdam, Netherlands) and 25 µL of RNAse solution (Sigma Aldrich, Missouri, United States). This mixture was incubated at 37 °C for 30 minutes before adding 30 µL of 0.375 µL CYQUANT GR solution (ThermoFisher, Carlsbad, California, United States) dissolved in 30 µL of PBS. A standard curve was prepared using 20X diluted 0.025 mg/mL DNA (Sigma Aldrich, Missouri, United States) dissolved in PBS. A linear trend line was fitted through the standard curve points. The measured values were corrected for background noise and plotted against the DNA concentration. The measured DNA content was calculated using equation 4.

$$DNA\ amount\ (ng) = \frac{(E_{520} - E_{520\ blanc}) - intercept\ trendline}{slope\ trendline} \cdot \frac{sample\ volume}{Total\ sample\ volume} \quad (4)$$

2.6.3 DMB assay

A 1,9-Dimethylmethylene-Blue (DMB) assay in flat 96-well plates was used to quantify sulphated glycosaminoglycan (GAG) content in samples. Sulphated GAG content was quantified based on a colorimetric measurement at $\lambda_1 = 530$ nm and $\lambda_2 = 590$ nm. A VersaMax microplate reader spectrophotometer (Molecular Devices, California, United States) was used to measure the absorbance. A standard curve was prepared using 10X diluted 0.5 mg/mL chondroitin sulfate C (CS; Sigma Aldrich, Missouri, United States) dissolved in phosphate buffer saline-ethylenediaminetetraacetic acid (PBS-EDTA) PBS (0.5 ng/mL). To measure the sulphated GAG content in the medium collected from the samples, CS was dissolved in DMEM medium to prepare the standard curve. The DMB solution was prepared by dissolving 0.016 grams of DMB (AppliChem GmbH, Darmstadt, Germany) in 5 mL of 100% EtOH in a glass vial and stirred overnight at room temperature. 2.37 grams of NaCl, 3.04 grams of glycine (Sigma Aldrich, Missouri, United States), and the DMB in EtOH solution were dissolved in 1 L water. The pH was adjusted to 1.75 using formic acid (Sigma Aldrich, Missouri, United States).
PBS-EDTA solution was prepared by dissolving 0.1 M of sodium phosphate dibasic dihydrate ($Na_2HPO_4.2H_2O$; Sigma Aldrich, Missouri, United States), sodium phosphate monobasic dihydrate ($H_2NaPO_4.2H_2O$; Sigma Aldrich, Missouri, United States) and 0.01 M ethylenediaminetetraacetic acid disodium salt (Na_2EDTA; Sigma Aldrich, Missouri, United States) in distilled water, and the pH was adjusted to 6.5 using 6 M NaOH and 6 M HCl.

To calculate the sulphated GAG content in each measured sample, 5 to 50 µL of each sample was filled up to 100 µL with PBS-EDTA solution (or with DMEM medium if measuring in DMEM containing samples) before adding 200 µL of DMB solution. The standard curve was used to calculate the calibration factor (F) required to quantify the sulphated GAG content in the samples, as shown in equation 5.

$$Sulphated\ GAG\ per\ sample\ (\mu g) = \frac{\frac{E_{530}}{E_{590}}}{F} \cdot \frac{sample\ volume}{total\ sample\ volume} \quad (5)$$

The calibration factor was calculated following equation 6 to 8.

$$X = \sum \left(\frac{E_{530}}{E_{590}} - \frac{E_{530\ blanc}}{E_{590\ blanc}}\right) \quad (6)$$

$$G = \sum all\ standard\ CS\ (\mu g) \quad (7)$$

$$Calbiration\ factor\ (F) = \frac{X}{G} \quad (8)$$

2.7 Histology staining

2.7.1 Cryostat sectioning

Freshly harvested samples were collected in 1.5 mL Eppendorf tubes filled with 4% formalin overnight before transferring them into a single use plastic mold filled with optimal cutting temperature compound (OCT; Sakura Finetek, Torrance, United States) and gently frozen down in liquid nitrogen. The frozen sample was stored at -80 °C before sectioning. A CryoStar NX70 solution (ThermoFisher, Carlsbad, California, United States) cryostat microtome was used for sectioning the samples at a thickness of 8 µm using a blade and environmental temperature of -35°C. Adhesive glass slides (Waldemar Knittel Glasbearbeitungs- GmbH, Braunschweig, Germany) were used to collect the sectioned specimens. The slides with specimens were dried at room temperature for 1 hour before freezing down at -80 °C overnight for histological/immunohistochemical staining.

2.7.2 Hematoxylin Eosin Staining

Cryosections were defrosted under a hairdryer for 60 minutes before opening the sections containing box. Afterwards, the samples were fixated on slides by pipetting ice-cold methanol (Sigma Aldrich, Missouri, United States) very gently on the slides and incubated for 10 minutes at room temperature. Due to the fragile nature of hydrogels, extra care was taken during washes and rehydration steps using pipets instead of dipping. After fixation, the slides were rinsed with distilled water two times for 3 minutes. Haematoxylin (Sigma Aldrich, Missouri, United States) solution was pipetted on top of the slides and incubated for 5 minutes at room temperature. The slides were rinsed with tap water for 10 minutes and dipped for 5 sec in distilled water before pipetting eosin (Merck, Darmstadt, Germany) very gently and incubated for 45 seconds. Finally, the slides were dehydrated in 70% EtOH for 10 seconds followed by 96% EtOH,100% EtOH and two times in O-Xylene (Sigma Aldrich, Missouri, United States) each step 1 minute at room temperature before mounting the slides with Depex (Merck, Darmstadt, Germany). The slides were dried at room temperature for at least one hour before using the slides for microscopic observation.

2.7.3 Thionin staining

Cryosections were defrosted under a hairdryer for 60 minutes before opening the sections containing box. After 60 minutes, the samples were fixated on slides by pipetting ice-cold methanol very gently on the slides and incubated for 10 minutes at room temperature. Due to the fragile nature of the hydrogels, extra care was taken during washes and rehydration steps using pipets instead of dipping. After fixation, the slides were rinsed with distilled water two times for 3 minutes. Thionin (Sigma Aldrich, Missouri, United States) solution was pipetted on top of the slides and incubated for 5 minutes. The slides were rinsed with 70% EtOH for 10 seconds, followed by a rinse with 96% of EtOH for 30 seconds.
Finally, the slides were dehydrated in 100% EtOH and two times in O-Xylene, each step 1 minute at room temperature before mounting the slides with Depex. The slides were dried at room temperature for at least one hour before using the slides for microscopic observation.

2.7.4 Safranin O staining

Cryosections were defrosted under a hairdryer for 60 minutes before opening the sections containing box. After 60 minutes, the samples were fixated on slides by pipetting ice-cold methanol very gently on the slides and incubated for 10 minutes at room temperature. Due to the fragile nature of the hydrogels, extra care was taken during washing and rehydration steps using pipets instead of dipping the slide in solution. After fixation, the slides were rinsed with distilled water two times for 3 minutes. 1 mg/ml of Light Green (Sigma Aldrich, Missouri, United States) solution in distilled water was pipetted very gently on top of the slides and incubated for 8 minutes at room temperature before rinsed with 1% acetic acid (Sigma Aldrich, Missouri, United States) twice for 10 seconds. 1 mg/mL of Safranin O (Sigma Aldrich, Missouri, United States) solution was pipetted on top of the slides and incubated for 12 minutes at room temperature before washing the slides with 96% EtOH twice for 30 seconds. Finally, the slides were dehydrated in 100% EtOH and two times in O-Xylene, each step 1 minute at room temperature before mounting the slides with Depex. The slides were dried at room temperature for at least one hour before using the slides for microscopic observation.

2.8 Rheological measurements

To characterize different Ha-Tyr hydrogel conditions material properties, a Kinexus Pro + rheometer (Malvern Panalytical, Malvern, United Kingdom) was used. For each measurement, a sample volume of 160 µL of Ha-Tyr hydrogel that was crosslinked *in situ* on the rheometer was compressed between two parallel impermeable surfaces to obtain a disk-like hydrogel with a height (h) of 0.5 mm and a diameter (Ø) of 20 mm as the initial dimensions. These dimensions were achieved using a stainless steel bottom plate and a PU20 SR3860 SS top plate (Malvern Panalytical, Malvern, United Kingdom) with Ø = 20 mm separated with an initial gap height (h) of 0.5 mm. The bottom plate was kept at 37°C and encapsulated within a sealing box (hood) to maintain a constant temperature and humidity throughout the experiment. Each sample was exposed to a series of preprogrammed sequence of measurements to characterise different gel conditions.
The gelation kinetics was first measured, followed by a frequency sweep test was performed using a frequency range from 0.1 to 100 Hz to determine the equilibrium gel modulus. Finally, a serial measurement of compression measurements was performed, followed by a serial measurement of decompression. The used rheometer settings are shown in appendix A.

2.8.1 Mesh size calculation based on the compression test

The dataset obtained from the first compression part was used to calculate the mesh size (ξ) of different gel conditions. The quantitative predictive equation obtained from Punter et al. (2020) [48] was used to calculate ξ, as shown in equation 9.

$$\frac{F}{\pi a^2} = T(t)\left(\frac{\eta a^2}{8k}\dot{\varepsilon} + M\varepsilon(t)\right) + \big(1 - T(t)\big)G\varepsilon \qquad (9)$$

In equation 9, F denotes for the measured force, a denotes for the radius of the gel, η denotes for the viscosity of pure water at 37 °C, k denotes for the permeability of the gel, $\dot{\varepsilon}$ means for

the compressive strain rate, and $M = K + 4G/3$ with K as the bulk modulus and G as shear modulus. After reaching the maximal fluid stress distribution, $T(t) \approx 1$ and simplifies the equation into equation 10.

$$\frac{F}{\pi a^2} = \frac{\eta a^2}{8k}\dot{\varepsilon} + M\varepsilon(t) \tag{10}$$

Fitting a linear least square model, the intercept of the linear part of the model was obtained to calculate the permeability of the gel. The linear least square model was fitted between t = 20 seconds and t = 100 seconds, since most of the obtained datasets showed some part of a linear region within this time window. The mesh size was calculated using the root square of the calculated gel permeability, as shown in equation 11.

$$mesh\ size\ (\zeta) \cong \sqrt{k} \tag{11}$$

A standardized MatLab ver. R2018b (MathWorks, Massachusetts, United States) script was used to calculate the mesh size, as shown in appendix B.

2.9 Flory-Rehner model

The Flory-Rehner model is an indirect method for calculating ξ using the swelling behavior of gels. The same procedure was used as described in Leach et al. (2003) [49] . Shortly, 50 µL hydrogel disks were swollen in DMEM medium at 37 °C for 72 hours. The gels were transferred in pre-weighed Eppendorf tubes. The samples were weighed to measure the swollen weight (W_s) of the gels before freeze-drying the samples for at least 10 hours. The weights of the dried samples were remeasured to obtain the dry weight of the gels (W_d). The swelling ratio (Q_d) was calculated from the two measured weights, as shown in equation 12.

$$Q_d = \frac{W_s}{W_d} \tag{12}$$

Using the equilibrium swelling theory, ξ was calculated. Therefore, the average molecular weight between crosslinks of the gel ($\overline{M}_c$) was calculated using the simplified Flory-Rehner model, as shown in equation 13.

$$Q_v^{\frac{5}{3}} \cong \frac{\overline{v}\,\overline{M_c}}{V_1}\left(\frac{1}{2} - \chi\right) \tag{13}$$

Q_v denotes for the swelling ratio, $\bar{v}$ denotes for the specific volume of the dry polymer, V_1 denotes for the molar volume of the solvent (18 mol/cm^3), and χ denotes for the Flory polymer solvent interaction parameter (0.473). Q_v was calculated using equation 14.

$$Q_v = 1 + \frac{\rho_p}{\rho_s}(Q_m - 1) \tag{14}$$

ρ_p denotes for the Ha-Tyr density (1.229 g/cm^3) and ρ_s denotes for the solvent density, which was assumed to be equal to the density of water (1 g/cm^3).
ξ of the swollen gel was calculated using equation 15.

$$\zeta \cong 0.1748 \sqrt{\overline{M_c}} Q_v^{\frac{1}{3}} \quad (15)$$

2.10 Statistics

The results were expressed as mean ± standard deviation (SD) if not stated differently. A statistical difference in gene expression and biochemical assays was determined using a one-way ANOVA statistical test with a Tukey test for multiple comparisons. A two-way ANOVA statistical test with a Tukey test for multiple comparisons was performed for the material characterisation. All statistics were performed in GraphPad Prism 8.4.2 (GraphPad Holdings, California, United States). The statical difference was considered for $p < 0.05$.

3

RESULTS

3.1 How do different crosslinking densities influence the gene expression of ECM remodeling genes and result in different matrix deposition?

3.1.1 Expression of ECM deposition related genes in cartilage like tissue

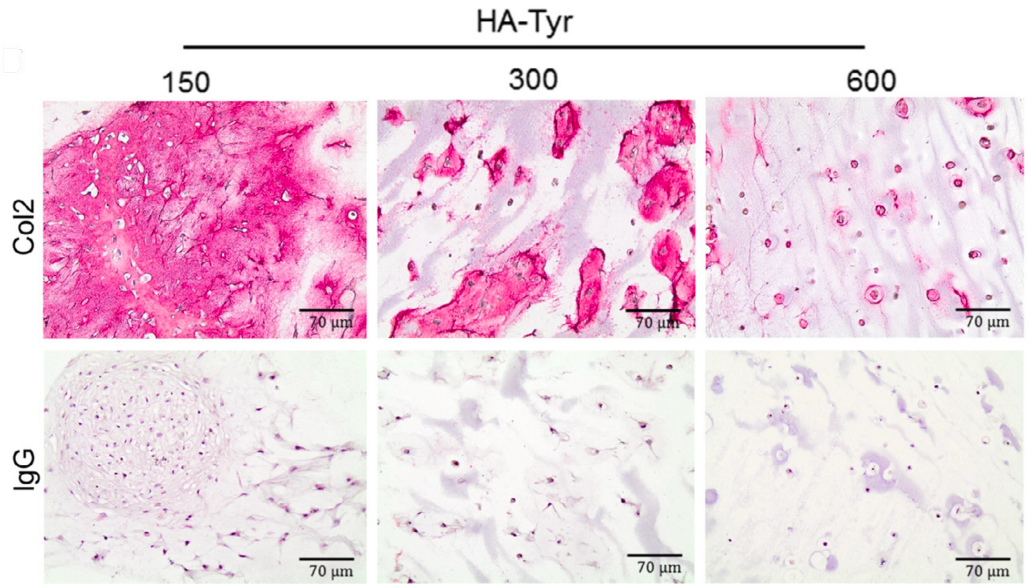

Figure 7: Immunohistological staining of chondrogenically differentiated MSCs in 3.5 % w/v Ha-Tyr gels crosslinked with either 150, 300 or 600 µM of H_2O_2 and cultured in full chondrogenic medium for 28 days. Staining was performed for collagen type II using primary antibody against collagen type 2 (stained in pink) and IgG isotope controls for demonstration of collagen staining specificity. Microscopic images were taken at 20X magnification. The pink staining represents the collagen type II specific staining in the matrix deposition of the gels. A decrease in collagen type II content in the matrix deposition was observed in gels crosslinked with higher H_2O_2 concentration. This figure is taken from the study of Vainieri et al. (2020) [46].

The histological staining for collagen type II data presented in the study of Vainieri et al. (2020) [46] on day 28 (fig. 7) was used as starting point. Tunable hydrogel properties (mesh size and gel stiffness) were achieved by varying the H_2O_2 concentration (150, 300 or 600 µM). Respectively, for the 150, 300, and 600 µM H_2O_2 crosslinked gel conditions, a mesh size of 184.99 ± 8.03 nm, 160.60 ± 5.04 nm and 130.85 ± 7.04 nm were reported, and a storage modulus (G') of ~ 70 Pa, ~ 500 Pa and ~ 3000 Pa were reported [46].
The immunohistochemical staining for collagen type II, using a primary antibody against collagen type II coupled with the secondary antibody F(ab) 2-labelled goat-anti mouse, (stained in pink) showed a decrease in collagen type II specific staining with increasing gel stiffness. However, no significant difference was observed at the gene expression level for both chondrogenic markers *COL2A1* and *ACAN* across the different gel conditions at two different time points (fig. 8). As potential housekeeper genes, *UBC, B2M* and *GAPDH* were measured (appendix C). *UBC* had the most constant expression across all samples and was used to normalize the other genes to.

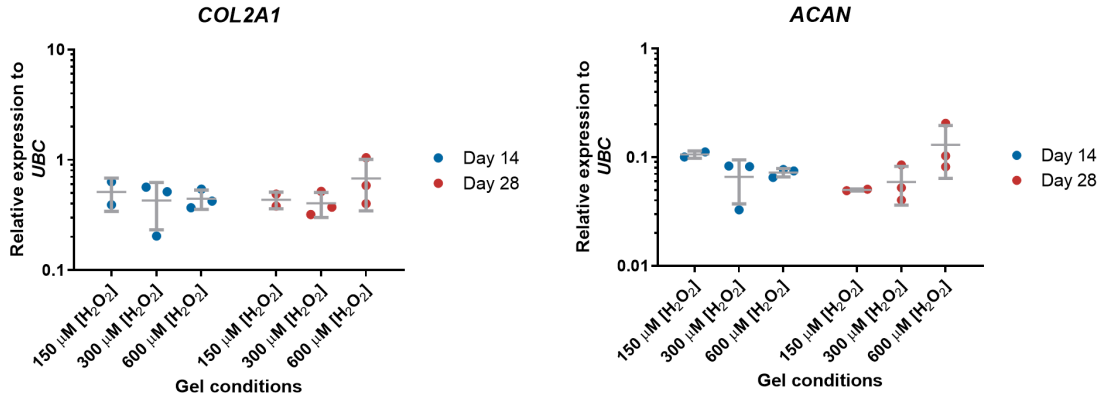

Figure 8: Relative gene expression levels for *COL2A1* and *ACAN* of MSCs embedded in 3.5% w/v Ha-Tyr hydrogels crosslinked with either 150, 300 or 600 µM of H_2O_2 and cultured for 14 and 28 days. No significant difference in relative gene expression between the different gel conditions was observed. The data are shown based on n=2 for gel condition 150 µM H_2O_2 and n=3 for gel conditions 300 and 600 µM H_2O_2 with mean ± SD.

Both chondrogenic markers were expressed in all three gel conditions, confirming chondrogenesis in each hydrogel condition. For *COL2A1* and *ACAN*, no significant differences in gene expression levels were observed between the gel conditions. This was true for gene expression levels on day 14 as well as day 28. For both genes, a trend towards lower gene expression levels was observed with increasing H_2O_2 concentration for crosslinking at day 14. Interestingly, the trend observed at day 14 changed at day 28 towards higher gene expression levels for *COL2A1* and *ACAN* with increasing H_2O_2 concentration for crosslinking.

3.1.2 Expression of ECM remodeling related genes in cartilage like tissue

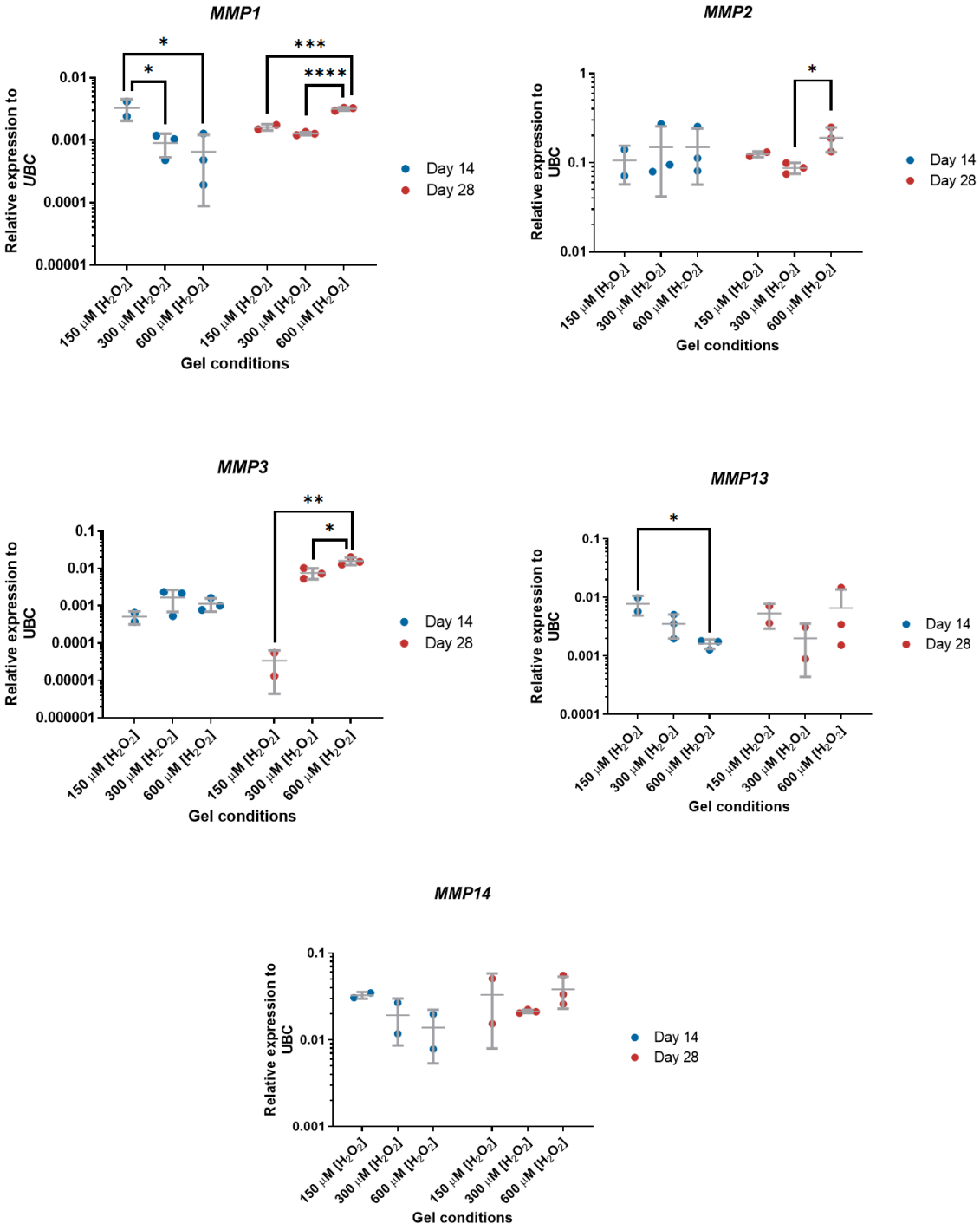

Figure 9: Relative gene expression levels for *MMP1, MPP2, MMP3, MMP13* and *MMP14* of MSCs embedded in 3.5% w/v Ha-Tyr hydrogels crosslinked with either 150, 300 or 600 µM of H_2O_2 and cultured for 14 and 28 days. The data are shown based on n=2 for gel condition 150 µM H_2O_2 and n=3 for gel conditions 300 and 600 µM H_2O_2 with mean ± SD. * = $p < 0.05$, ** = $p < 0.01$, *** = $p < 0.001$, and **** = $p < 0.0001$.

To evaluate if expression in ECM remodeling genes might give some more insight into the observed differences in histological staining (fig. 7), expression levels of ECM remodeling genes were measured. Gene expression levels for collagen degrading enzymes (collagenase) *MMP1, MMP2, MMP3, MMP13* and *MMP14* were measured (fig. 9). A higher expression for *MMP1* was measured in gel conditions crosslinked with 150 µM H_2O_2 compared to gel conditions crosslinked with 300 µM H_2O_2 and 600 µM H_2O_2 on day 14. Furthermore, a trend toward a lower expression level of *MMP1* was observed for cells cultured in gel conditions crosslinked with higher H_2O_2 concentration. The trend observed on day 14 changed on day 28 towards higher gene expression levels in gel conditions crosslinked with higher H_2O_2 concentration. No significant differences in gene expression levels for *MMP2* and *MMP3* were observed between the gel conditions on day 14. A trend towards higher gene expression levels for *MMP2* and *MMP3* was observed for MSCs cultured in gel conditions crosslinked with higher H_2O_2 concentration. On day 28, higher expression levels of *MMP2* and *MMP3* were measured in gel condition crosslinked with 600 µM H_2O_2 compared to gel condition crosslinked with 300 µM H_2O_2. For *MMP13* and *MMP14,* a trend towards lower gene expression levels was observed in gels crosslinked with a higher concentration of H_2O_2. Thereby, a higher expression level of *MMP13* was measured in the gel condition crosslinked with 150 µM H_2O_2 compared to the gel condition crosslinked with 600 µM H_2O_2 at day 14. Looking at all MMPs together, it was observed that the highest expression levels were measured for *MMP2* and *MMP14*, and the lowest gene expression was measured for *MMP3*. Additionally, a general trend towards a higher expression level of *MMPs* with increasing gel stiffness was observed on day 28. No general trend was observed for the gene expression patterns on day 14.

Besides the expression of collagen degrading enzymes, the expression levels of MMP inhibitors *TIMP1* and *TIMP2* were measured (fig.10). No significant differences in gene expression levels for *TIMP1* and *TIMP2* were measured across the different gel conditions on day 14 and day 28. Furthermore, no clear trend was observed in the expression pattern of *TIMP1* across the other gel conditions on days 14 and 28. For *TIMP2*, a trend towards higher expression levels in gel conditions crosslinked with higher H_2O_2 concentration was observed for day 14 and 28. Higher expression levels of *TIMP2* were measured in all gel conditions compared to *TIMP1* in the same gel condition.

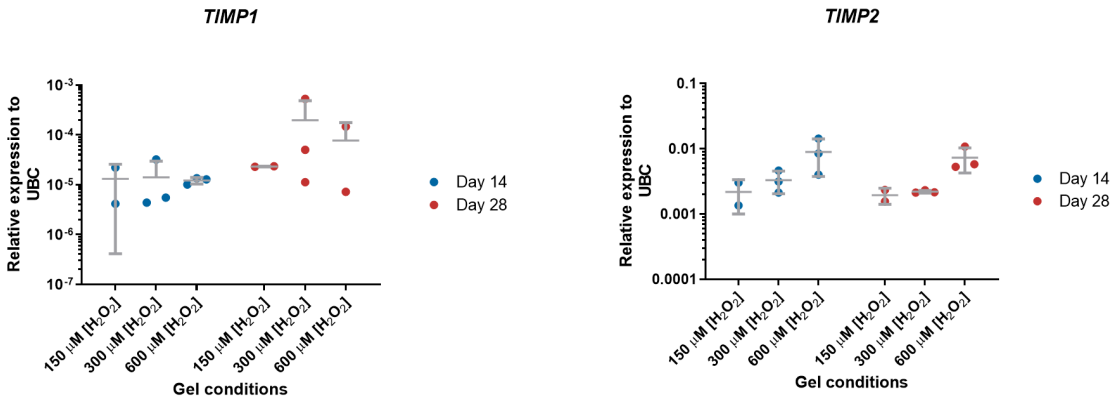

Figure 10: Relative gene expression levels for *TIMP1* and *TIMP2* of MSCs embedded in 3.5 % w/v Ha-Tyr hydrogels crosslinked with either 150, 300 or 600 µM of H_2O_2 and cultured for 14 and 28 days. No significant difference in relative gene expression between the different gel conditions was observed. The data are shown based on n=2 for gel condition 150 µM H_2O_2 and n=3 for gel conditions 300 and 600 µM H_2O_2 with mean ± SD.

The expression levels for the aggrecan degrading enzymes (aggrecanase) *ADAMTS4* and *ADAMTS5* were measured (fig. 11). No significant differences in gene expression levels for *ADAMTS4* and *ADAMTS5* were measured across the different gel conditions on day 14 and day 28. A trend towards lower expression levels for *ADAMTS4* and *ADAMTS5* was measured in gels crosslinked with a higher concentration of H_2O_2 on day 14. The trend observed on day 14 changed on day 28 towards higher gene expression levels in gel conditions crosslinked with higher H_2O_2 concentration. Higher expression levels for *ADAMTS4* were measured in all gel conditions compared to *ADAMTS5* in the same gel condition.

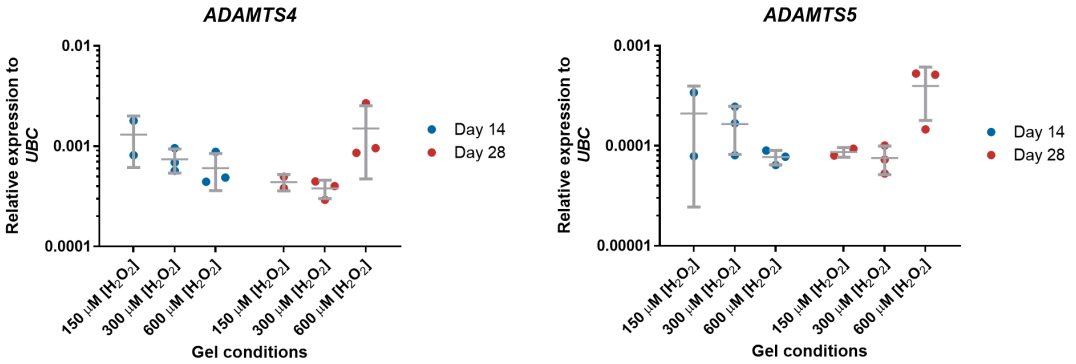

Figure 11: Relative gene expression levels for *ADAMTS4* and *ADAMTS5* of MSCs embedded in 3.5 % w/v Ha-Tyr hydrogels crosslinked with either 150, 300 or 600 µM of H_2O_2 and cultured for 14 and 28 days. No significant difference in relative gene expression between the different gel conditions was observed. The data are shown based on n=2 for gel condition 150 µM H_2O_2 and n=3 for gel conditions 300 and 600 µM H_2O_2 with mean ± SD.

3.2 Which gel conditions are required to investigate the effect of the isolated material properties on Ha-Tyr based hydrogels?

3.2.1 Gel stiffness

First, the gelation kinetics (fig. 12) of gel conditions with a polymer concentration of 1.5 % or 3.5 % w/v Ha-Tyr and crosslinked with 150, 300 or 600 µM H_2O_2 were measured over a time course of 1 hour. The individual replicates are shown in Appendix D. Throughout the rest of the thesis, abbreviations will refer to the different gel conditions as stated in table 3.

Table 3: Abbreviations list for the different gel conditions used during the material characterization part.

Gel condition	Abbreviation
1.5 % w/v Ha-Tyr crosslinked with 150 µM H_2O_2	1.5% 150
1.5 % w/v Ha-Tyr crosslinked with 300 µM H_2O_2	1.5% 300
1.5 % w/v Ha-Tyr crosslinked with 600 µM H_2O_2	1.5% 600
3.5 % w/v Ha-Tyr crosslinked with 150 µM H_2O_2	3.5% 150
3.5 % w/v Ha-Tyr crosslinked with 300 µM H_2O_2	3.5% 300
3.5 % w/v Ha-Tyr crosslinked with 600 µM H_2O_2	3.5% 600

All gel conditions showed similar polymerization kinetics. The storage modulus (G') rapidly increased within the first 1000 seconds of gelation, followed by a plateau phase. It was observed that between 1000 and 2000 seconds, all gel conditions reached equilibrium at a gel condition-specific G'. The required time needed for reaching the plateau phase for storage modulus was defined as the gelation time, which did not show a dependency for H_2O_2 or polymer concentration (appendix D). However, for the gel condition 3.5 % 60, a slight decrease in gel stiffness was measured during the equilibrium phase due to measuring a sudden reduction in gel stiffness in one of the replicates (appendix D). Furthermore, gel conditions 1.5% 150 and 3.5 % 300 showed overlapping gelation kinetics.
Additionally, the gelation curves showed an increase in gel stiffness using a higher H_2O_2 concentration for crosslinking while maintaining a constant polymer concentration. Increasing the polymer concentration while maintaining a continuous H_2O_2 concentration for crosslinking again resulted in stiffer gels.

To validate if this observation was true, each gel conditions plateau value was plotted against its polymer concentration (fig. 13). A two-way ANOVA with a Tukey posthoc test was performed to validate the effect of the two parameters on gel stiffness and their interaction. The statistical test yielded a p-value of 0.0415 for the interaction between the two parameters indicating that the interaction between H_2O_2 and polymer concentration is considered significant. Furthermore, a p-value of 0.0008 and <0.0001 were calculated respectively for the effect of polymer concentration and H_2O_2, proofing that both parameters independently from each do impact the gel stiffness. For gel conditions crosslinked with 150 µM H_2O_2, the G' increased from 184.83 ± 47.20 Pa to 265.33 ± 83.17 Pa when changing the polymer concentration from 1.5 % w/v to 3.5 % w/v Ha-Tyr. Respectively, for gel conditions 300 µM H_2O_2 and 600 µM H_2O_2, the G' increased from 528.63 ± 77.19 Pa to 1027.6 ± 209.99 Pa and from 1036.00 ± 262.17 Pa to 1869.33 ± 275.55 Pa when changing the polymer concentration from 1.5 % w/v to 3.5 % w/v Ha-Tyr.

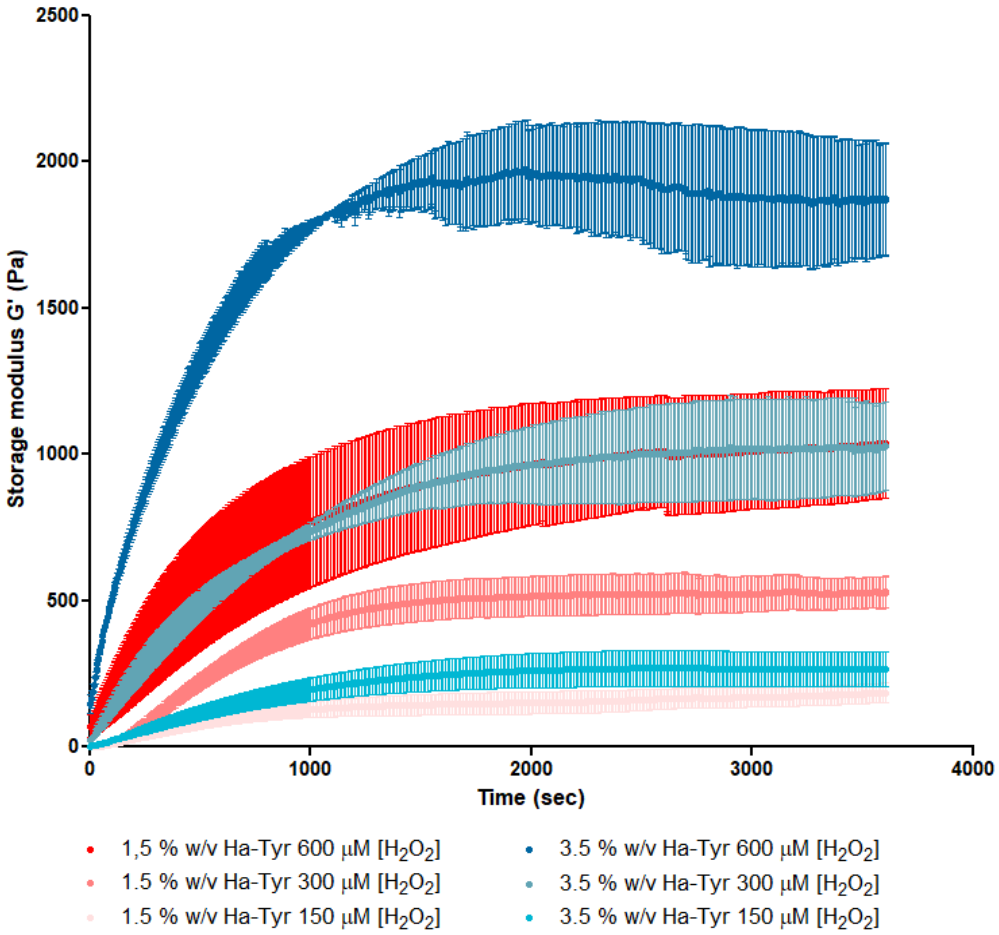

Figure 12: The gelation kinetics of Ha-Tyr gels crosslinked with different concentrations of H_2O_2 measured over a time course of 1 hour. In red, gel conditions having a polymer concentration of 1.5 % w/v Ha-Tyr, and in blue, the gel conditions having a polymer

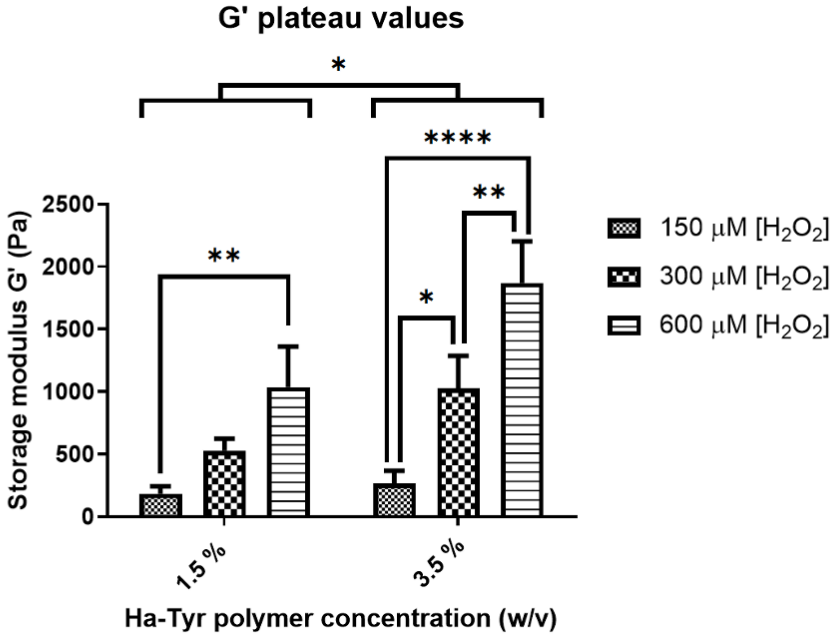

Figure 13: The plateau values of each gel condition plotted against its polymer concentration. The data are shown in triplicate gel sample with mean ± SEM for each time point. * = $p < 0.05$, ** = $p < 0.01$, *** = $p < 0.001$, and **** = $p < 0.0001$.

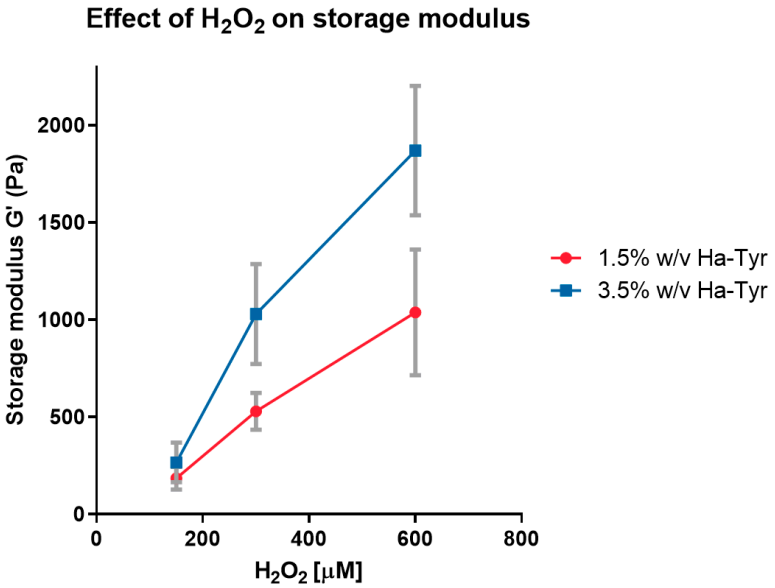

Figure 14: H_2O_2 concentration plotted against the measured equilibrium storage modulus (G') for both polymer concentration of Ha-Tyr hydrogels. The data are shown in triplicate gel sample with mean ± SD.

The equilibrium storage modulus was plotted against the H_2O_2 concentration (fig. 14) to estimate the range of possible matching gel stiffness that could be obtained. Gel conditions having a similar G' ranging between ~ 200 Pa up to ~1000 Pa could be obtained by adjusting the polymer concentration between 1.5 % w/v and 3.5 % w/v and the H_2O_2 concentration between 150 µM and 600 µM.

3.2.2 Mesh size

The mesh size (ξ) for each gel condition was calculated utilizing multiple data points extracted from unconfined compression. From this data set, the permeability (k) of the gels was calculated to obtain ξ (fig. 15). The application of this methodology gave an indication of ξ of Ha-Tyr hydrogels in an unswollen state. For gel conditions having a polymer concentration of 1.5 % w/v Ha-Tyr crosslinked with 150, 300 or 600 µM H_2O_2, a mesh size of 120.00 ± 31.82 nm, 76.39 ± 16.15 nm and 79.77 ± 13.19 nm were measured. For gel conditions having a polymer concentration of 3.5 % w/v Ha-Tyr crosslinked with 150, 300 or 600 µM H_2O_2, a mesh size of 838.32 ± 351.07 nm, 97.89 ± 17.70 nm and 78.72 ± 52.94 nm were measured.
Gel condition 3.5% 150 having a mesh size of at least 8 times higher in comparison to the rest of the gel conditions was classified as an inaccurate mesh size estimation. A two-way ANOVA yielded no significant difference in mesh size between the rest of the gel conditions. A trend towards smaller ξ with increasing H_2O_2 concentration independently of the polymer concentration. When comparing the ξ of gel conditions crosslinked with the same H_2O_2 concentration and different polymer concentration, it was observed that gel conditions having a higher polymer concentration yielded bigger mesh sizes.

Besides the unconfined compression methodology, the swelling ratio of gels was measured to estimate ξ utilizing the Flory-Rehner model. Evaluating the ξ via the Flory-Rehner model gave an estimation of the mesh size of our gels during the swollen state. The data obtained from the Flory-Rehner model are shown in appendix E. The Flory-Rehner model yielded mesh sizes ranging between 406.92 ± 145.91 nm and 188.22 ± 52.27 nm.

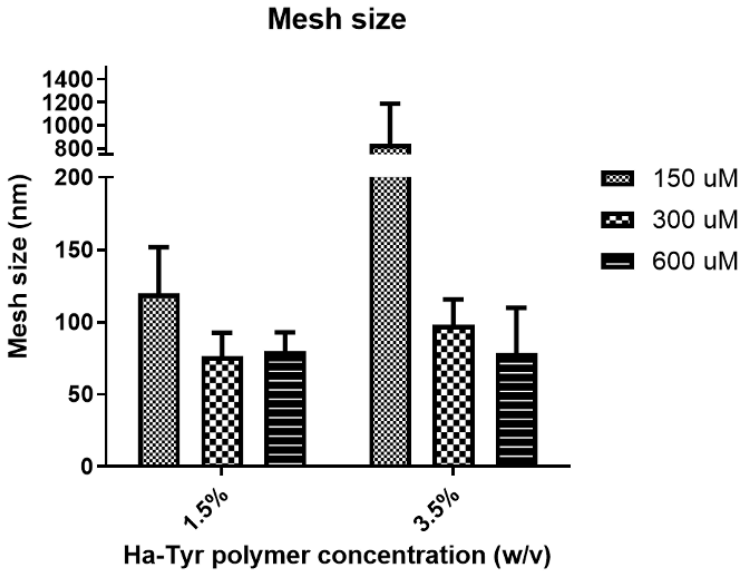

Figure 15: The average calculated mesh size using the unconfined compression test and the permeability of the gel. The data are shown in triplicate gel sample with mean ± SD.

3.2.3 Uncoupling mesh size & stiffness

The mesh size and gel stiffness were uncoupled from each other by generating gel conditions with different crosslinking densities. For the uncoupling, ξ estimation via model fitting on the unconfined compression data set was used. ξ and G' for each gel condition were plotted against each other (fig. 16) highlighting which gel conditions can be used to investigate the effect of mesh size and gel stiffness independently from each other. Uncoupling of gel stiffness and mesh size using the dataset from the Flory-Rehner model estimation yielded a similar distribution of the gel conditions, as shown in appendix E. A trend towards smaller mesh size with increasing gel stiffness was observed independently of the polymer concentration.
Based on the calculated ξ and measured G', three gel conditions were strategically selected (the red box in fig. 16) to investigate the effect of material properties on the matrix deposition of MSCs. Gel conditions 3.5 % w/v Ha-Tyr crosslinked with either 300 µM or 600 µM and the gel condition 1.5 % w/w Ha-Tyr crosslinked with 600 µM H_2O_2 were selected. This selection of gel conditions allowed the evaluation of whether gel stiffness, polymer concentration or H_2O_2 concentration does have an impact on the chondrogenesis and matrix deposition of MSCs.

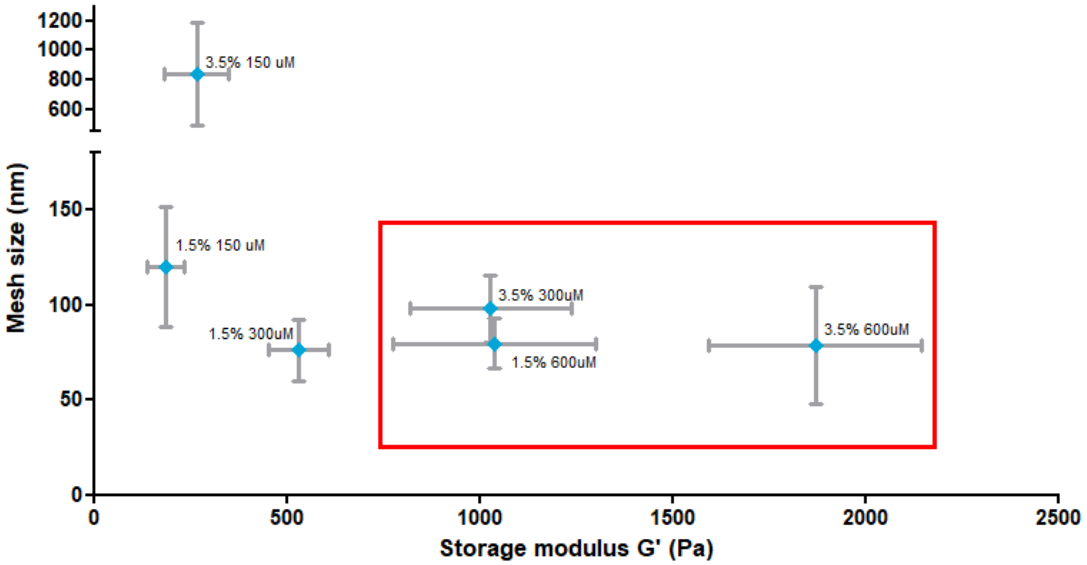

Figure 16: The storage modulus (G') and mesh size plotted against each other for each gel condition to uncouple the two material properties from each other. In the red box, the three gel conditions selected for the effect of material properties on matrix deposition of MSCs are shown. The data are shown in triplicate gel sample with mean ± SD.

3.3 What is the effect of material properties on the matrix deposition of chondrogenic differentiation of MSCs?

3.3.1 Expression levels chondrogenic markers

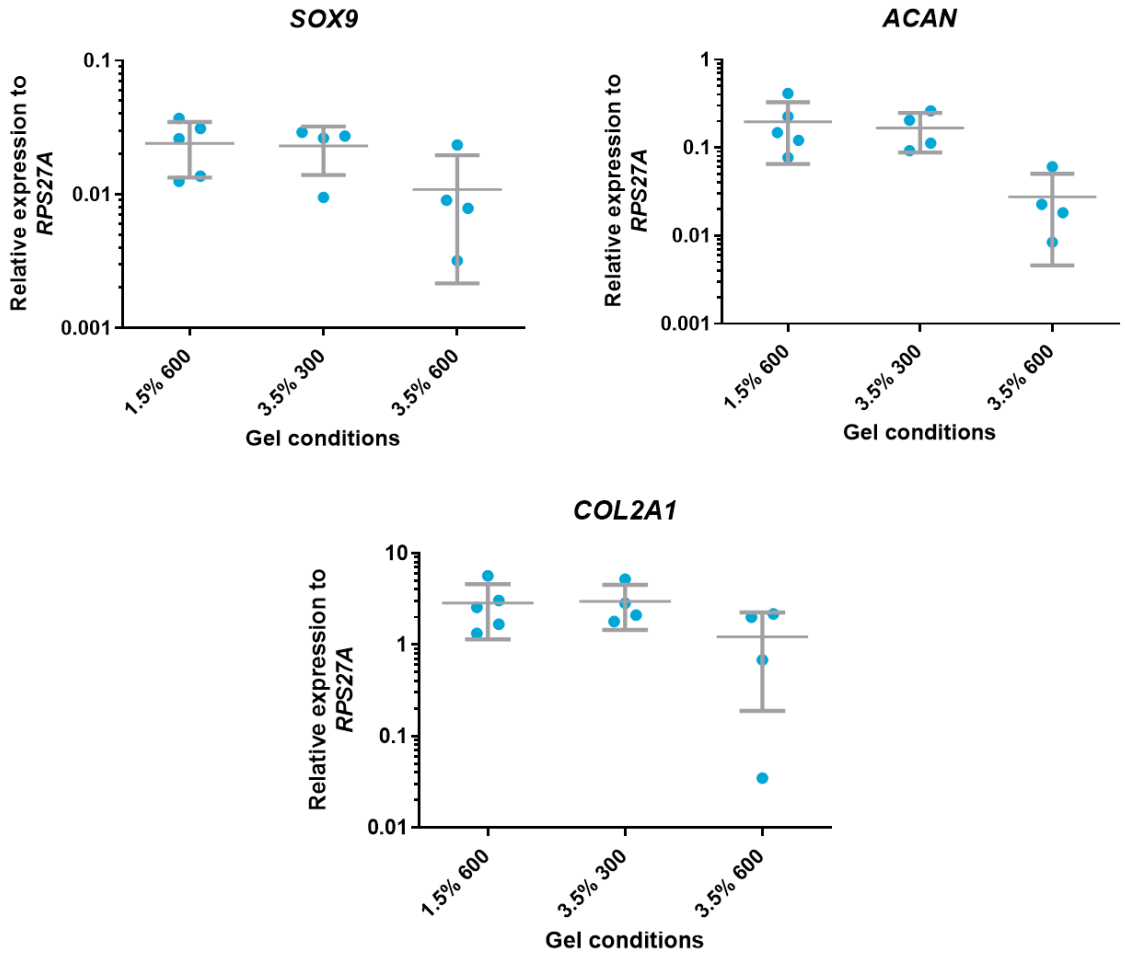

Figure 17: The relative gene expression levels for the chondrogenic markers *SOX9, ACAN* and *COL2A1* of P-MSCs embedded in 3.5% w/v Ha-Tyr hydrogels crosslinked with either 300 or 600 µM of H_2O_2 and 1.5% w/v Ha-Tyr hydrogels crosslinked with either 600 µM of H_2O_2. No significant difference in relative gene expression between the different gel conditions was observed. The data are shown based on n=5 for gel condition 1.5 % 600 and n=4 for gel conditions 3.5% 300 and 3.5% 600 with mean ± SD.

The three selected gel conditions were seeded with P-MSCs and cultured for 14 days in a full chondrogenic medium. They were used to evaluate the effect of material properties on cartilage-like matrix deposition of chondrogenic differentiated P-MSCs. First, the gene expression of chondrogenic markers *SOX9*, *COL2A1* and *ACAN* were measured to validate the chondrogenic potential of the cells embedded within the different gel conditions (fig. 17). As potential housekeeper genes, *UBC, B2M* and *RPS27A* were measured (appendix F). *RPS27A* had the most stable expression across all samples and was used to normalize the other genes to. All three chondrogenic markers were expressed in all three gel conditions, confirming chondrogenesis in each gel condition. No significant differences in gene expression were found between the three gel conditions. Gel condition 3.5% 600 repeatedly showed a trend towards lower gene expression levels for all three chondrogenic markers when compared to the gel conditions 1.5% 600 and 3.5% 300.

3.3.2 Biochemical assays

GAG and DNA content were measured for all three gel conditions (fig. 18). DNA content was detected in all three gel conditions with P-MSCs embedded within the hydrogels for 14 days. The GAG production within each construct was normalized to DNA. Prior to normalization, the possible interference of Ha-Tyr with the biochemical assay was validated. Therefore, a DMB assay with cell-free Ha-Tyr gels was performed. The measured GAG content was below the detection level (appendix F) and was assumed not to interfere with the measurement. Gel condition 3.5% 300 showed a significant difference ($p < 0.0001$) in GAG/DNA content when compared to gel conditions 1.5% 600 and 3.5% 600. No difference in GAG/DNA content was measured between gel conditions 1.5% 600 and 3.5% 600.

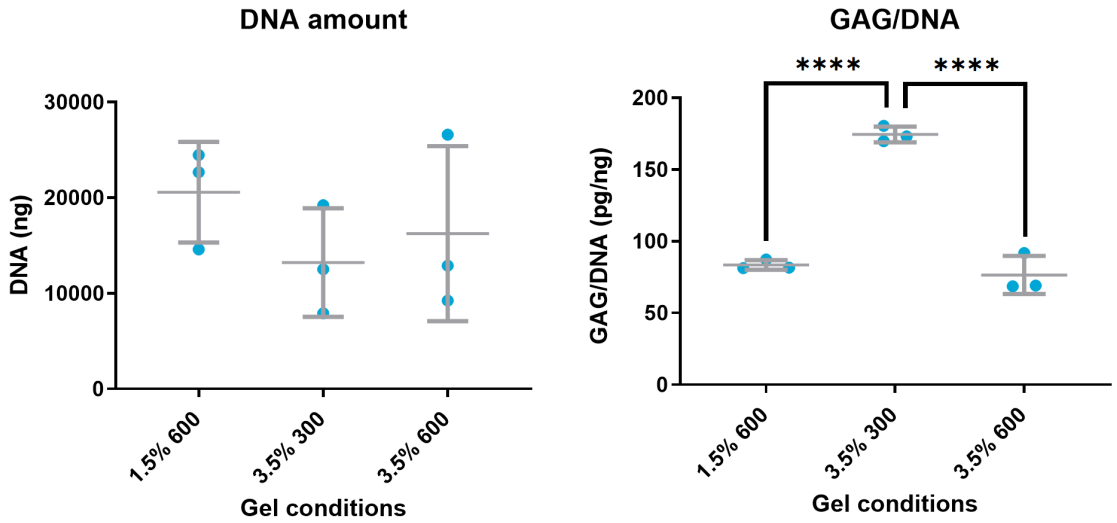

Figure 18: The DNA and GAG/DNA content measured in each gel condition after 14 days of culture in a full chondrogenic medium. Data are shown in triplicate with mean ± SD and **** = $p < 0.0001$.

3.3.3 Expression levels of ECM remodeling related genes

As mentioned before, microenvironmental cues do play a role in the remodeling of the extracellular matrix. For cartilage-like tissue, the two main components of the ECM are collagen and aggrecan molecules. The gene expression levels for collagen degrading enzymes (collagenase) *MMP1*, *MMP3* and *MMP13* were measured (fig. 19). In addition, the expression levels for the aggrecan degrading enzymes (aggrecanases) *ADAMTS4* and *ADAMTS5* were measured (fig. 20). *MMP1* was expressed in all three gel conditions, and no significant difference was observed at the gene expression level. A trend towards a higher expression of *MMP1* with increasing stiffness was observed. *MMP3* and *MMP13* were expressed in all three gel conditions. A higher expression of *MMP3* was measured in gel condition 1.5% 600 when compared to 3.5% 600. *MMP3* and *MMP13* showed a trend towards lower expression with higher polymer concentration. Both *ADAMTS4* and *ADAMTS5* were expressed in all three conditions, and no significant difference nor a trend was observed at the gene expression level.

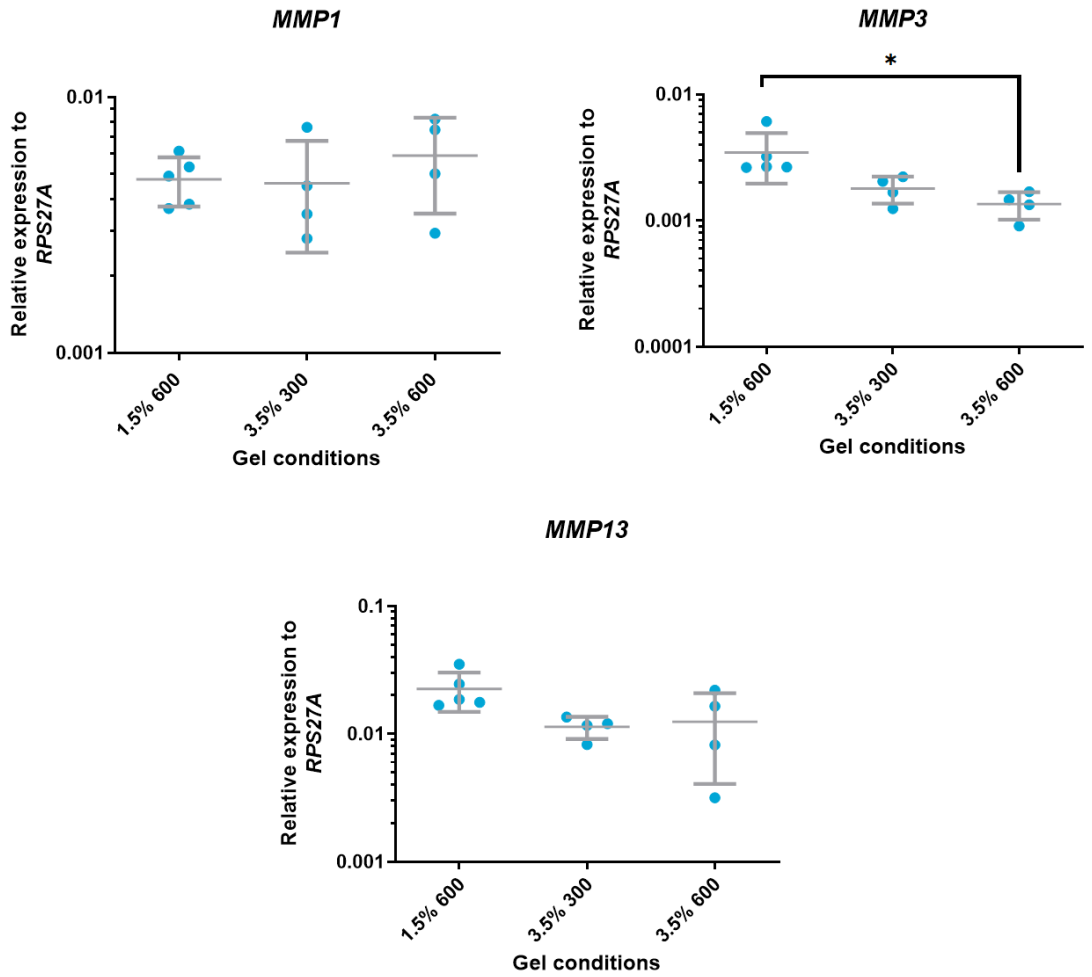

Figure19: The relative gene expression levels for *MMP1*, *MMP3* and *MMP13* of P-MSCs embedded in 3.5% w/v Ha-Tyr hydrogels crosslinked with either 300 or 600 µM of H_2O_2 and 1.5% w/v Ha-Tyr hydrogels crosslinked with either 600 µM of H_2O_2. The data are shown based on n=5 for gel condition 1.5 % 600 and n=4 for gel conditions 3.5% 300 and 3.5% 600 with mean ± SD. The data are shown based on n=5 for gel condition 1.5 % 600 and n=4 for gel conditions 3.5% 300 and 3.5% 600 with mean ± SD and * = $p < 0.05$.

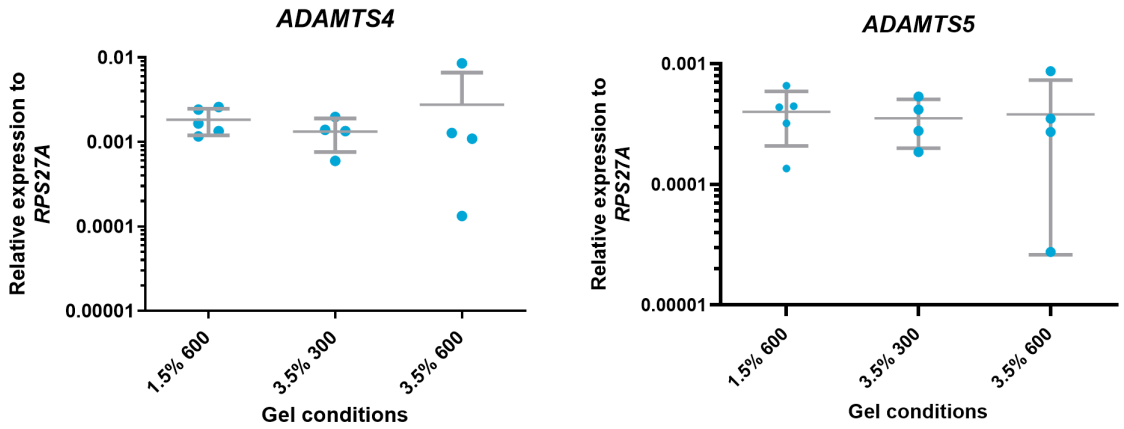

Figure 20: The relative gene expression levels for *ADAMTS4* and *ADAMTS5* of P-MSCs embedded in 3.5% w/v Ha-Tyr hydrogels crosslinked with either 300 or 600 µM of H_2O_2 and 1.5% w/v Ha-Tyr hydrogels crosslinked with either 600 µM of H_2O_2. No significant difference in relative gene expression between the different gel conditions was observed. The data are shown based on n=5 for gel condition 1.5 % 600 and n=4 for gel conditions 3.5% 300 and 3.5% 600 with mean ± SD.

4

DISCUSSION

In this study, we investigated the effect of H_2O_2 and polymer concentration on the gel stiffness and mesh size of Ha-Tyr based hydrogels, followed by a comparison of different hydrogels for their support for chondrogenic differentiation and cartilage-like matrix deposition of MSCs *in vitro*. Our study confirmed that the gel stiffness of Ha-Tyr based hydrogels is polymer concentration and H_2O_2 concentration dependent [50, 51, 52, 53]. Adjusting these two parameters independently from each other, different gel conditions having matching bulk stiffness could be achieved. Finding gel conditions with similar G' allowed the evaluation of gel stiffness on the chondrogenic potential of MSCs independently from other material properties like mesh size. Additionally, our study indicates that the mesh size of Ha-Tyr shows a trend towards bigger mesh sizes with increasing polymer concentration and decreasing H_2O_2 concentration. Translation of the effect of material properties on the cartilage-like matrix deposition of chondrogenic differentiating MSCs indicated towards reduced matrix deposition with increasing crosslinking. Additionally, the dynamic microenvironment cells are cultured in resulted in changing expression patterns over time. Cells are capable of sensing and responding to the continuous changes of their microenvironment which have resulted in the expression of ECM remodeling genes like *MMPs*, *TIMPs*, and *ADAMTSs* [54, 55]. The most noticeable response towards the differences in microenvironmental cues was seen in the expression levels of *MMP1* and *MMP3*, indicating that these two genes might play a pivotal role in the accumulation of ECM components.

Our approach is based on the tunability of hydrogels and their potential to support cartilage tissue engineering purposes. The advantage of the used strategy to uncouple gel stiffness and mesh size from each other opens the possibility to evaluate the effect of isolated material properties on the chondrogenic potential of MSCs, which helps to identify mechanotransductional regulators for cartilage tissue engineering purposes. This obtained knowledge could be used for the development of smart biomaterials for tissue engineering purposes. The used uncoupling strategy could be applied for different types of tissue engineering purposes to evaluate the effect of gel stiffness and mesh size independently from each other. Furthermore, it allows better controllability of cell differentiation and cellular behaviour that is not possible using conventional culturing strategies [56]. Ultimately, it may result in the development of smart biomaterials capable of directing cells towards a specific phenotype without the need for additional factors such as chemical stimulators.

Comparison of the findings with those of other studies indicated that the material properties of Ha-Tyr based hydrogels can be tuned via adjustment of a couple of parameters [50, 51, 52, 57]. One of these tunable parameters for Ha-Tyr hydrogels is the gelation time required to achieve equilibrium in the stiffness of the gels. The gelation time is considered an important parameter in hydrogels since it affects the spatial distribution of crosslinks [58, 53]. Additionally, it is an important parameter for tissue engineering application, since the gelation time is one of the parameters that define whether irregularly shaped defects could be filled with the hydrogel to obtain cohesion between the native tissue and the biomaterial [58, 53]. The gel kinetics measurement showed a rapid increase in G' that reaches equilibrium between 1000- and 2000-seconds during crosslinking when using an HRP concentration of 0.2 U/mL. These results reflect those of Abu-Hakmed et al. (2016) [57], who also found that using an HRP concentration of 0.24 U/mL reaches equilibrium after ~ 25 minutes (~1500 seconds) of crosslinking. Reducing the HRP concentration increased the duration of reaching equilibrium, while adjustments in the polymer concentration or H_2O_2 concentration did not affect the gelation time [57, 53]. Our measured gel kinetics also indicated nondependency for H_2O_2 or polymer concentration, which are in line with those of previous studies [57, 53]. One unanticipated finding was that gel conditions crosslinked with 600 µM of H_2O_2 independently of the polymer concentration showed for some measurements a decrease over time in G' during polymerization, which indicates structural instability within these gel conditions [59, 60, 61]. These structural instabilities might have been the consequence of the inhomogeneous distribution of the formed crosslinks causing failure of the gel [59]. Another possibility might have been the consequence of the buckling of the formed crosslinks in combination with the inhomogeneous distribution of the crosslinks [60, 61]. According to Kan and Zheng (2009) [61], the formed crosslinks are assumed to be slender elastic columns while the polymers are considered rigid bodies. During the buckling effect, the elastic columns are not strong enough to withstand the weight of the polymer and start to buckle together causing the gel to collapse. Meanwhile, some crosslinks could break resulting in the loss of gel stiffness [60, 61]. Another possibility to explain the observed behaviour could be at the enzyme activity level. It has been reported that HRP activity decreases with increasing concentration of H_2O_2 [53, 62]. Exceeding the catabolic capacity of HRP at a high concentration of H_2O_2 (>1 mM) may inhibit the enzyme activity due to destabilization of the enzyme itself [53, 62]. This may initiate the formation of unstable internal structures resulting in the failure of gel crosslinked with a high concentration of H_2O_2. Knowledge regarding the negative effect of high H_2O_2 concentration on Ha-Tyr is an important point for future research. A titration experiment with different concentrations of H_2O_2 will reveal the maximum concentration of H_2O_2 that can be used without introducing instabilities within the internal structures. The used HRP concentration does need to be taken into account within the experimental setup since HRP concentration determines the total catalytic capacity [57, 53, 50]. Additionally, HRP concentration has been reported as a potential regulator for gel stiffness of Ha-Tyr based hydrogels [57, 53, 50]. Previous studies highlighted that reducing the HRP concentration below 0.1 U/mL reduced the final gel stiffness, whereas, increasing the HRP above 0.1 U/mL had no effect on the gel stiffness [50, 53, 57]. Therefore, the HRP concentration cannot be neglected in future experimental setups.

Besides the HRP concentration, the H_2O_2 concentration was identified as a tunable parameter for Ha-Tyr hydrogels. Several reports have shown a strong relationship between H_2O_2 concentration and gel stiffness [50, 51, 52, 53]. On the other hand, no studies were identified in literature investigating the effect of polymer concentration of Ha-Tyr based hydrogels on the gel stiffness. The effect of polymer concentration has been investigated in a chitosan-based hydrogel [59]. They illustrated that increasing the polymer concentration increased the

stiffness of the gel [59]. In the current study, the resulting hydrogels ranged in G' between ~180 Pa and ~1800 Pa, which is in line with those of other studies using similar gel conditions [50, 51, 52, 53]. Consistent with the literature, our results indicated a positive correlation between polymer concentration and gel stiffness as well as for H_2O_2 concentration and gel stiffness [50, 51, 52, 53] [59]. Additionally, the ANOVA (two-way) showed that H_2O_2 and polymer concentration were statically significant, indicating that these two parameters are dependent on each other for the gel stiffness. To the best of our knowledge, no findings regarding this dependency between polymer and H_2O_2 concentration for the gel stiffness in Ha-Tyr based hydrogels has been reported in literature.
This combination of findings provides some support for the conceptual premise that the H_2O_2 and polymer concentration could be used for tuning the gel stiffness of Ha-Tyr hydrogels. Utilizing this unique approach of tuning material properties in hydrogels, matching material properties were achieved to investigate isolated material properties.

Unfortunately, the used techniques for ξ determination did not allow for a precise estimation of ξ. Therefore, it has limited the current study to the evaluation of matching stiffness rather than the uncoupling of gel stiffness and mesh size from each other to evaluate the effect of isolated material properties. But the obtained ξ estimations were sufficient to reveal some effects of polymer and H_2O_2 concentration on ξ. The mesh size determination via model fitting on the unconfined compression data set gave an ξ estimation ranging between ~75 nm and ~120 nm, whereas, the mesh size determination via the Flory-Rehner model gave an estimation ranging between ~180 nm and ~400 nm. Comparison with previous studies reported ξ ranging between ~100 nm and ~200 nm, indicating that most of our estimated ξ were in order of magnitude consistent with previously reported for this material [46, 52, 63]
Comparison of the two methods for ξ estimation illustrated that the Flory-Rehner model yielded larger ξ when compared to estimation via model fitting. A possible explanation for this phenomenon might have been the fact that for the Flory-Rehner model swollen gels were used, whereas for the model fitting method unswollen gels were used. Hydrophilic polymer networks in aquas solution attract the solvent into the polymer network due to the osmotic pressure causing the gel to swell [64, 65, 66]. During the swelling state, the mesh size of the polymer network within the hydrogel expands resulting in larger mesh sizes [64, 65, 66].
For both methods, a trend towards smaller ξ was observed with increasing crosslinking density, which is consistent with previous studies [46, 52, 63]. Comparison of ξ of gel conditions crosslinked with the same concentration of H_2O_2 and different polymer concentration repeatedly showed a bigger mesh size for gel conditions having a higher polymer concentration. This phenomenon might have been the consequence of the difference in crosslinking density. Factors that play a role in the crosslinking density in Ha-Tyr based hydrogels are H_2O_2 concentration, HRP concentration, polymer concentration, and DS_{mol} for tyramine [51]. In our experimental setup, the HRP concentration and DS_{mol} for tyramine were fixed parameters, whereas, the H_2O_2 and polymer concentration were the tunable parameters. Increasing the polymer concentration while maintaining the amount of H_2O_2 for crosslinking increases the potential crosslinking points within the gel. This might result in a lower crosslinking density causing bigger mesh sizes (fig. 21). Based on this theory, our experimental setup should yield the lowest crosslinking density in gel condition 3.5% 150. The estimated ξ for these gel conditions were indeed the largest one. However, it was classified as an inaccurate estimation of ξ, since the calculated mesh size was at least 8 times higher than previous reports [46, 52, 63]. A possible explanation for this might be that microgels were formed within the gel as a consequence of the low crosslinking points [67]. Instead of a single polymer network, a couple of unconnected smaller polymer networks may have been formed (fig. 22). Since the microgels are in theory not connected, their theoretical

distance between each other is infinitely large. This phenomena of the formation of microgels might have interfered with the experimental output resulting in the inaccurate mesh size determination.

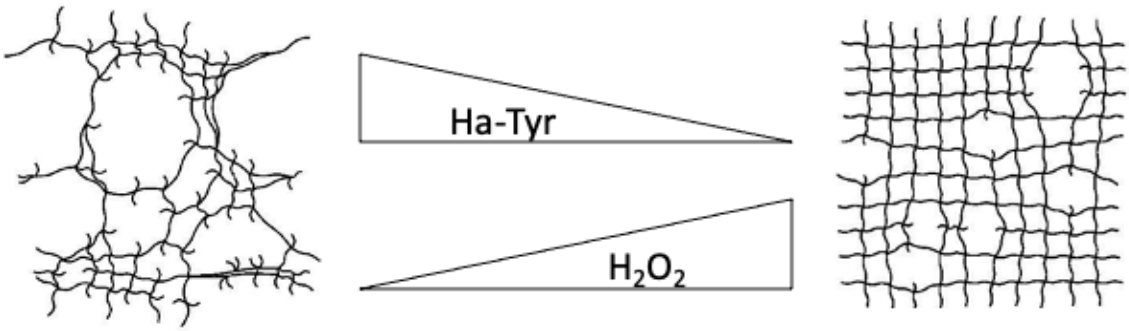

Figure 21: A schematic illustration of the effect of H_2O_2 and polymer concentration on the crosslinking density of Ha-Tyr based hydrogels causing differences in mesh sizes.

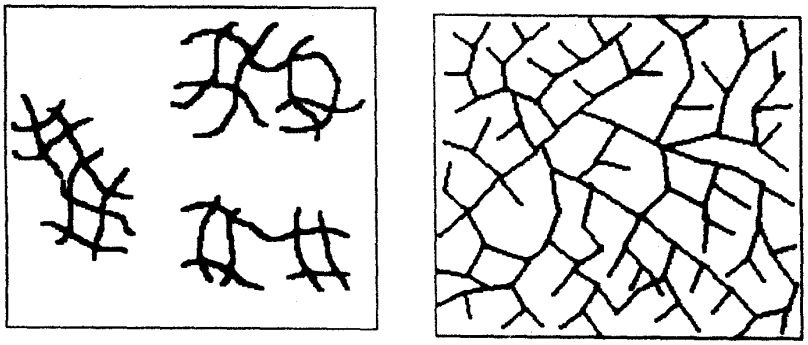

Figure 22: A schematic representation of the formation of unconnected polymer networks on one side and the formation of one big polymer network on the other side depending on the amount of crosslinks formed within the entire gel [67].

Due to insufficient precision in ξ determination, complete uncoupling of the gel stiffness and mesh size was not achieved. But the used unique approach for uncoupling gel stiffness and mesh size revealed the distribution of gel conditions, which was unknown before. Using both ξ estimation techniques for uncoupling yielded similar gel distribution when plotting the gel stiffness against the mesh size indicated that gel conditions having matching material properties could be achieved utilizing the methodology. However, to successfully evaluate the effect of stiffness while maintaining comparable mesh size, improvement in the ξ determination is required. In future investigations, it might be possible to improve the precision of mesh size estimation via the Flory-Rehner model by increasing the sample volume. A bigger sample volume could improve the determination of the swelling ratio resulting in a more precise estimation of the mesh size. Another possibility is the use of a diffusion-based technique such as fluorescent recovery after photobleaching (FRAP) for mesh size determination [63]. Different size of fluorescein-labelled dextran molecules will be photobleached to measure the fluorescence recovery time for the determination of the mesh size [63]. Our calculated mesh sizes could be used as a starting point for the experimental setup to decide which particle sizes should be used for the mesh size determination. For mesh size determination, a microscopic based technique such as a cryogenic-temperature scanning electron microscopy (cryo-SEM) could be used [68]. Preliminary work performed for the optimization of cryosectioning (appendix H) could be used as starting point for the cryosectioning procedure necessary for this particular technique.

The selected gel conditions (1.5% 600, 3.5% 300 and 3.5% 600) were used to investigate the effect of gel stiffness, H_2O_2 concentration and polymer concentration on the chondrogenic potential and matrix deposition of cartilage-like tissue. Therefore, MSCs were encapsulated and cultured in full chondrogenic differentiation medium for up to 14 days. Chondrogenesis took place in all tested hydrogels, as indicated through the gene expression levels of *SOX9, ACAN*, and *COL2A1*. Repeatedly, gel condition 3.5% 600 showed a trend towards lower gene expression level when compared to gel conditions 1.5% 600 and 3.5% 300 indicating towards reduced chondrogenic potential with increasing gel stiffness. This finding supports the work of other studies in this area linking substrate stiffness with the chondrogenic potential of MSCs [39, 41, 19]. To develop a full picture of the chondrogenic potential of MSCs within these gel conditions, additional studies investigating the cartilage-like matrix deposition are needed. This type of data could be obtained via histological staining for aggrecan deposition and immunohistochemical staining for collagen type II deposition. Preliminary work performed for the optimization of cryosectioning (appendix H) could be used as starting point for the sectioning procedure required prior to histological and immunohistochemical staining.

Another possibility is the use of biochemical assays to measure quantitatively the matrix deposition of cartilage-like tissue. One interesting finding from the biochemical assay for GAG deposition per cell is that gel condition 3.5% 300 showed a significantly higher GAG deposition per cell when compared to the gel conditions crosslinked with 600 µM of H_2O_2. This result may be explained by our previously mentioned theory regarding the effect of polymer and H_2O_2 concentration on the crosslinking density (fig. 21). Increasing the polymer concentration while maintaining a similar H_2O_2 concentration for crosslinking increases the likelihood of potential crosslinking points within the gel resulting in a lower crosslinking density within the gel. According to this theory, within this series of gel condition 3.5% 300 should yield the lowest crosslinking density, whereas, gel condition 1.5% 600 should yield the highest crosslinking density. The more disconnected polymer network, due to the lower crosslinking density, enables contraction of the gel by the cells resulting in the formation of cell aggregates [52]. Cell aggregate creates regions with a high cellular density which favours chondrogenic differentiation of MSCs and ultimately the cartilage matrix deposition [52]. From microscopic observation at day 7 (appendix I), higher numbers of cell aggregates were seen in the gel conditions having a polymer concentration of 3.5% w/v Ha-Tyr when compared to gel condition 1.5% 600. Additionally, our pilot study regarding the effect of cell density (appendix J) showed an increased expression level of chondrogenic markers *SOX9, ACAN* and *COL2A1* with increasing cell density, supporting the positive effect of higher cell density on the chondrogenic differentiation potential for MSCs. Additionally, previous studies have reported reduced MSCs metabolic activity with increasing concentration of H_2O_2 [50, 69]. The combination of findings proves some support for the premise that difference in crosslinking density, as a consequence of the difference in H_2O_2 concentration, rather than gel stiffness may function as the driving force for ECM deposition of cartilage-like tissue in Ha-Tyr based hydrogels.

A similar observation of reduced ECM deposition with increasing crosslinking density was observed in the study of Vainieri et al. (2020) [46]. However, no difference was detected at the expression level for *COL2A1.* This mismatch between immunohistological staining and gene expression levels for collagen type II may have been the response to the difference in environmental cues. As a response to the different material properties, the expression of levels for ECM remodeling genes like *MMPs* were regulated via mechanotransductional pathways [54]. Expression levels for ECM remodeling genes at day 28, showed a general trend towards higher gene expression levels for *MMPs* with increasing crosslinking density.

In particular, *MMP1* and *MMP3* showed a strong modulation with increasing crosslinking density at day 28. As a consequence of the high crosslinking density, the diffusivity for nutrients might be restrained when compared to lower crosslinking density regions. As a response, MSCs might enhance their gene expression levels for *MMP1* and *MMP3.* MMP-3 is known to activate the precursor of MMP-1 and degrades collagen as well [70, 71]. The higher expression levels may result in more active MMP-1 and MMP-3, which enables the remodeling of the ECM to improve nutrient diffusivity. The activity of MMPs as a response to impaired nutrient diffusivity may explain some of the observed difference in histological staining. For future experiments, a diffusion-based technique like FRAP in combination with silencing the genes for *MMP1* and *MMP3* could be used to evaluate this hypothesis.

Comparison of the expression patterns of genes involved in matrix remodelling like *MMPs*, *TIMPs*, and *ADAMTSs* at day 14 to the once at day 28, showed alterations in the expression pattern across the different gel conditions. *MMP1, MMP13* and *MMP14* showed a trend towards higher expression with lower crosslinking density at day 14, while this trend changed towards a higher expression level for these genes with increasing crosslinking density at day 28. This change in expression pattern may have been the consequence of MSC differentiation towards chondrocytes [72]. According to Assis-Ribas et al. (2018) [72], MSCs differentiation is a process that occurs in two phases. The first phase, also called commitment, is characterized by the decision of the cell towards a specific cell phenotype depending on the differentiation triggers. Once MSCs are committed, the differentiation will proceed even in absence of differentiation triggers. The second phase, also called maturation, involves morphological changes to differentiate into the committed cell type (in our case chondrocytes) [72]. Knowing that chondrocytes do have a round cell morphology, increased production of MMP-13 may help MSCs during the late stage of chondrogenic differentiation to keep their round morphology by degrading attachment points to the ECM [55, 73]. After maturation, the expression of MMP is only required for the remodeling of the ECM. Therefore, the expression level may reduce at later time points. This potential explanation for changing expression pattern in *MMP13* might also be true for *MMP1* and *MMP14*. But no supporting evidence has been found in literature. Another possibility might be that hydrogel degradation results in changing mechanical properties over time within the gel [56]. These changes in mechanics may affect cellular responses resulting in mechanotransductional responses by altering the gene expression level of ECM remodelling genes like *MMP1, MMP13*, and *MMP14*. Material characterization of gels embedded with cells at serial time points may help to reveal the relation between changing MMP expression patterns over time.

While *MMP1* and *MMP3* showed the strongest modulation over the different gel conditions, *MMP2* showed the highest expression level independently from the gel conditions. Previous studies have shown a positive correlation between *MMP2* expression and the chondrogenic potential of MSCs [55, 74, 75]. Silencing of *MMP2* expression inhibited chondrogenic differentiation and therefore is stated as being an important gene for chondrogenic differentiation [55, 74, 75]. The functionality of MMP-2 (also known as gelatinase) has been associated with the removal of fragments of the ECM [55, 74, 75]. Their proteolytic activity does not harm intact collagen networks but only degrades fragmented collagen networks as a consequence of damaged ECM [75]. As a consequence of the high expression level in combination with The expression of *MMP2* can be used as an additional chondrogenic marker to validate chondrogenic differentiation within MSCs.

5

FUTURE RECOMMENDATION

This thesis aimed to evaluate the effect of material properties on the chondrogenic potential and matrix deposition of cartilage like tissue in MSCs cultured in Ha-Tyr hydrogels. The experimental outputs resulted in the conformation of existing literature as well as in the development of new theories. Furthermore, it revealed some weaknesses of this study that needs improvement in future studies as well as new theories and hypothesis that requires further investigation to understand how material properties affect cellular responses.

First of all, improved mesh size determination is needed. This study was limited by the absence of gel conditions having matching ξ with significantly different G' and limited the complete uncoupling of the mesh size and gel stiffness from each other. In future studies, methods like FRAP and cryoSEM may be used for the determination of ξ within the gel conditions. Our estimation of the mesh size may function as the starting point to decide which size of particles may be suitable for estimating the mesh size within the hydrogel constructs.

Secondly, an important material property that has not been investigated within this study is the degradation rate of Ha-Tyr hydrogels. Hydrogel degradation results in an alteration in mechanical properties within the gel over time, which may affect cellular behaviour over time. Loss in mass of the gel over time as well as rheological measurements at serial time points may reveal some of the cellular responses to changes in mechanical properties over time.

Our study has illustrated that both H_2O_2 concentration as well as polymer concentration can be used as a tunable parameter for gel stiffness. Additional parameters that have been mentioned as a tunable parameter for Ha-Tyr hydrogels are the DS_{mol} (%) and HRP concentration. In literature, all the studies related to the tunability of Ha-Tyr hydrogel material properties are limited to a combination of the two of the previously mentioned parameters. No study has been identified in literature evaluating the dependency of three or more of the previously mentioned tunable parameters on each other. Extending the gel stiffness characterization by including a third tunable parameter such as HRP concentration may improve the understanding of the tunability characteristics of Ha-Tyr hydrogels. Repeating the gel stiffness characterization at different HRP concentrations will yield a 3D plot for gel stiffness and a better characterization of Ha-Tyr hydrogels.

A further study could also assess the effect of inclusion of cells on the material properties. All material characterizations were performed in cell-free hydrogels. The inclusion of cells may result in slight changes in material properties. Therefore, material characterization of gels embedded with cells may give a better representation of the actual forces experienced by

cells. Switching from measurements at global scale via rheology towards measurements at local scale via nano-indentation would also improve the understanding of the actual forces experienced by cells.

Another direction for future research is the development of a computational model for gel stiffness of Ha-Tyr hydrogels. Using the model, a prediction of gel stiffness could be achieved by varying the polymer concentration and H_2O_2 concentration independently from each other. The model could be extended by the inclusion of HRP concentration-related data points for further improvement of the model. After improved mesh size determination, a computational model for the mesh size could be made. The same tunable parameters could be included as stated before. The study of Campbell et al. (2020) [76] could be used as starting point for the model. They developed a computational model capable of predicting the mesh size in alginate-based hydrogels [76].

The question raised by this study is at the translational level of the ECM remodelling proteins. During this study, gene expression levels for ECM remodeling genes like *MMPs, TIMPs* and *ADAMTSs* were measured. However, no investigation was performed at the protein translational level. For instance, the turnover of collagen depends on the overall collagen production and collagenolytic activity within the construct [77]. This collagenolytic activity on his turn depends on the balance between the amount of active MMP enzymes, TIMPs, and other enzyme activators like MMP-3 [77]. Measurements at the gene expression level gave an indication of which genes were expressed as a response to certain stimuli. But it does not indicate how much of each gene was translated into a functional protein. The obtained gene expression level data helps to identify potential candidates that may have played a role in the observed histological data. But protein quantification data would help to identify to which extent each enzyme was responsible for the observed histological difference.

More broadly, research is also needed to include donor variability as well as serial time points. Each donor may respond slightly different to the same experimental setup, which yields some variance in the experimental outcome. This variance is used to estimate the general response of cells to the experimental setup. If a single donor is used for the experimental setup, no statements could be made regarding the general cellular response to the experimental setup. Therefore, it may bias the experimental outcome.
Additional time points will help reveal the responsiveness of MSCs to the dynamic conditions experienced by cells.

Finally, interesting will the lower the TGF-β concentration used in the chondrogenic medium to unmask the effect material properties on chondrogenic differentiation. By reducing the TGF-β concentration the chemical cue to direct cell differentiation will be lowered. As a result, smaller alterations in gene expression or matrix deposition may become more noticeable. A first pilot study using alginate beads with different concentration of TGF-β concentration (appendix K) could be used as a starting point.

6

CONCLUSION

The engineering of tunable hydrogels like Ha-Tyr opens the possibility to tailor hydrogel material properties to control and regulate cellular responses in MSCs via mechanotransduction pathways [51, 57]. However, the interconnectivity of material properties in hydrogels by the crosslinking density limits the identification of chondrogenic differentiation cues [39, 41, 42, 19]. Therefore, knowledge is needed of the effect of isolated material properties on the chondrogenic potential of MSCs. This project was undertaken to evaluate the effects of substrate stiffness and mesh size on the chondrogenic differentiation potential of MSCs. The evidence from this study confirmed that the gel stiffness of Ha-Tyr based hydrogels is polymer concentration and H_2O_2 concentration dependent. Adjusting these two parameters independently from each other, different gel conditions having matching bulk stiffness could be achieved. Finding gel conditions with matching gel stiffness opened the possibility to evaluate the effect of isolated material properties, like mesh size, on the chondrogenic potential of MSCs.

Unfortunately, the mesh size determination was not precise enough for complete uncoupling of the gel stiffness and mesh size from each other. In spite of its limitations, the findings indicate that the mesh size shows a trend towards larger mesh size with increasing polymer concentration and lower H_2O_2 concentration. As a potential mechanism for this phenomenon, the likelihood of potential crosslinking points resulting in different crosslinking densities has been addressed. In particular, at low crosslinking density conditions, it may result in the formation of unconnected or branched polymer networks. The natural progression of this work is to analyze the spatial distribution of the polymer network and their connectivity using techniques like cryoSEM and FRAP.

Translation of the effect of material properties on the chondrogenic potential of MSCs indicated towards reduced cartilage-like matrix deposition with increasing crosslinking density. These findings suggest that in general the matrix deposition of cartilage-like tissue is driven by the crosslinking density rather than gel stiffness. Lower crosslinking density gel conditions enabled contraction of gels for the formation of cell aggregates that showed a beneficial effect on cartilage-like matrix deposition. As a consequence of the high crosslinking density, the diffusivity for nutrients might be restrained when compared to lower crosslinking density regions. As a response, MSCs might enhance their gene expression levels for *MMP1* and *MMP3*.

Our unique approach based on the tunability of hydrogels to uncouple gel stiffness and mesh size from each other opened the possibility to evaluate the effect of isolated material properties on the chondrogenic potential of MSCs. The information obtained helps to identify mechanotransductional regulators that could be used for the development of smart biomaterials for tissue engineering purposes. Ultimately, it brings us a step closer towards the development of functional cartilage tissue that could be used as a possible therapeutic strategy for OA patients.

7

REFERENCE

[1] A. J. Sophia Fox, A. Bedi and S. A. Rodeo, "The basic science of articular cartilage: Structure, composition, and function," *Sports Health,* vol. 1, no. 6, pp. 461-469, 2009.

[2] G. Pattapa, J. Zellner, B. Johnstone, D. Docheva and P. Angela , "Cells under pressure - the relationship between hydrostatic pressure and mesenchymal stem cell chondrogenesis," *European cells & materials,* vol. 37, pp. 360-381, 2019.

[3] R. L. Davies and N. J. Kuiper, "Regenerative Medicine: A Review of the Evolution of Autologous Chondrocyte Implantation (ACI) Therapy," *Bioengineering,* vol. 6, no. 1, pp. 1-16, 2019.

[4] A. Mobasheri, S. D. Carter, P. Martin-Vasallo and M. Shakibaei, "Integrins and stretch activated ion channels; putative components of functional cell surface mechanoreceptors in articular chondrocytes," *Cell Biology International,* vol. 26, no. 1, pp. 1-18, 2002.

[5] R. L. Mauck, B. A. Byers, X. Yuan and R. S. Tuan, "Regulation of cartilaginous ECM gene transcription by chondrocytes and MSCs in 3D culture in response to dynamic loading," *Biomechanics and Modeling in Mechanobiology,* vol. 6, pp. 113-125, 2007.

[6] T. Nishida and S. Kubota, "Roles of CCN2 as a mechano-sensing regulator of chondrocyte differentiation," *Japanese Dental Science Review,* vol. 56, no. 1, pp. 119-126, 2020.

[7] H. Akkiraju and A. Nohe, "Role of Chondrocytes in Cartilage Formation, Progression of Osteoarthritis and Cartilage Regeneration," *Journal of Developmental Biology,* vol. 3, no. 4, pp. 177-192, 2015.

[8] F. Safshekan, M. Tafazzoli-Shadpour, M. A. Shokrgozar, N. Haghighipour, R. Mahdian and A. Hemmati, "Intermittent Hydrostatic Pressure Enhances Growth Factor-Induced Chondroinduction of Human Adipose-Derived Mesenchymal Stem Cells," *Artifical Organs,* vol. 35, no. 12, pp. 1065-1071, 2012.

[9] J. C. Silva, C. S. Moura, G. Borrecho, A. P. Alves de Matos, C. L. da Silva, J. M. Cabral, P. J. Bártolo and F. C. Ferreira, "Extruded Bioreactor Perfusion Culture Supports the Chondrogenic Differentiation of Human Mesenchymal Stem/Stromal Cells in 3D Porous Poly(-Caprolactone) Scaffolds," *Biotechnology,* vol. 15, no. 2, pp. 1-14, 2020.

[10] C. R. Harrell, B. S. Markovic, C. Fellabaum, A. Arsenijevic and V. Volarevic, "Mesenchymal stem cell-based therapy of osteoarthritis: Current knowledge and future perspectives," *Biomedicine & Pharmacotherapy,* vol. 109, pp. 2318-2326, 2019.

[11] D. Chen, J. Shen , W. Zhoa, T. Wang, L. Han, J. L. Hamilton and H.-J. Im, "Osteoarthritis: toward a comprehensive understanding of pathological mechanism," *Bone Research,* vol. 5, pp. 1-13, 2017.

[12] R. Zhang, J. Ma, J. Han, W. Zhang and J. Ma, "Mesenchymal stem cell related therapies for cartilage lesions and osteoarthritis," *American Journal of Translational Research,* vol. 11, no. 10, pp. 6275-6289, 2019.

[13] A. C. Thomas, T. Hubbard-Turner, E. A. Wikstrom and R. M. Palmieri-Smith, "Epidemiology of Posttraumatic Osteoarthritis," *Journal of athletic training,* vol. 52, no. 6, pp. 491-496, 2017.

[14] L. J. Sandell and T. Aigner, "Articular cartilage and changes in Arthritis: Cell biology of osteoarthritis," *Arthritis Research & Therapy,* vol. 3, pp. 107-113, 2001.

[15] "Chronic diseases and health promotion," World Health Organization, [Online]. Available: https://www.who.int/chp/topics/rheumatic/en/. [Accessed 7 2 2021].

[16] N. Nasiri, S. Hosseini, M. Alini, A. Khademhosseini and M. Baghaban Eslaminejad, "Targeted cell delivery for articular cartilage regeneration and osteoarthritis treatment," *Drug Discovery Today,* vol. 24, no. 11, pp. 2212-2224, 2019.

[17] "Overview osteoarthrithis," NHS, 19 8 2019. [Online]. Available: https://www.nhs.uk/conditions/osteoarthritis/ . [Accessed 7 2 2021].

[18] A. Mobasheri, G. Kalamegam, G. Musumeci and M. E. Batt, "Chondrocyte and mesenchymal stem cell-based therapies for cartilage repair in osteoarthritis and related orthopaedic conditions," *Maturitas,* vol. 78, no. 3, pp. 188-198, 2014.

[19] A. X. Sun, H. Lin, M. R. Fritch, H. Shen, P. G. Alexander, M. DeHart and R. S. Tuan, "Chondrogenesis of human bone marrow mesenchymal stem cells in 3-dimensional, photocrosslinked hydrogel constructs: Effect of cell seeding density and material stiffness," *Acta Biomaterialia,* vol. 58, pp. 302-311, 2017.

[20] R. Nerem, H. Sage, C. A. Kelley and L. A. McNicol, "Symposium summary," *Annals of the New York Academy of Sciences ,* vol. 961, no. 1, pp. 386-389, 2002.

[21] M. W. Kessler and D. A. Grande, "tissue engineering and cartilage," *organogenesis,* vol. 4, no. 1, pp. 28-32, 2008.

[22] R. Langer and J. P. Vacanti, "Tissue Engineering," *Science ,* vol. 261, no. 5110, pp. 920-926, 1993.

[23] S. Caddeo, M. Boffito and S. Sartori, "Tissue Engineering Approaches in the Design of Healthy and Pathological In Vitro Tissue Models," *Frontiers in Bioengineering and Biotechnology,* vol. 5, no. 40, 2017.

[24] A. Cochis, S. Grad, M. J. Stoddart, S. Faré, L. Altomare, B. Azzimonti, M. Alini and L. Rimondini, "Bioreactor mechanically guided 3D mesenchymal stem cell chondrogenesis using a biocompatible novel thermo-reversible methylcellulose-baed hydrogel," *Scientific Reports,* vol. 7:45018, pp. 1-12, 2017.

[25] Y.-N. Wu, Z. Yang, J. H. Hui, H.-W. Ouyang and E. H. Lee, "Cartilaginous ECM component-modification of the micro-bead culture system for chondrogenic differentiation of mesenchymal stem cells," *Biomaterials,* vol. 28, no. 28, pp. 4056-4067, 2007.

[26] O. Schätti, S. Grad, J. Goldhahn, Z. Li, M. Alini and M. J. Stoddart, "A combination of shear and dynamic compression leads to mechanically induced chondrogenesis of human mesenchymal stem cells," *European Cells and Materials ,* vol. 22, pp. 214-225, 2011.

[27] S. D. Thorpe, C. T. Buckley, A. J. Steward and D. J. Kelly, "European Society of Biomechanics S.M. Perren Award 2012: the external mechanical environment can override the influence of local substrate in determining stem cell fate," *Journal of Biomechanics,* vol. 45, no. 15, pp. 2483-2492, 2012.

[28] Y. Zhang, S. Chen and M. Pei, "Biomechanical signals guiding stem cell cartilage engineering: From molecular adapyion to tissue functionality," *European Cells and Materials,* vol. 31, pp. 59-78, 2016.

[29] J. Hoa, Y. Zhang, D. Jing, Y. Shen, G. Tang, S. Huang and Z. Zhoa, "Mechanobiology of mesenchymal stem cells: Perspective into mechanical induction of MSC fate," *Acta Biomaterialia,* vol. 20, pp. 1-9, 2015.

[30] K. Haase and A. E. Pelling, "Investigating cell mechanics with atomic force microscopy," *Journal of the royal society interface,* vol. 12, no. 104, pp. 1-16, 2015.

[31] L. Li, J. Eyckmans and C. S. Chen, "Designer biomaterials for mechanobiology," *Nature materials ,* vol. 16, pp. 1164-1168, 2017.

[32] P. M. Tsimbouri, "Adult Stem Cell Responses to Nanostimuli," *Journal of Functional Biomaterials,* vol. 6, pp. 598-622, 2015.

[33] D. Schumann, R. Kujat, M. Nerlich and P. Angele, "Mechanobiological conditioning of stem cells for cartilage tissue engineering," *Bio-Medical Materials and Engineering ,* vol. 16, pp. 37-52, 2006.

[34] V. Terraciano, N. Hwang, L. Moroni, H. B. Park, Z. Zhang, J. Mizrahi, D. Seliktar and J. Elisseeff, "Differential Response of Adult and Embryonic Mesenchymal Progenitor Cells to Mechanical Compression in Hydrogels," *Stem Cells ,* vol. 25, no. 11, pp. 2730-2738, 2007.

[35] B. Matthews, D. Overby, R. Mannix and D. Ingber, "Cellular adaptation to mechanical stress: Role of integrins, Rho, cytoskeletal tension and mechanosensitive ion channels," *Journal of Cell Science,* vol. 119, no. 3, pp. 508-518, 2006.

[36] C.-C. Lin and K. S. Anseth, "PEG hydrogels for the controlled release of biomolecules in regenerative medicine," *Pharmaceutical Research,* vol. 26, no. 3, pp. 631-643, 2009.

[37] M. S. Rehmann, K. M. Skeens, P. M. Kharkar, E. M. Ford, E. Maverakis, K. H. Lee and A. M. Kloxin, "Tuning and predicting mesh size and protein release from step growth hydrogels," *Biomacromolecules,* vol. 18, no. 10, pp. 3131-3142, 2017.

[38] R. P. Wool, "7 - Properties of Triglyceride-Based Thermosets," in *Bio-Based Polymers and Composites*, Academic Press, 2005, pp. 202-255.

[39] C. M. Murphy, A. Matsiko, M. G. Haugh, J. P. Gleeson and F. J. O'Brien, "Mesenchymal stem cell fate is regulated by the composition and mechanical properties of collagen–glycosaminoglycan scaffolds," *Journal of the mechanical behavior of biomedical materials,* vol. 11, pp. 53-62, 2012.

[40] M. Selig, J. C. Lauer, M. L. Hart and B. Rolauffs, "Mechanotransduction and Stiffness-Sensing: Mechanisms and Opportunities to Control Multiple Molecular Aspects of Cell Phenotype as a Design Cornerstone of Cell-Instructive Biomaterials for Articular Cartilage Repair," *International journal of Molecular Science,* vol. 21, no. 15, p. 5399, 2020.

[41] Y. Wu, Z. Yang, J. B. K. Law, A. Y. He, A. A. Abbas, V. Denslin, T. Kamarul, J. H. Hui and E. H. Lee, "The Combined Effect of Substrate Stiffness and Surface Topography on Chondrogenic Differentiation of Mesenchymal Stem Cells," *Tissue Engineering ,* vol. 23, no. 1, pp. 43-54, 2017.

[42] R. Goldshmid, S. Cohen, Y. Shachaf, I. Kupershmit, O. Sarig-Nadir, D. Seliktar and R. Wechsler, "Steric Interference of Adhesion Supports In-Vitro Chondrogenesis of Mesenchymal Stem Cells on Hydrogels for Cartilage Repair," *scientific reports,* vol. 5, pp. 1-13, 2015.

[43] L. Bian, C. Hou, E. Tous, R. Rai, R. L. Mauck and J. A. Burdick, "The influence of hyaluronic acid hydrogel crosslinking density and macromolecular diffusivity on human MSC chondrogenesis and hypertrophy," *Biomaterials,* vol. 34, pp. 413-421, 2013.

[44] D. J. Munoz-Pinto, A. S. Bulick and M. S. Hahn, "Uncoupled investigation of scaffold modulus and mesh size on smooth muscle cell behavior," *Journal of Biomedical Materials Research Part A,* vol. 90, no. 1, pp. 303-319, 2009.

[45] B. Grigoryan, *INVESTIGATION OF UNCOUPLED EFFECT OF MESH AND MODULUS ON MESENCHYMAL STEM CELL DIFFERENTIATION,* Texas: Texas A&M University, 2012.

[46] M. L. Vainieri, A. Lolli, N. Kops, D. D'Arti, D. Eglin, A. Yayon, M. Alini, S. Grad, K. Sivasubramaniyan and G. J. van Osch, "Evaluation of biomimetic hyaluronic-based hydrogels with enhanced endogenous cell recruitment and cartilage matrix formation," *Acta Biomaterialia,* vol. 101, pp. 293-303, 2020.

[47] C. A. Knuth, C. H. Kiernan, V. Palomares Cabeza, J. Lehmann, J. Witte-Bouma, D. ten Berge, P. A. Brama, E. B. Wolvuis, E. M. Strabbing, S. M. Koudstaal, R. Narcisi and E. Farrell, "Isolating paediatric mesenchymal stem cells with enhanced expansion and differentiation capabilities," *Tissue Engineering ,* vol. 24, no. 6, pp. 313-321, 2018.

[48] M. T. Punter, B. E. Vos, B. M. Mulder and G. H. Koenderink, "Poroelasticity of (bio)polymer networks during compression: theory and experiment," *Soft Matter,* vol. 16, pp. 1298-1305, 2020.

[49] J. B. Leach, K. A. Bivens, C. W. Patrick and C. E. Schmidt, "Photocrosslinked Hyaluronic Acid Hydrogels: Natural, Biodegradable Tissue Engineering Scaffolds," *Biotechnology and bioengineering,* vol. 82, no. 5, pp. 578-589, 2003.

[50] P. Behrendt, Y. Ladner, M. J. Stoddart, S. Lippross, M. Alini, D. Eglin and A. R. Armiento, "Articular Joint-Simulating Mechanical Load Activates Endogenous TGF-β in a Highly Cellularized Bioadhesive Hydrogel for Cartilage Repair," *The American journal of sports medicine,* vol. 48, no. 1, pp. 210-221, 2020.

[51] C. Loebel, T. Stauber, M. D'Este, M. Alini, M. Zenobi-Wong and D. Eglin, "Fabrication of Cell-Compatible Hyaluronan Hydrogels with a Wide Range of Biophysical Properties Through High Tyramine Functionalization," *Journal of Materials Chemistry B,* vol. 5, no. 12, pp. 2355-2363, 2017.

[52] W. S. Toh, T. C. Lim, M. Kurisawa and M. Spector, "Modulation of mesenchymal stem cell chondrogenesis in a tunable hyaluronic acid hydrogel microenvironment," *Biomaterials,* vol. 33, pp. 3835-3845, 2012.

[53] F. Lee, J. E. Chung and M. Kurisawa, "An injectable enzymatically crosslinked hyaluronic acid-tyramine hydrogel system with independent tunig of mechanical strength and gelation rate," *Soft Matter ,* vol. 4, pp. 880-887, 2008.

[54] F. Djouad, B. Delorme, M. Maurice, C. Bony, F. Apparailly, P. Louis-Plence, F. Canovas, P. Charbord, D. Noël and C. Jorgensen, "Microenvironmental changes during differentiation of mesenchymal stem cells towards chondrocytes," *Arthritis Research & Therapy,* vol. 9, no. 2, 2007.

[55] S. G. Almalki and D. K. Agrawal, "Effect of matrix metalloproteinases on the fate of mesenchymal stem cells," *Stem Cell Research & Therapy,* vol. 7, no. 1, 2016.

[56] S. R. Caliari and J. A. Burdick, "A practical guide to hydrogels for cell culture," *Nature methods,* vol. 13, no. 3, pp. 405-414, 2016.

[57] A. Abu-Hakmed, A. Kung, B. R. Mintz, S. Kamal, J. A. Cooper, X. L. Lu and L. Q. Wan, "Sequential gelation of tyramine-substituted hyaluronic acid hydrogels enhances mechanical integrity and cell viability," *Medical & biological engineering & computing,* vol. 54, no. 12, pp. 1893-1902, 2016.

[58] S. Moeinzadeh and E. Jabbari, "Gelation characterrisitic, physico-mechanical properties and degradation kinetics of micellar hydrogels," *European polymer journal,* vol. 72, pp. 566-576, 2015.

[59] L. Weng, X. Chen and W. Chen, "rheological Characterization of in situr Crosslinkable Hydrogels Formulated from Oxidized Dextran and N-Carboxyethyl Chitosan," *Biomacromolecules,* vol. 8, no. 4, pp. 1109-1115, 2007.

[60] A. Rajan, R. Pramanik, A. Narayanan and A. Arockiarajan, "Mechanics of viscoelastic buckling in slender hydrogels," *Matrials Research Express,* vol. 6, no. 5, pp. 1-21, 2019.

[61] F. Kan and L. Zheng , "Buckling Analysis of Soft Nanostructure in Nanoimprinting," *Chinese Physics Letters,* vol. 26, no. 12, pp. 1-4, 2009.

[62] L. P. Budnikova and A. N. Eryomin, "Synthesis and Properties of Horseradish Peroxidase Copolymers," *applied Biochemistry and Microbiology,* vol. 42, pp. 127-133, 2006.

[63] J. Karvinen, T. O. Ihalainen, M. T. Calejo and I. Jönkkäri, "Characterization of the microstructure of hydrazone crosslinked polysaccharide-based hydrogels through rheological and diffusion studies," *Materials Science & Engineering C,* vol. 94, pp. 1056-1066, 2019.

[64] F. Ganji, S. Vasheghani-Farahani and E. Vasheghani-Farahani, "Theoretical Description of Hydrogel Swelling: A Review," *Iranian Polymer Journal,* vol. 19, no. 5, pp. 375-398, 2010.

[65] D. Klinger and K. Landfester, "Stimuli-responsive microgels for the loading and relase of functional compounds: Fundamental concepts and applications," *Polymer,* vol. 53, pp. 5209-5231, 2012.

[66] H. Holback, Y. Yeo and K. Park, "Hydrogel swelling behavior and its biomedical applications," in *Biomedical Hydrogels*, Woodhead Publishing Limited , 2011, pp. 3-24.

[67] H. B. Bohidar, "Dynamics in thermoreversible polymer gels," *Current Science ,* vol. 88, no. 8, pp. 1008-1017, 2001.

[68] C. Marmorat, A. Arinstain, N. Koifman, Y. Talmon, E. Zussman and M. Rafailovich, "Cryo-Imaging of Hydrogels supermolecular Structure," *Scientific Reports,* vol. 6, 2016.

[69] R. A. Denu and P. Hematti, "Effects of Oxidative Stress on Mesenchymal Stem Cell Biology," *Oxidative medicine and cellular longevity,* pp. 1-9, 2016.

[70] M. Mathieu, M. Iampietro, P. Chuchana, D. Guérit, F. Djouad, D. Noël and C. Jorgensen, "Involvement of Angioopoietin-like 4 in Matrix Remodeling during Chondrogenic differentiation of Mesenchymal Stem Cells," *Journal of Biollogical Chemistry,* vol. 289, no. 12, pp. 8402-8412, 2014.

[71] S. Ye, P. Eriksson, A. Hamsten, M. Kurkinen, S. E. Humphries and A. M. Henney , "Progression of coronary atherosclerosis with a comoon genetic variant of the human stromelysin-1 promoter which resutls in reduced gene expression," *The Journal of Biological Chemistry,* vol. 271, no. 22, pp. 13055-13060, 1996.

[72] T. Assis-Ribas, M. F. Forni, S. M. Winnischofer, M. C. Sogayar and M. Trombetta-Lima, "Extracellular matrix dynamics during mesenchymal stem cells differentiation," *Developmental Biology,* vol. 437, no. 2, pp. 63-74, 2018.

[73] S. Kondo, C. Shukunami, Y. Morioka, N. Matsumoto, R. Takahashi, J. Oh, T. Atsumi, A. Umezawa, A. Kudo, H. Kitayama, Y. Hiraki and M. Noda, "Dual effects of the membrane-anchored MMP regulator RECK on chondrogenic differentiaiton of ATDC5 cells," *Journal of Cell Science,* vol. 120, no. 5, pp. 849-857, 2007.

[74] Y. Arai, S. Park, B. Choi, K.-W. Ko, W. C. Choi, J.-M. Lee, D.-W. Han, H.-K. Park, I. Han and S.-H. Lee, "Enhancement of Matrix Metalloproteinase-2 (MMP2) as a Potnetial Chondrogenic Marker during Chondrogenic Differentiation of Human Adipose-Derived Stem Cells," *International Journal of Molecular Sciences,* vol. 17, no. 6, p. 963, 2016.

[75] J. Denkovskij, E. Bagdonas, I. Kusleviciute, Z. Mackiewicz, A. Unguryte, N. Porvaneckas, S. Fleury, V. Algirdas, C. Jorgensen and E. Bernotiene, "Paracrine Potential of the Human Adipose Tissue-Derived Stem Cells to Modulare Balance between Matrix Metalloproteinases and Their Inhibitors in the Osteoarthritic Cartilage In Vitro," *Stem Cells international,* pp. 1-13, 2017.

[76] K. T. Campbell, K. Wyscozynski, D. J. Hadley and E. A. Silva, "Computational-Based Design of Hydrogels with Predictable Mesh properties," *ACS Biomaterials Science & Engineering ,* vol. 6, no. 1, pp. 308-319, 2020.

[77] W. C. Duivenvoorden, H. W. Hirte and G. Singh, "Quantification of matrix metalloproteinase activity in plasma of patients enrolled in a BAY 12-9566 phase I study," *International Journal of Cancer,* vol. 91, no. 6, pp. 857-862, 2001.

[78] V. P. Mane, M. A. Heuer, P. Hillyer, M. B. Navarro and R. L. Rabin, "Systematic Method for Determining an Ideal Housekeeping Gene for Real-Time PCR Analysis," *Journal of Biomolecular Techniques,* vol. 19, no. 5, pp. 342-347, 2008.

[79] I. A. Ho, K. Y. Chan, W.-H. Ng, C. M. Guo, K. M. Hui, P. Cheang and P. Y. Lam, "Matrix Metalloproteinase 1 Is Necessary for the Migration of Human Bone Marrow-Derived Mesenchymal Stem Cells Toward Human Glioma," *Stem Cells,* vol. 27, pp. 1366-1375, 2009.

[80] A. B. inc., *Lifeink 200 Instructions - Mixing Cells to the Collagen Bioink [Video]. YouTube. https://www.youtube.com/watch?v=hY9O6Ozrfis,* www.youtube.com, 2017.

A

APPENDIX

An overview of the preprogrammed setting used for rheological measurements (table A1).

Table A1: An overview of the preprogrammed rheometer set-up used to characterize each hydrogel sample.

Characterization	Applied Values			Sampling	
	Frequency (Hz)	Target shear strain (%)	Gap (mm)	Number	Interval (sec)
Gelation kinetics:					
Oscillation Single Frequency	1.00	0.50		720	5.0
Frequency sweep test:					
Oscillation Frequency Table	0.1 - 100	0.50		20	0.01 - 10.0
Serial set of compression:					
Set Gap			0.4		
Oscillation Single Frequency (1)	1.00	0.50		1000	0.10
Set Gap (1)			0.5		
Oscillation Single Frequency (2)	1.00	0.50		1000	0.10
Set Gap (2)			0.4		
Oscillation Single Frequency (3)	1.00	0.50		1000	0.10
Set Gap (3)			0.50		
Oscillation Single Frequency (4)	1.00	0.50		1000	0.10
Serial set of decompression:					
Set Gap (4)			0.40		
Oscillation Single Frequency (5)	1.00	0.50		1000	0.10
Set Gap (5)			0.50		
Oscillation Single Frequency (6)	1.00	0.50		1000	0.10
Set Gap (6)			0.40		
Oscillation Single Frequency (7)	1.00	0.50		1000	0.10
Set Gap (7)			0.50		
Oscillation Single Frequency (8)	1.00	0.50		1000	0.10

B

APPENDIX

MatLab code that has been used to analyse the data obtained from the rheology measurement.

```
clear all;
close all;
clc;

%% import data
All_raw_data = xlsread('measurement 5 3.5% 600uM.xls');
Raw_data_gelation = All_raw_data(1:720,:);
Raw_frequency_sweep = All_raw_data(721:781,:);
Raw_Compression1_data = All_raw_data(782:993,:);

Time_action_gelation = Raw_data_gelation(:,4);
Storage_gelation = Raw_data_gelation(:,9);

Freq_sweep = Raw_frequency_sweep(:,6);
Freq_sweep_store_mod = Raw_frequency_sweep(:,9);

Time_action_compression = Raw_Compression1_data(:,4);
Normal_force_compression = Raw_Compression1_data(:,11);
Gap_compression = Raw_Compression1_data(:,12);

%% Parameters
a = 10*10^-3;           %[m] 20mm diameter of compressor
h = 0.5*10^-3;          %[m] 0.5 mm height of the gel
n = 0.6913*10^-3;       %

%% Gelation curve
figure
scatter(Time_action_gelation,Storage_gelation);
title('Storage modulus VS time','FontSize', 20);
xlabel('Time (s)','FontSize', 14);
ylabel('Storage modulus (Pa)','FontSize', 14);
grid on

final_value_storage_Gelation = Storage_gelation(end,1)
Maximal_G_gelation = max(Storage_gelation)

difference = (Maximal_G_gelation -
final_value_storage_Gelation)/final_value_storage_Gelation*100
threshold = 15;
```

```
if (difference < threshold)
    disp('Drop in storage modulus is below the threshold value')
else
    disp('Drop in storage modulus is above the threshold value')
end

%% Frequency sweep
figure
scatter(Freq_sweep,Freq_sweep_store_mod);
title('Storage modulus VS Frequency','FontSize', 20);
xlabel('Frequency(Hz)','FontSize', 14);
ylabel('Storage Modulus (Pa)','FontSize', 14);
grid on

figure
loglog(Freq_sweep,Freq_sweep_store_mod);
title('Storage modulus VS Frequency','FontSize', 20);
xlabel('Frequency(Hz)','FontSize', 14);
ylabel('Storage Modulus (Pa)','FontSize', 14);
grid on

Gelation time
subplot(2,1,1);
plot(Storage_gelation, 'b.-', 'Markersize', 11);
grid on;
xlabel('Index')
ylabel('Y Signal');

gel=diff(Storage_gelation);

subplot(2,1,2);
plot(gel, 'b.-', 'Markersize', 11);
grid on;
xlabel('Index')
ylabel('Y Signal');
gelpoint=find(gel<0.2);

%% Rescaling normal force first compression part
A = Normal_force_compression(1,1);
Rescaled_normal_force = Normal_force_compression - A;

figure
scatter(Time_action_compression,Rescaled_normal_force);
title('Normal force VS time','FontSize', 14);
xlabel('Time (s)','FontSize', 14);
ylabel('Normal force (N)','FontSize', 14);
grid on

%% First Compressive strain
B = Gap_compression(1,1);
C = B - Gap_compression;
Compressive_strain = C./B;
Coefficients = polyfit(Time_action_compression, Compressive_strain, 1);
Strain_rate = Coefficients(1);
Strain =
Strain_rate*Time_action_compression(length(Time_action_compression),1);

figure
scatter(Time_action_compression,Compressive_strain);
title('Compressive strain VS time','FontSize', 20);
xlabel('Time (s)','FontSize', 14);
```

```
ylabel('Compressive strain','FontSize', 14);

%% Stress VS Strain first one
Compressive_stress = Rescaled_normal_force./(pi*a^2);
e = 1/8*Strain_rate*n*a^2;

figure
scatter(Compressive_strain,Compressive_stress)
title('Stress VS strain curve','FontSize', 20)
xlabel('Compressive strain','FontSize', 14)
ylabel('Compressive stress','FontSize', 14)

%% Calculation mesh size
Compressive_stress = Rescaled_normal_force./(pi*a^2);

figure
scatter(Time_action_compression,Compressive_stress)
title('Stress VS time curve','FontSize', 20)
xlabel('Time','FontSize', 14)
ylabel('Compressive stress (Pa)','FontSize', 14)
grid on

linear_time_20 = Time_action_compression(42:200,1);
linear_force_20 = Rescaled_normal_force(42:200,1);

linear_time_40 = Time_action_compression(82:200,1);
linear_force_40 = Rescaled_normal_force(82:200,1);

linear_time_60 = Time_action_compression(122:200,1);
linear_force_60 = Rescaled_normal_force(122:200,1);

linear_time_80 = Time_action_compression(162:200,1);
linear_force_80 = Rescaled_normal_force(162:200,1);

X_20 = [ones(length(linear_time_20),1) linear_time_20];
X1_20 = [ones(length(Time_action_compression),1) Time_action_compression];
b_20 = X_20\linear_force_20;
intercept_20 = b_20(1,1)
slope_20 = b_20(2,1)
yCalc2_20 = X_20*b_20;
yCalc3_20 = X1_20*b_20;

X_40 = [ones(length(linear_time_40),1) linear_time_40];
X1_40 = [ones(length(Time_action_compression),1) Time_action_compression];
b_40 = X_40\linear_force_40;
intercept_40 = b_40(1,1)
slope_40 = b_40(2,1)
yCalc2_40 = X_40*b_40;
yCalc3_40 = X1_40*b_40;

X_60 = [ones(length(linear_time_60),1) linear_time_60];
X1_60 = [ones(length(Time_action_compression),1) Time_action_compression];
b_60 = X_60\linear_force_60;
intercept_60 = b_60(1,1)
slope_60 = b_60(2,1)
yCalc2_60 = X_60*b_60;
yCalc3_60 = X1_60*b_60;

X_80 = [ones(length(linear_time_80),1) linear_time_80];
X1_80 = [ones(length(Time_action_compression),1) Time_action_compression];
```

```
b_80 = X_80\linear_force_80;
intercept_80 = b_80(1,1)
slope_80 = b_80(2,1)
yCalc2_80 = X_80*b_80;
yCalc3_80 = X1_80*b_80;

Rsq_20 = 1 - sum((linear_force_20 - yCalc2_20).^2)/sum((linear_force_20 -
mean(linear_force_20)).^2)
Rsq_40 = 1 - sum((linear_force_40 - yCalc2_40).^2)/sum((linear_force_40 -
mean(linear_force_40)).^2)
Rsq_60 = 1 - sum((linear_force_60 - yCalc2_60).^2)/sum((linear_force_60 -
mean(linear_force_60)).^2)
Rsq_80 = 1 - sum((linear_force_80 - yCalc2_80).^2)/sum((linear_force_80 -
mean(linear_force_80)).^2)


figure
scatter(Time_action_compression,Rescaled_normal_force,'k');
hold on
plot(Time_action_compression,yCalc3_20,'r','LineWidth', 2)
hold on
plot(Time_action_compression,yCalc3_40,'b','LineWidth', 2)
hold on
plot(Time_action_compression,yCalc3_60,'m','LineWidth', 2)
hold on
plot(Time_action_compression,yCalc3_80,'c','LineWidth', 2)
title('Linear least sequare fitting' ,'FontSize', 20)
xlabel('Time (s)','FontSize', 14);
ylabel('Normal force (N)','FontSize', 14)
legend('Data','Linear least square fit 20-100 sec','Linear least square fit
40-100 sec','Linear least square fit 60-100 sec','Linear least square fit
80-100 sec','Location','best','FontSize', 14);
grid on

k_20=(n*a^4*pi*Strain_rate)/(8*intercept_20);
mesh_size_20 = sqrt(k_20)*10^9

k_40=(n*a^4*pi*Strain_rate)/(8*intercept_40);
mesh_size_40 = sqrt(k_40)*10^9

k_60=(n*a^4*pi*Strain_rate)/(8*intercept_60);
mesh_size_60 = sqrt(k_60)*10^9

k_80=(n*a^4*pi*Strain_rate)/(8*intercept_80);
mesh_size_80 = sqrt(k_80)*10^9

av_intercept= (intercept_20+intercept_40+intercept_60+intercept_80)/4

K_average=(n*a^4*pi*Strain_rate)/(8*av_intercept);
av_mesh = sqrt(K_average)*10^9

%% Mesh size calculaton automated
intercept = zeros(121,1);
slope = zeros(121,1);
for i = 42:162  %loop between 20-100 untill 80-100 sec
    linear_time = Time_action_compression(i:200,1);
    linear_force = Rescaled_normal_force(i:200,1);

    X = [ones(length(linear_time),1) linear_time];
X1 = [ones(length(Time_action_compression),1) Time_action_compression];
b = X\linear_force;
```

```
intercept(i-41,1) = b(1,1);
slope(i-41,1) = b(2,1);
end

intercept_filter = zeros(121,1);

for i= 1: length (intercept_filter)
    if  (intercept(i,1) > 0);
        intercept_filter(i,1) = 1;
    else
         intercept_filter(i,1) = 0;
    end
end

slope_filter = zeros(121,1);

for i= 1: length (slope_filter)
    if  (slope(i,1) > 0)
        slope_filter(i,1) = 1;
    else
         slope_filter(i,1) = 0;
    end
end

combined_filters = [intercept_filter slope_filter];
sum_filters = sum(combined_filters,2);

idx = find(sum_filters == 2);
Mesh_size_filter = zeros(length(idx),1);

for i = 1: length(idx)
   AA = idx(i,1);
   Mesh_size_filter(i,1) = intercept (AA,1);
end

av_filter_intercept = sum(Mesh_size_filter)/ length(idx)

K_average_filter=(n*a^4*pi*Strain_rate)/(8*av_filter_intercept);
av_mesh_filter = sqrt(K_average_filter)*10^9
```

C

APPENDIX

To quantify the relative gene expression level, each measured gene expression was normalized against a housekeeper gene(s). Housekeeper genes are constitutive genes required for maintenance within cells. Therefore, it is assumed that housekeeper genes are expressed at similar expression levels across different experimental conditions [78]. Using the same amount of RNA as input, we can assume that a smaller variance in gene expression for the housekeeper genes will better compare gene expression patterns across other conditions. The measured Cq value is dependent on the threshold value used during the measurement. A higher Cq value indicates a lower expression level for the gene. Cq values higher than 36 were considered as not expressed. cDNA samples obtained from MSCs embedded in Ha-Tyr hydrogels with 3.5% of polymer concentration and crosslinked with either 150, 300, 600 µM of H_2O_2 from the study of Vainieri et al. (2020) [46] at day 14 and day 28 were available for investigation of gene expression patterns. The housekeeper genes expression levels for *GAPDH, B2M* and *UBC,* were measured and used to calculate the expression level of the best of 3 housekeeper genes, as shown in equation C1.

$$Best\ of\ 3\ house\ keeper\ gene = \sqrt[3]{GAPDH \cdot UBC \cdot B2M} \qquad (C1)$$

Based on the measured and calculated Cq values (fig. C1), *UBC* had the most constant expression across all samples. *UBC* was selected to normalize the other genes to.

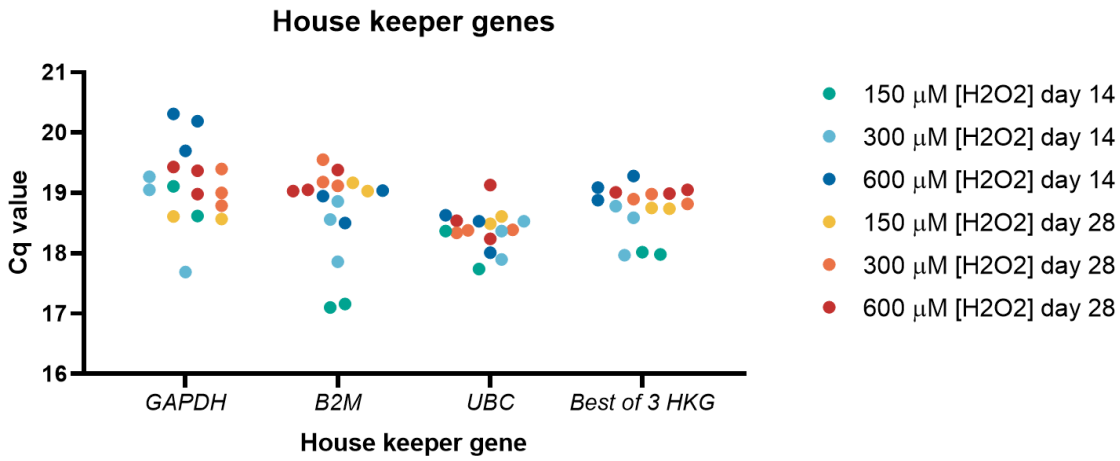

Figure C1: The measured Cq values for the house keeper genes *GAPDH, B2M* and *UBC* for different gel condition samples harvested at day 14 and 28. Also, Cq value of the calculated best of 3 housekeeper gene value was plotted for day 14 and 28.

D

APPENDIX

The individual replicates of the measurements used to obtain the average gelation curve are shown in fig. D1. The gel conditions containing a polymer concentration of 3.5 % w/v Ha-Tyr are denoted in blue, and gels containing a polymer concentration of 1.5 % w/v Ha-Tyr are presented in red. The gel condition 3.5 % w/v Ha-Tyr crosslinked with 600 µM H_2O_2

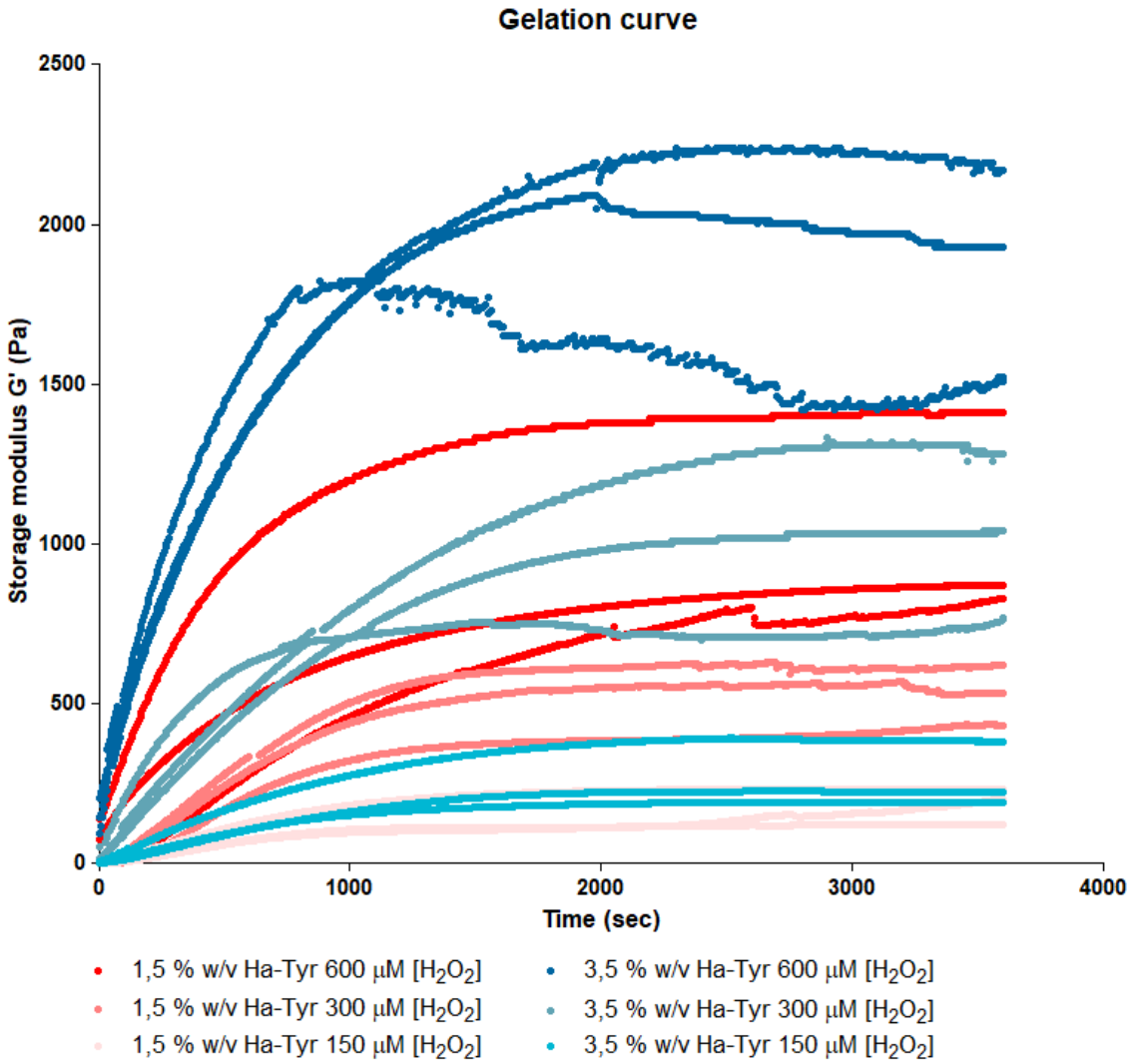

Figure D1: The measured individual replicates for the gelation kinetics. The gel conditions containing a polymer concentration of 3.5 % w/v Ha-Tyr are denoted in blue, and gels containing a polymer concentration of 1.5 % w/v Ha-Tyr are represented in red.

showed a sudden drop in storage modulus. In fig. D2, all individual replicates crosslinked with 600 µM H_2O_2 are presented to illustrate the sudden drop in G' in some of these gel conditions. In Fig. D3, the gelation times obtained from the rheological measurements are presented. The gelation was defined as the time required to reach G' equilibrium. Thereby, it was assumed that a gel reached an equilibrium state in G' if the difference between measured G'< 0.2 Pa.

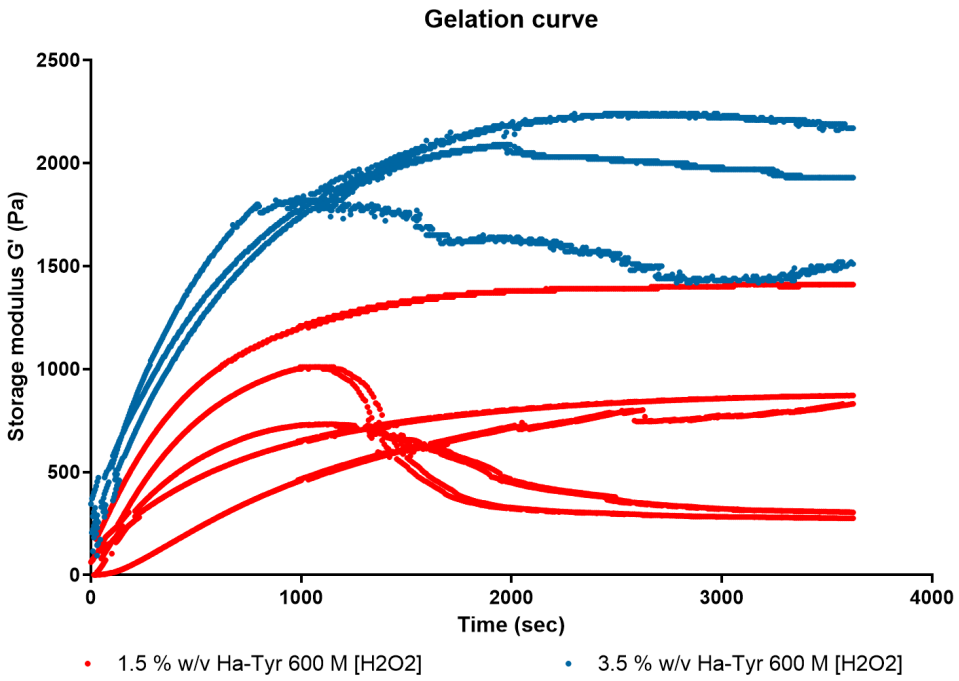

Figure D2: The measured individual replicates for the gelation kinetics crosslinked with 600 µM H_2O_2. The gel conditions containing a polymer concentration of 3.5 % w/v Ha-Tyr are denoted in blue, and gels containing a polymer concentration of 1.5 % w/v Ha-Tyr are represented in red.

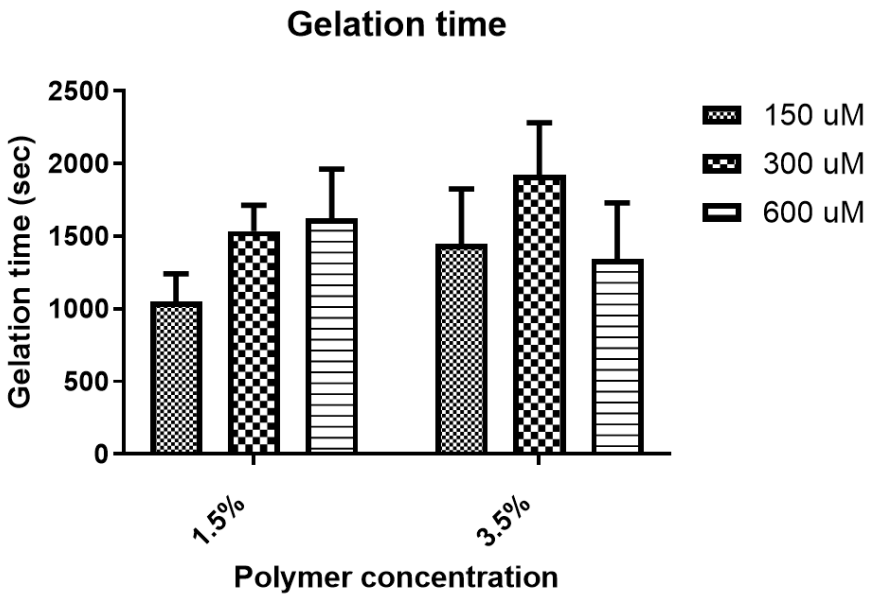

Figure D3: The measured individual replicates for the gelation time crosslinked with 600 µM H_2O_2. The data are shown based on n=3 with mean ± SD.

E

APPENDIX

The measured swelling ratio and calculated Flory-Rehner model (fig. E1). As a sample size, 50 µL was used for each gel. The uncoupling of storage modulus and mesh size using the Flory-Rehner mesh estimation showed a similar distribution is shown in fig. E2.

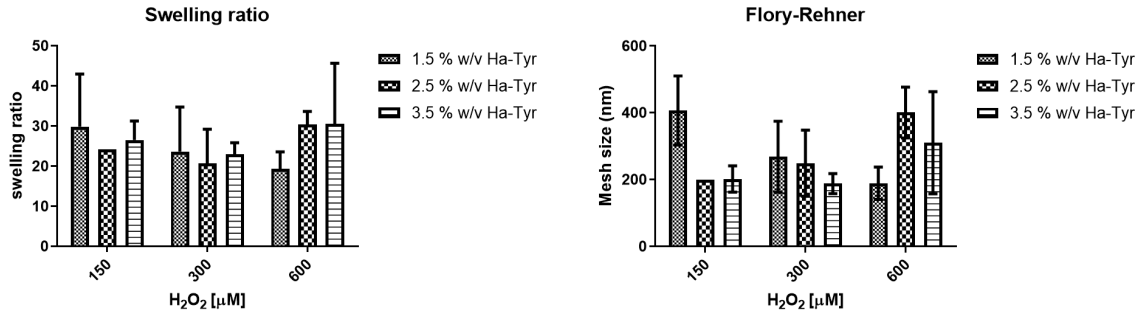

Figure E1: The measured swelling ratio and calculated mesh size using the Flory-Rehner model in different gel condition. The data are shown based on n=3 with mean ± SD. For gel condition 2.5% crosslinked with 150 µM H_2O_2 two data points were excluded as a consequence of wrong measurement.

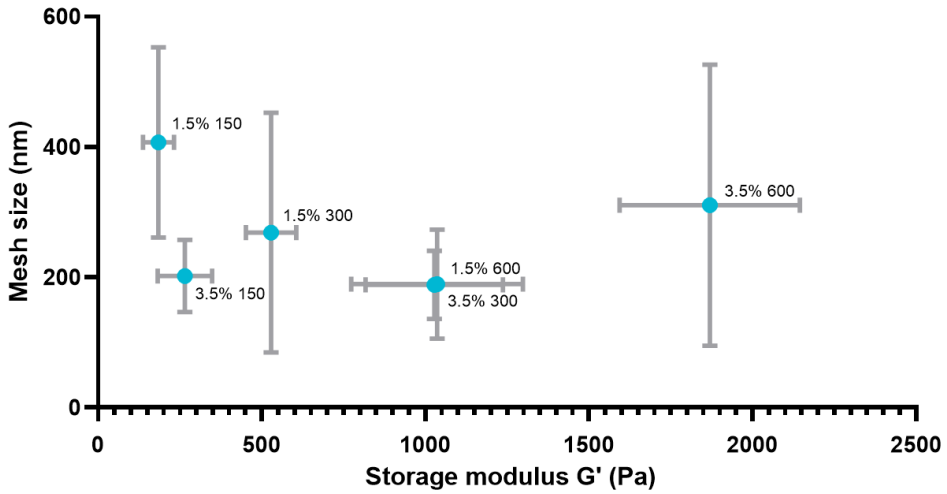

Figure E2: The storage modulus (G') and mesh size plotted against each other for each gel condition to uncouple the two material properties from each other. The Flory-Rehner estimation was used for mesh size determination. The data are shown in triplicate gel sample with mean ± SD.

F

APPENDIX

To quantify the relative gene expression level, each measured gene expression was normalized against a housekeeper gene(s). Housekeeper genes are constitutive genes required for maintenance within cells. Therefore, it is assumed that housekeeper genes are expressed at similar expression levels across different experimental conditions [78]. Using the same amount of RNA as input, we can assume that a smaller variance in gene expression for the housekeeper genes will better compare gene expression patterns across other conditions. The measured Cq value depends on the threshold value used during the measurement. A higher Cq value indicates a lower expression level for the gene. Cq values higher than 36 were considered as not expressed.
cDNA samples obtained from MSCs embedded in Ha-Tyr hydrogels with 3.5% of polymer concentration and crosslinked with either 150, 300, 600 µM of H_2O_2 from the study of Vainieri et al. (2020) [46] at day 14 and day 28 were available for investigation of gene expression patterns. The housekeeper genes expression levels for *RPS27A, B2M* and *UBC,* were measured and used to calculate the expression level of the best of 3 housekeeper genes, as shown in equation F1.

$$Best\ of\ 3\ house\ keeper\ gene = \sqrt[3]{RPS27A \cdot UBC \cdot B2M} \qquad (F1)$$

Based on the measured and calculated Cq values (fig. F1), *RPS27A* had the most constant expression across all samples. *RPS27A* was selected to normalize the other genes to.

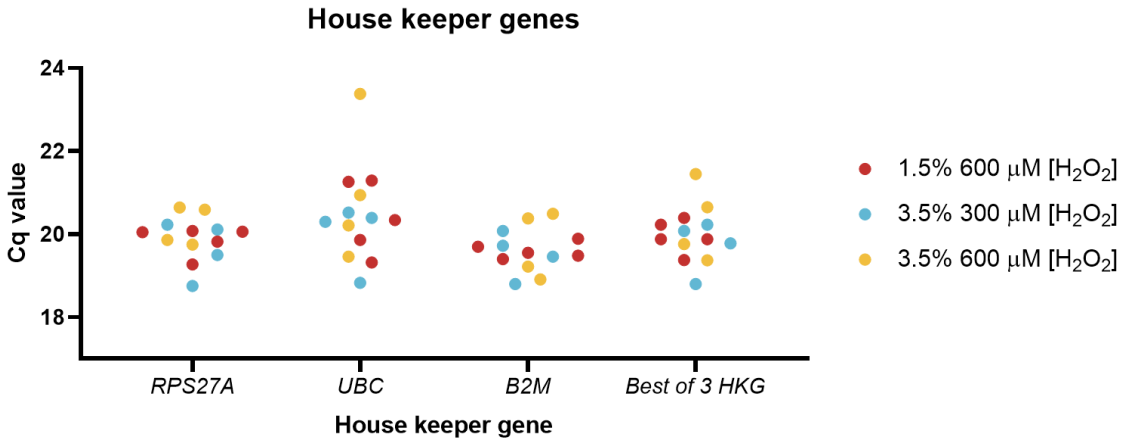

Figure F1: The measured Cq values for the house keeper genes *RPS27A, B2M* and *UBC* for different gel condition samples harvested at day 14. Also, Cq value of the calculated best of 3 housekeeper gene value was plotted for day 14.

G

APPENDIX

The GAG content within empty gel conditions were measured via a DMB assay to validate possible interference within the measurement (fig. G1). All measured values were below the detection limit. Therefore, it was assumed that the Ha-Tyr polymer does not interfere with the DMB assay for GAG quantification.

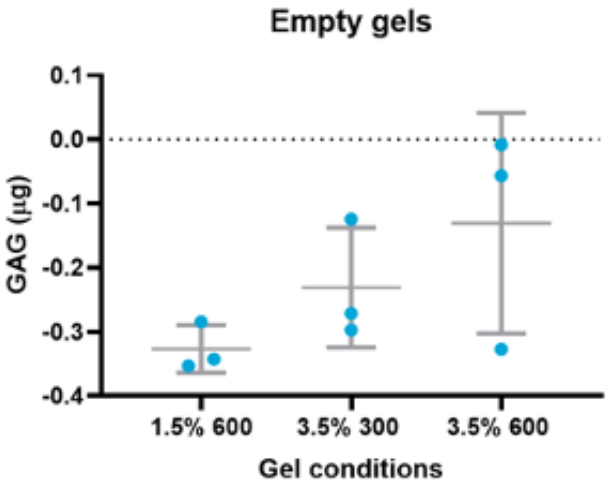

Figure G1: A DMB assay on empty hydrogels. All measured samples were below detection level. The data are shown in triplicate gel sample with mean ± SD.

H

APPENDIX

Cryosection optimization was performed at varying blade and sample temperatures. Sections and stained with Saf-O, Thionin and H&E. A general trend of improved cutting with lower blade temperature was observed.

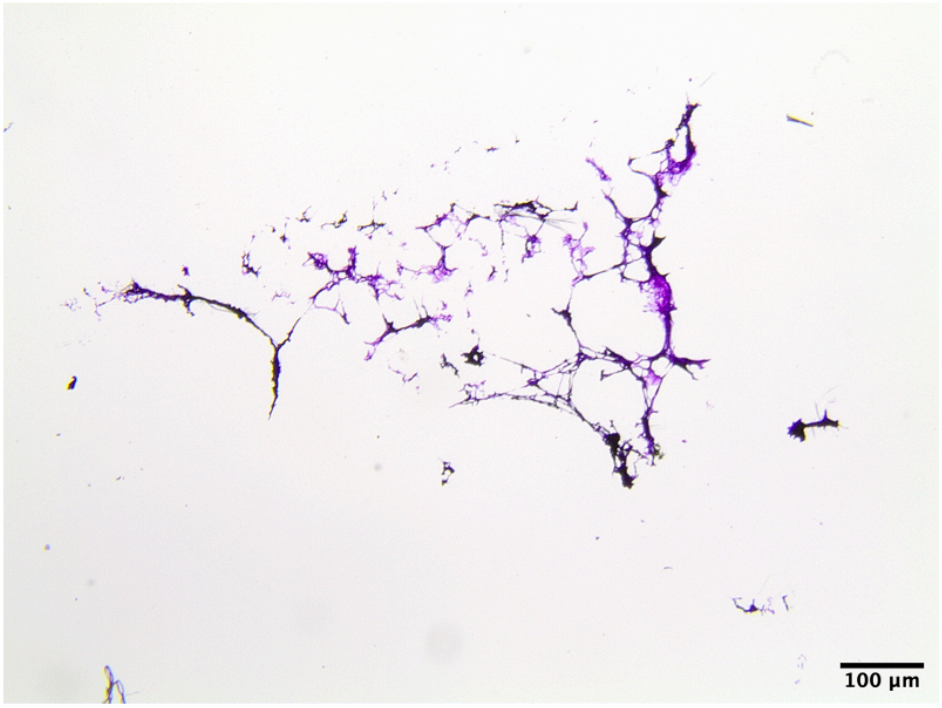

Figure H1: Thionin stained empty 1.5% 150 Ha-Tyr hydrogel. The gel had been sectioned with a sample and blade temperature of respectively -20 °C and -25 °C. Image was taken at 10 times magnification

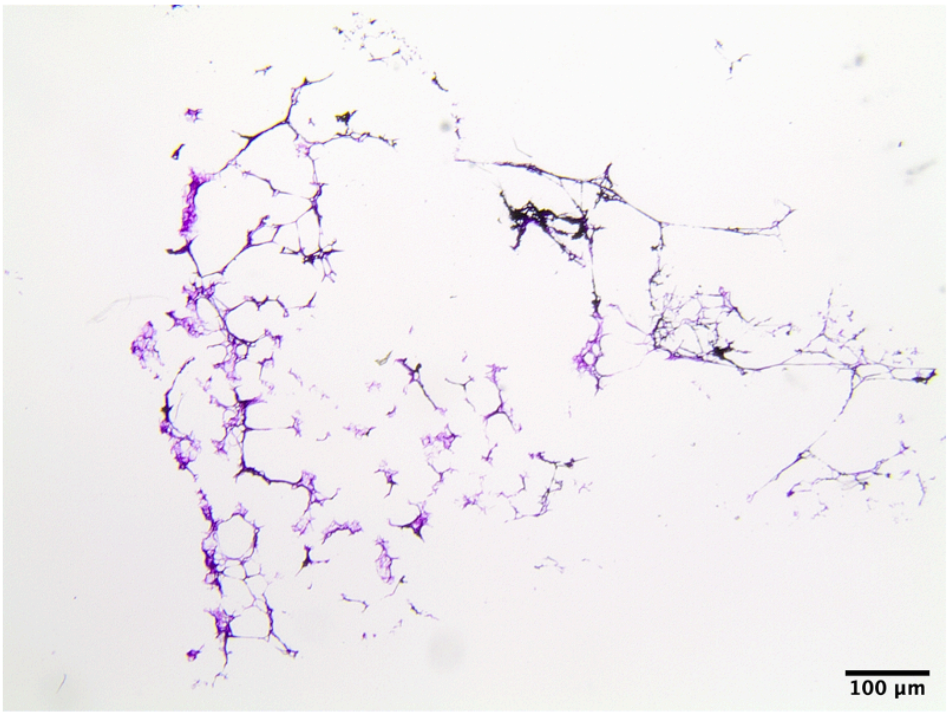

Figure H2: Thionin stained empty 1.5% 150 Ha-Tyr hydrogel. The gel had been sectioned with a sample and blade temperature of respectively -25 °C and -30 °C. Image was taken at 10 times magnification.

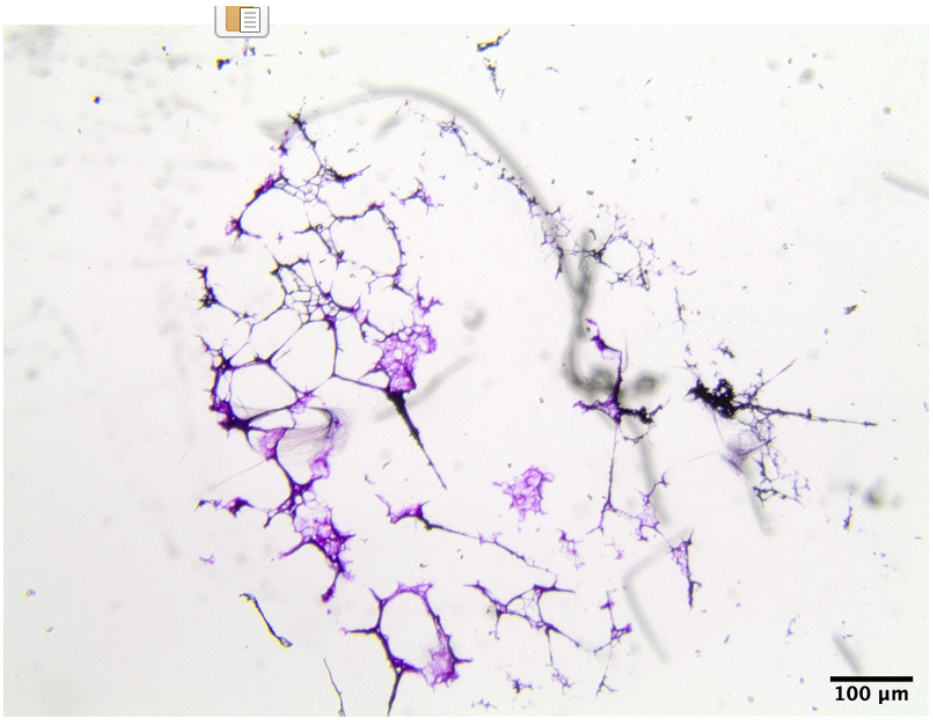

Figure H3: Thionin stained empty 1.5% 150 Ha-Tyr hydrogel. The gel had been sectioned with a sample and blade temperature of respectively -30 °C and -35 °C. Image was taken at 10 times magnification.

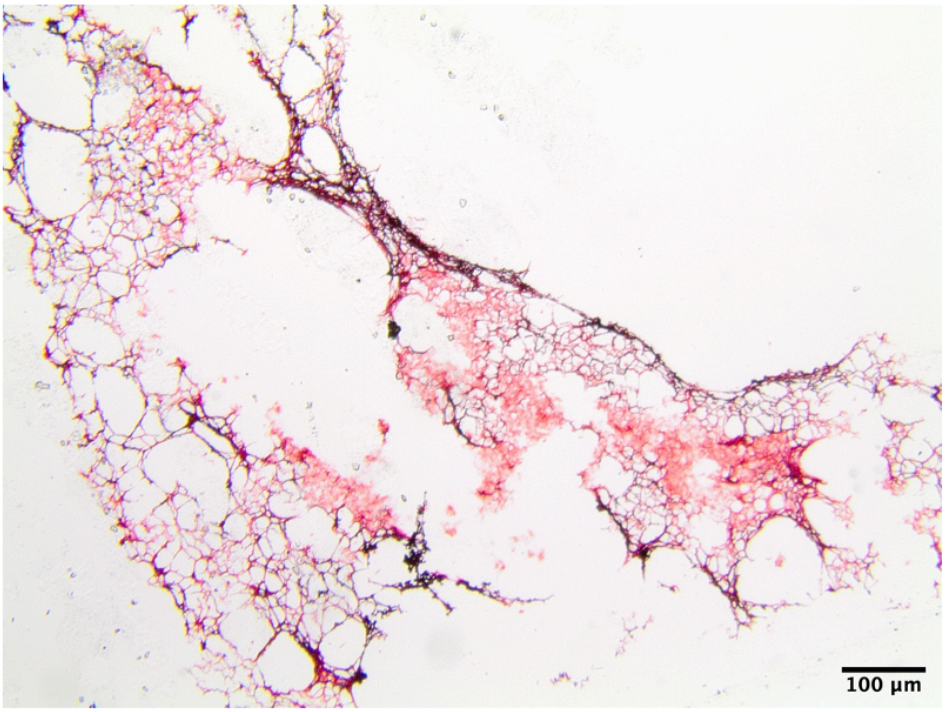

Figure H4: Safran-O stained empty 1.5% 150 Ha-Tyr hydrogel. The gel had been sectioned with a sample and blade temperature of respectively -35 °C and -35 °C. Image was taken at 10 times magnification.

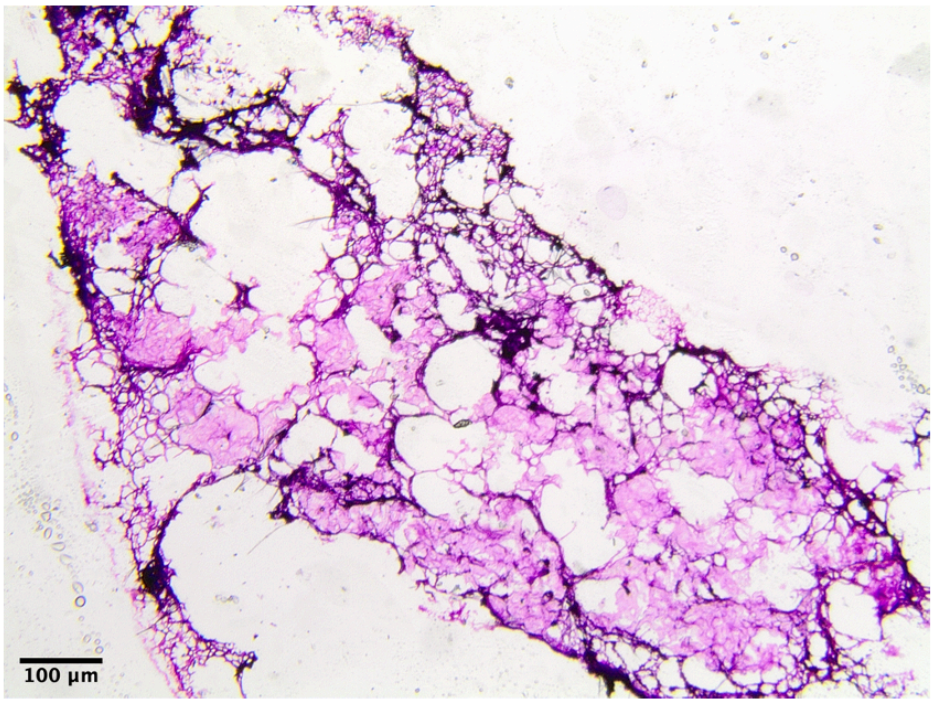

Figure H5: Thionin stained empty 1.5% 150 Ha-Tyr hydrogel. The gel had been sectioned with a sample and blade temperature of respectively -35 °C and -35 °C. Image was taken at 10 times magnification.

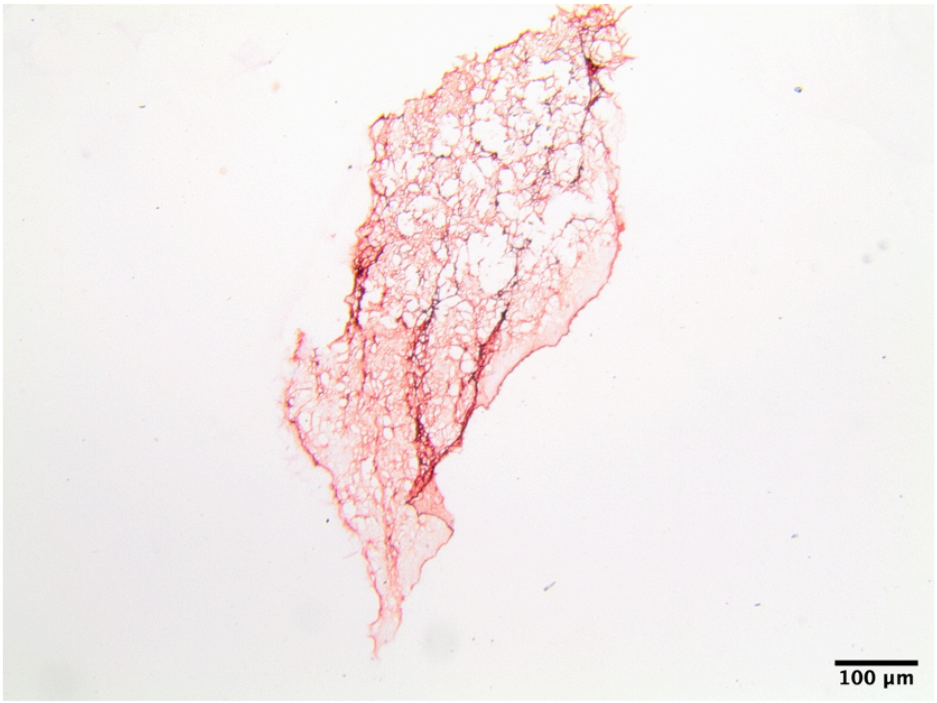

Figure H6: Safranin-O stained 1.5% 150 Ha-Tyr hydrogel cultured for 2 days in full chondrogenic medium. The gel had been sectioned with a sample and blade temperature of respectively -35 °C and -35 °C. Image was taken at 10 times magnification.

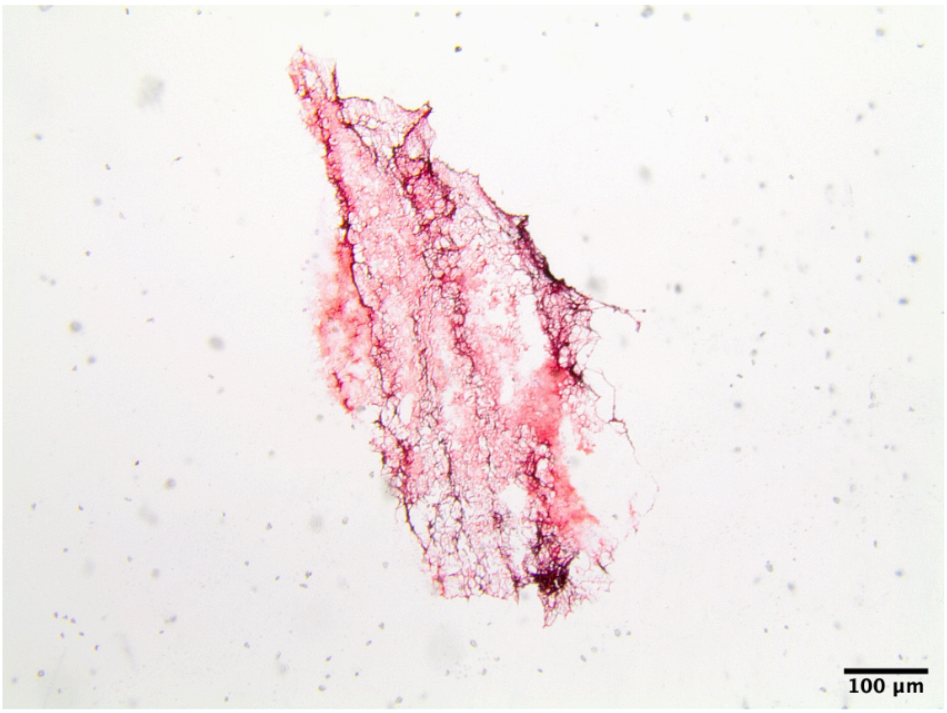

Figure H7: Safranin-O stained 1.5% 150 Ha-Tyr hydrogel cultured for 2 days in full chondrogenic medium. The gel had been sectioned with a sample and blade temperature of respectively -35 °C and -35 °C. Image was taken at 10 times magnification.

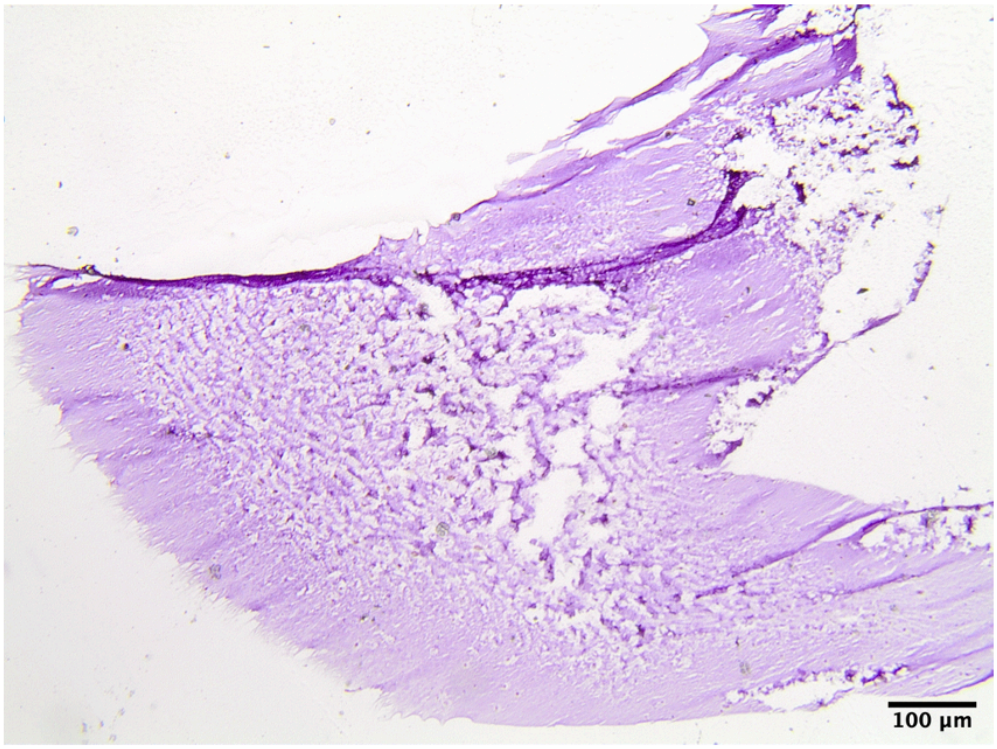

Figure H8: Thionin stained 1.5% 150 Ha-Tyr hydrogel cultured for 4 days in full chondrogenic medium. The gel had been sectioned with a sample and blade temperature of respectively -35 °C and -35 °C. Image was taken at 10 times magnification.

I

APPENDIX

Microscopic observation of the three selected gel conditions at day 7 of culture. All gels were cultured in full chondrogenic medium. In Fig. I1, the microscopic observation of gel condition 1.5% w/v Ha-Tyr crosslinked with 600 µM of H_2O_2 at day 7. In Fig. I2, the microscopic observation of gel condition 3.5% w/v Ha-Tyr crosslinked with 300 µM of H_2O_2 at day 7. In Fig. I1, the microscopic observation of gel condition 3.5% w/v Ha-Tyr crosslinked with 600 µM of H_2O_2 at day 7.

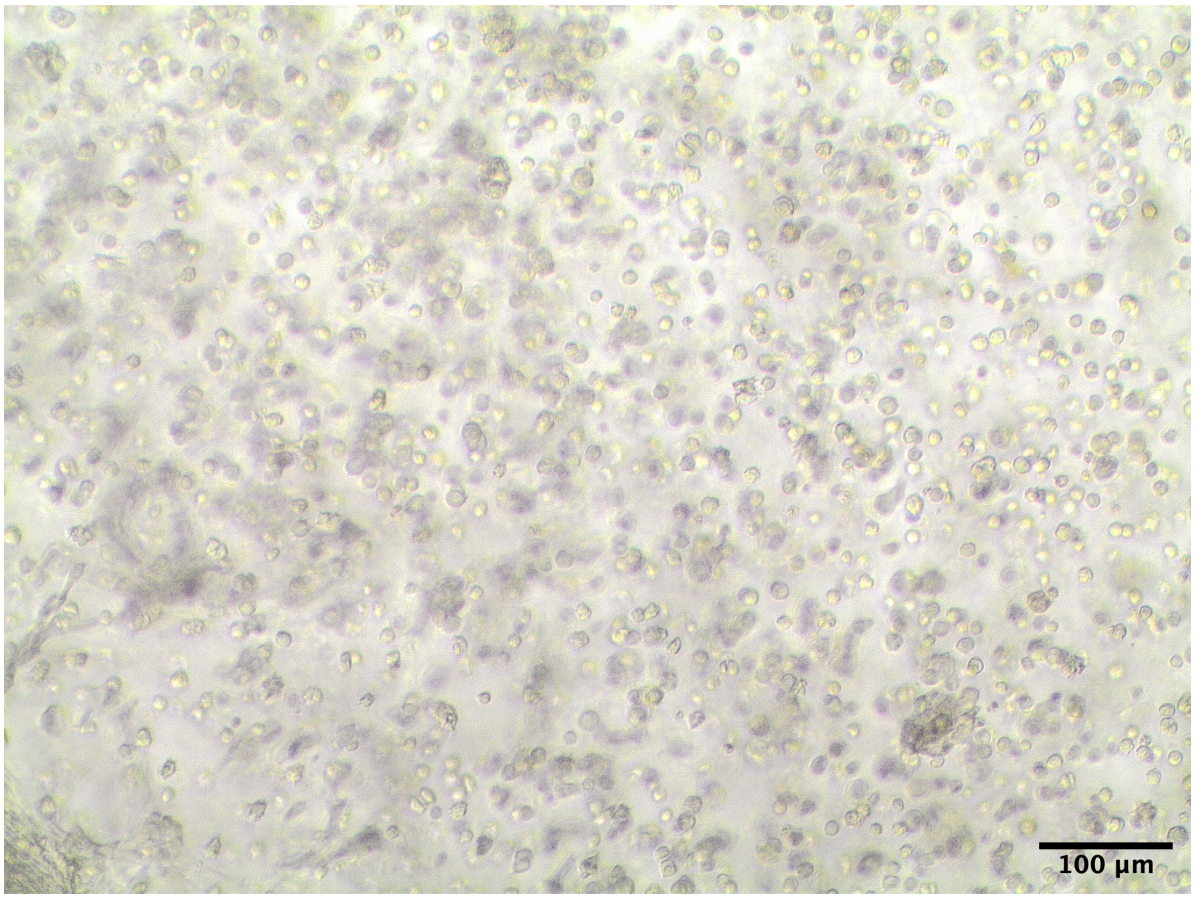

Figure I1: Microscopic observation of gel condition 1.5% w/v Ha-Tyr crosslinked with 600 µM of H_2O_2 at day 7. The image has been taken at a magnification of 40 times.

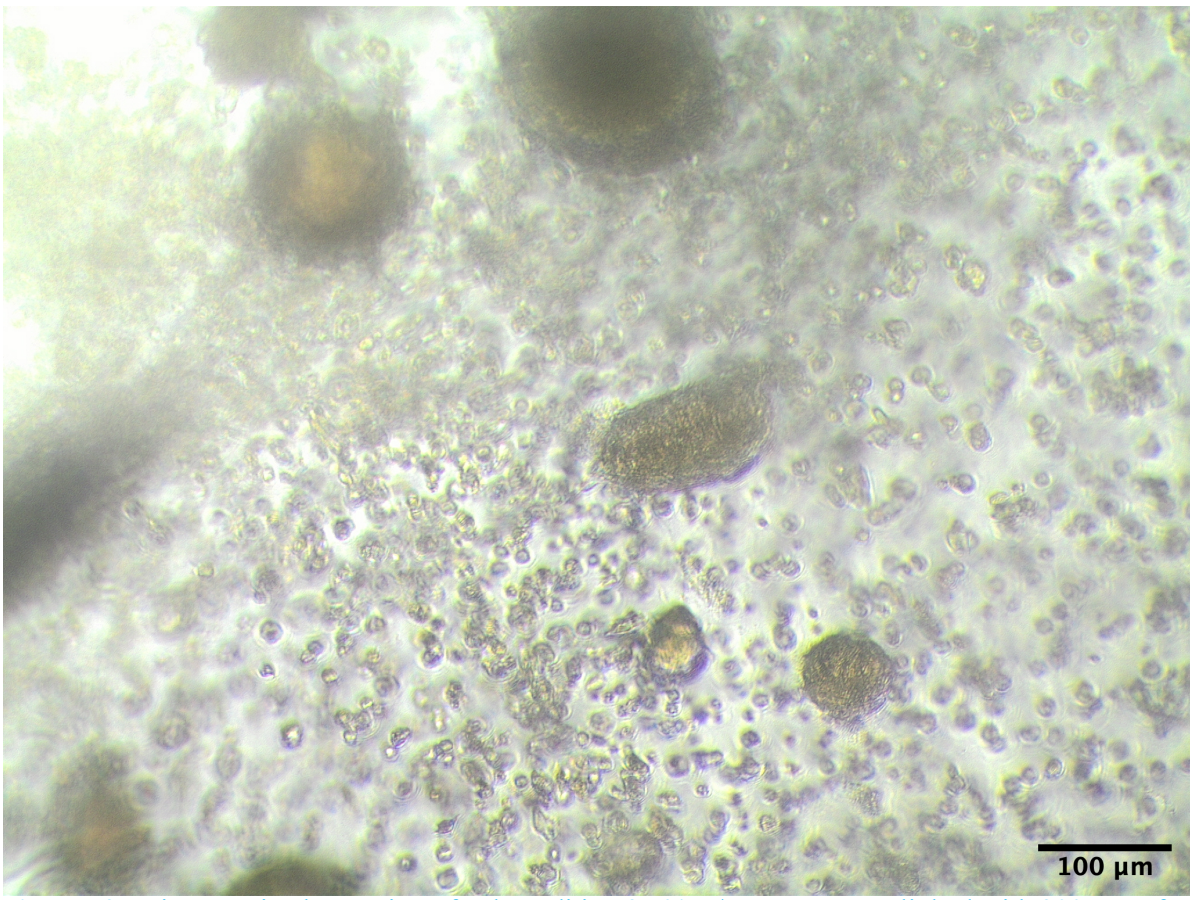

Figure I2: Microscopic observation of gel condition 3.5% w/v Ha-Tyr crosslinked with 300 µM of H_2O_2 at day 7. The image has been taken at a magnification of 40 times.

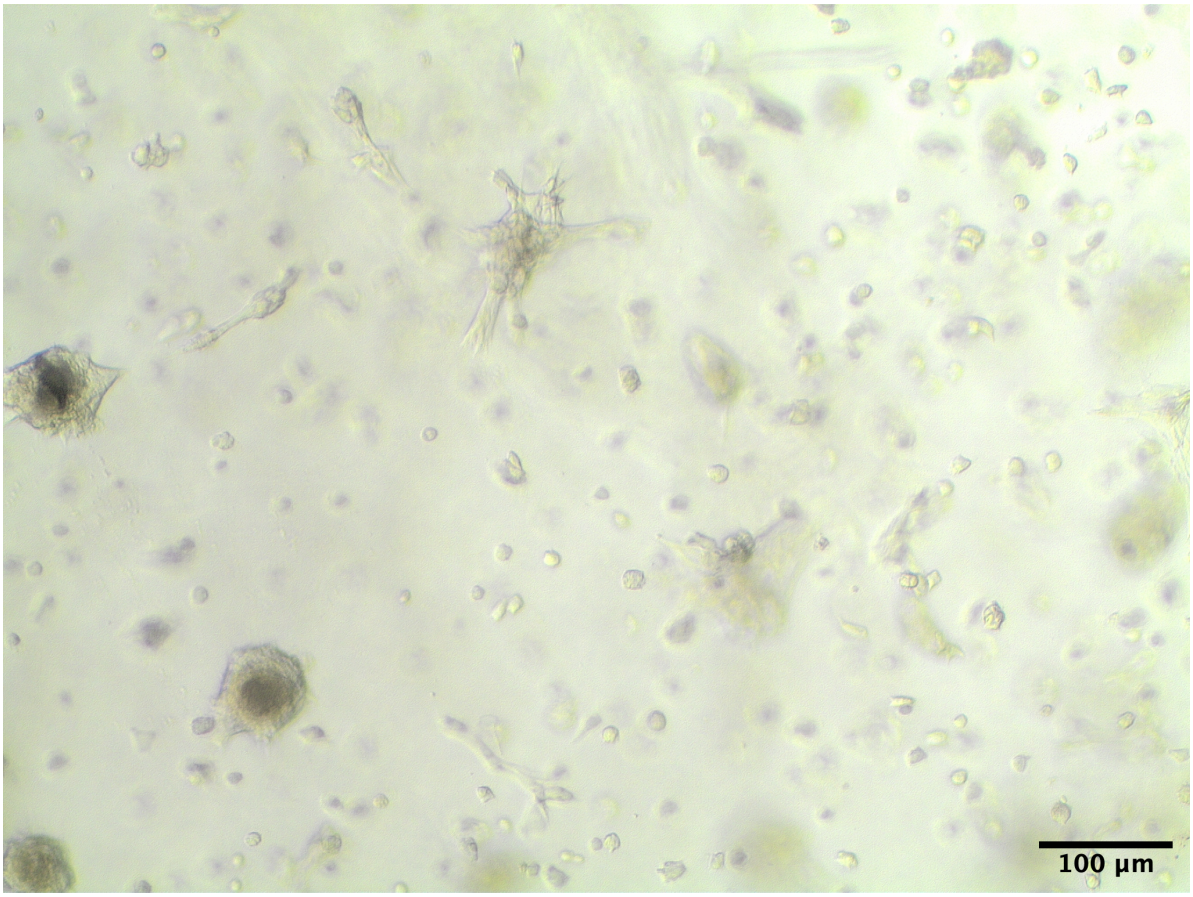

Figure I3: Microscopic observation of gel condition 3.5% w/v Ha-Tyr crosslinked with 600 µM of H_2O_2 at day 7. The image has been taken at a magnification of 40 times.

J

APPENDIX

A pilot study evaluating the effect of cell density on the chondrogenic potential of MSC embedded in alginate beads. Chondrogenesis was assessed based on measuring the gene expression levels for the chondrogenic markers *COL2A1, ACAN* and *SOX9*. The alginate beads were cultured in chondrogenic medium containing 0 ng/mL TGF-β or 10 ng/mL TGF-β for 14 days. A trend towards increased gene expression levels were measured with increasing crosslinking density as well as a higher TGF-β concentration.

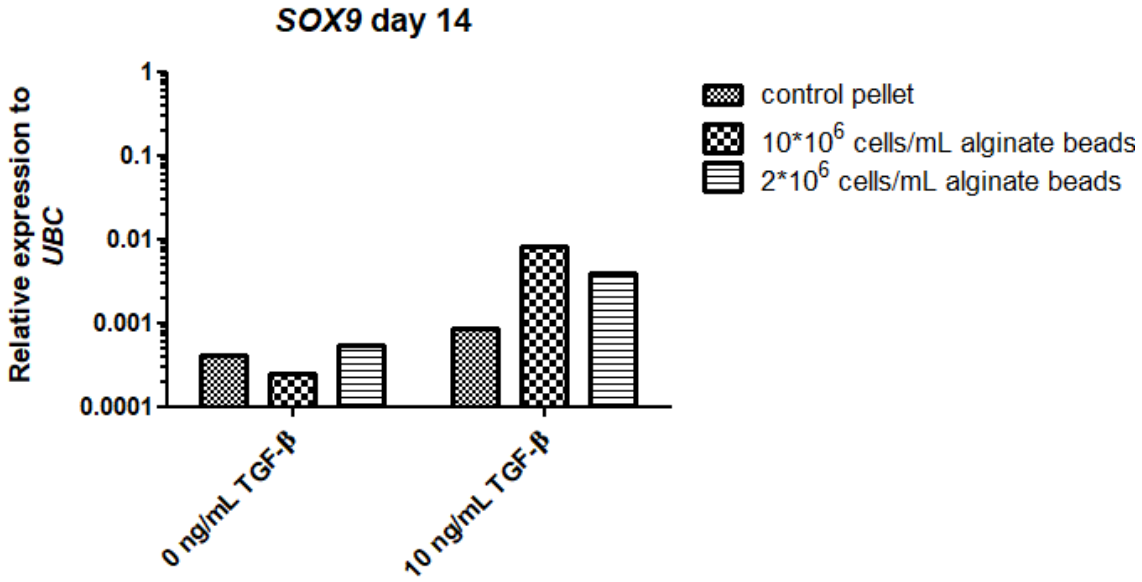

Figure J1: The relative gene expression level for the chondrogenic marker *SOX9* of P-MSCs embedded in alginate at a cell density of either $2 \cdot 10^6$ cells/mL or $10 \cdot 10^6$ cells/mL. The samples were cultured for 14 days in chondrogenic medium with either 0 ng/mL TGF-β or 10 ng/mL TGF-β.

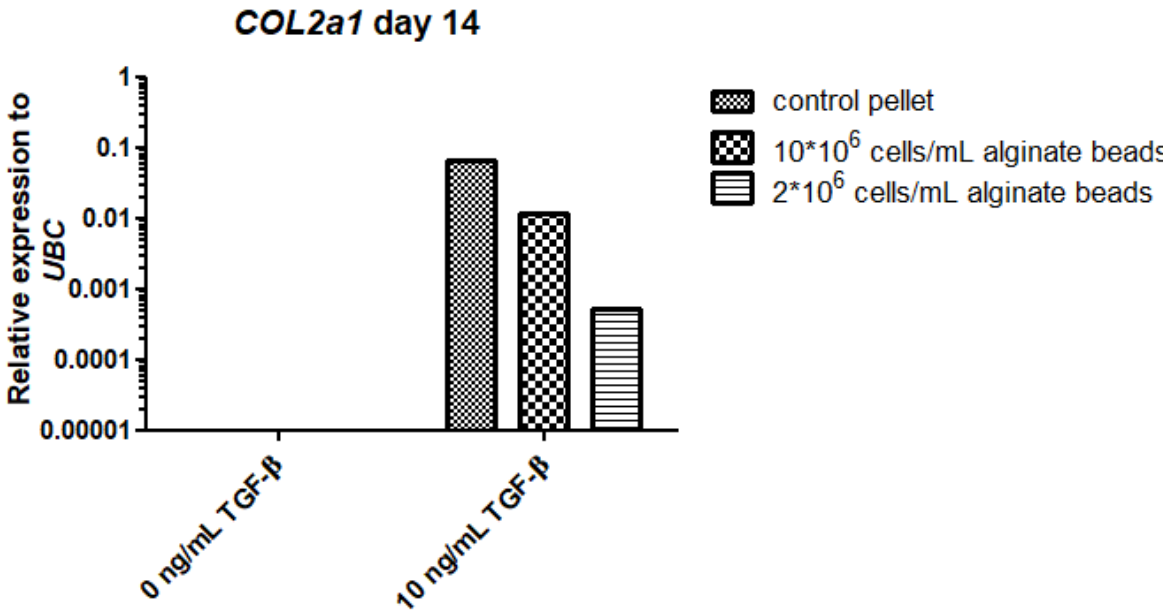

Figure J3: The relative gene expression level for the chondrogenic marker *COL2A1* of P-MSCs embedded in alginate at a cell density of either $2 \cdot 10^6$ cells/mL or $10 \cdot 10^6$ cells/mL. The samples were cultured for 14 days in chondrogenic medium with either 0 ng/mL TGF-β or 10 ng/mL TGF-β.

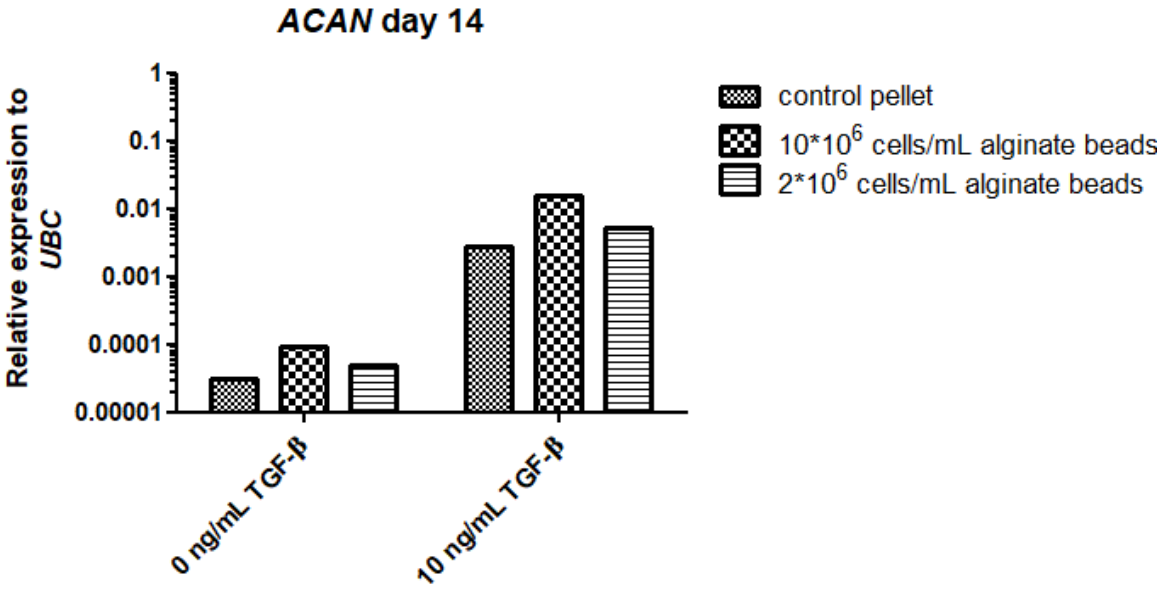

Figure J2: The relative gene expression level for the chondrogenic marker *ACAN* of P-MSCs embedded in alginate at a cell density of either $2 \cdot 10^6$ cells/mL or $10 \cdot 10^6$ cells/mL. The samples were cultured for 14 days in chondrogenic medium with either 0 ng/mL TGF-β or 10 ng/mL TGF-β.

K

APPENDIX

A pilot study evaluating the effect of TGF-β concentration on the chondrogenic potential of MSC embedded in alginate beads. Chondrogenesis was assessed by measuring the gene expression levels for the chondrogenic markers *COL2A1, ACAN* and *SOX9*. The alginate beads were cultured in chondrogenic medium ranging between 0 and 10 ng/mL TGF-β for 14 days. A trend towards increased gene expression levels were measured with increasing TGF-β concentration.

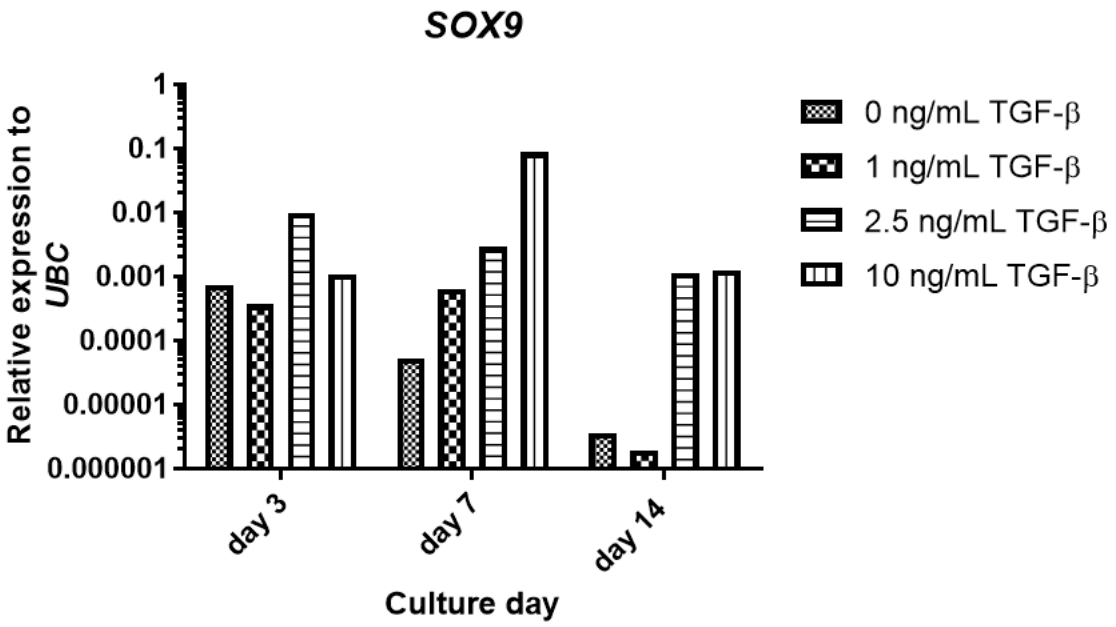

Figure K1: The relative gene expression level for the chondrogenic marker *SOX9* of P-MSCs embedded in alginate at a cell density of either $2 \cdot 10^6$ cells/mL and varying concentrations TGF-β between 0 and 10 ng/mL TGF-β.

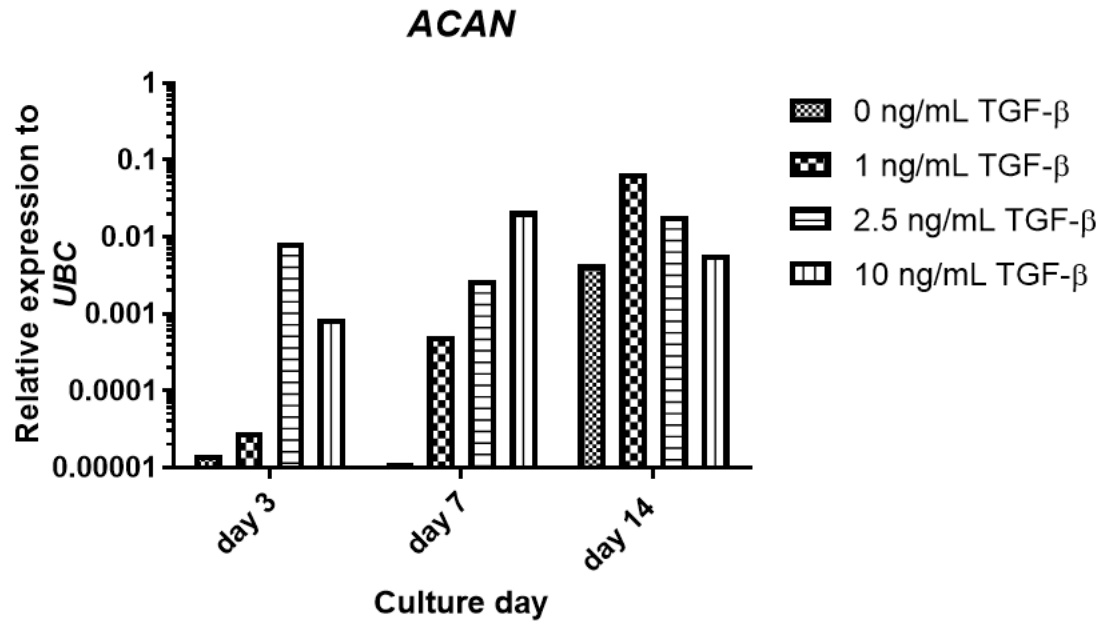

Figure K2: The relative gene expression level for the chondrogenic marker *ACAN* of P-MSCs embedded in alginate at a cell density of either $2 \cdot 10^6$ cells/mL and varying concentrations TGF-β between 0 and 10 ng/mL TGF-β.

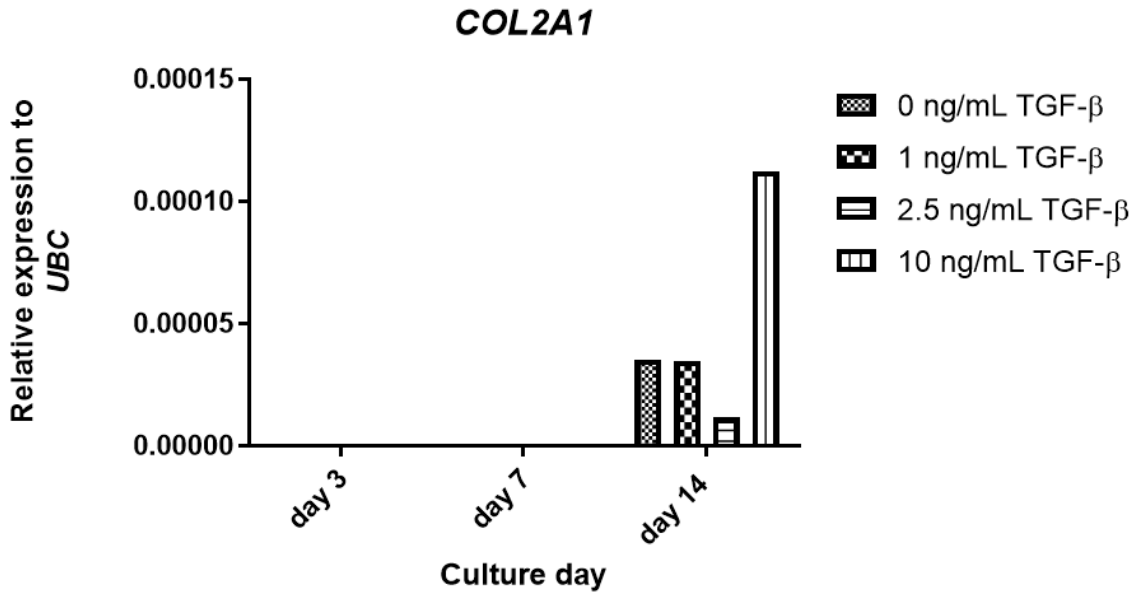

Figure K3: The relative gene expression level for the chondrogenic marker *COL2A1* of P-MSCs embedded in alginate at a cell density of either $2 \cdot 10^6$ cells/mL and varying concentrations TGF-β between 0 and 10 ng/mL TGF-β.